PRODUCTION PERFORMANCE MODELING THROUGH INTEGRATION OF RESERVOIR AND PRODUCTION NETWORK WITH ASPHALTENE DEPOSITION

A Dissertation

by

ERNESTO VALBUENA OLIVARES

Submitted to the Office of Graduate and Professional Studies of
Texas A&M University
in partial fulfillment of the requirements for the degree of

DOCTOR OF PHILOSOPHY

Chair of Committee,	Maria Barrufet
Co-Chair of Committee,	John Killough
Committee Members,	Thomas Blasingame
	Eduardo Gildin
	Michael King
Head of Department,	Daniel Hill

May 2015

Major Subject: Petroleum Engineering

ABSTRACT

This study proposes the development of a new integrated reservoir-network compositional simulator with asphaltene modeling in production pipelines. Reservoir and network simulators are developed with a fully-implicit formulation, allowing stand-alone runs to analyze specific areas of interest for reservoir and production engineers. The same simulation platform allows to perform tightly-coupled runs to assess mutual interaction between subsurface and surface components.

Fluid phase behavior is modeled through phase equilibria calculations, using Peng-Robinson equation of state with volume translation. Rigorous vapor/liquid/liquid-dense equilibria calculations are performed to model asphaltene precipitation in network pipelines using a thermodynamically consistent sequential approach. Asphaltene deposition in the internal pipe walls is estimated through a mechanistic solid transport model. Compositional delumping is performed from reservoir to network fluid descriptions to improve fluid characterization for asphaltene modeling in pipelines.

The proposed combination of tight coupling with fully-implicit formulation for oil, gas, water flow in reservoir and network, and sequential approach for solid precipitation and deposition in the pipeline system, provides a robust and flexible methodology for additional applications of solid deposition, e.g. hydrates and waxes. This approach also enables evaluation of inhibitor injection and artificial gas lift installation on asphaltene deposition and production performance.

Integrated reservoir-network modeling provides more representative reservoir performance forecasts than conventional stand-alone methods, as it allows to simulate complex interactions between reservoir and surface facilities. Solids precipitation and deposition in networks have a negative impact on production rates, pressure management, and field operations. Flow assurance techniques based on adequate estimates of potentially

blocking phases (hydrates, waxes, asphaltenes) are crucial to achieve good production performance. The modeling approach developed in this research allows to forecast asphaltene precipitation and accumulation in pipelines under multiple production conditions, including pressure and temperature gradients, fluid composition, production rates, gas lift, and inhibitor injection.

ACKNOWLEDGEMENTS

To my **wife Karin**, you are the cornerstone of my life. Your love and encouragement always drive me to be my best.

To **Dr. Maria Barrufet**, for her invaluable teachings, passion, and friendship. Your dedication inspires me in the pursue of knowledge. There are no words to describe my gratitude to you.

To **Dr. John Killough**, for his unconditional trust and support. Your words of advice served to guide my research journey.

To **Dr. Thomas Blasingame**, **Dr. Eduardo Gildin**, and **Dr. Michael King**, for their guidance, suggestions, and support during my career at Texas A&M, and as my advisory committee members during the development of this research.

To the **professors and staff of the Petroleum Engineering Department of Texas A&M University** at College Station, for their lessons and academic integrity.

To my **mother Elizabeth** and **father Eduardo**, for their endless encouragement, advice, and love. For being my role models in life. Walking the path of excellent would be very difficult without you.

My appreciations to all of you.

NOMENCLATURE

Acronyms

ADM	asphaltene deposition modeling
BC	boundary condition
BHP	bottomhole pressure
BIC	binary interaction coefficient
ECL	Eclipse simulator (Schlumberger)
EOS	equation of state
IMPES	implicit in pressure and explicit in saturation
IPR	inflow performance relationship
MSW	multi-segment well
PR	Peng-Robinson (EOS)
PVT	pressure/volume/temperature
QC	quality check
VLE	vapor/liquid equilibria
VLLE	vapor/liquid/liquid-dense equilibria

Variables

$(a\alpha)$	EOS mixture parameter (quadratic mixing rule)
Δ_τ	time differential operator
Δp_A	acceleration pressure drop, psi
Δp_F	frictional pressure drop, psi
Δp_{PE}	potential energy pressure drop, psi
A	area, ft^2
A	cubic EOS coefficient
a_i	EOS parameter for component i
$a_{\alpha\eta}$	transmissibility of phase α between central and neighbor η gridblocks, lbmol/day/psi

B	cubic EOS coefficient
b	EOS mixture parameter (linear mixing rule)
b_i	EOS parameter for component i
B_w	water volumetric factor, bbl/STB
BHP	well bottomhole pressure (at reference depth), psia
$\tilde{C}_b$	bulk fluid precipitated asphaltene molar concentration, lbmol/ft^3
$\tilde{C}_{wall}$	deposited asphaltene molar concentration, lbmol/ft^3
c_i	volume translation correction factor for component i
c_{rock}	rock compressibility, psi^{-1}
D	diameter, in or ft
D_B	Brownian diffusivity
d_p	asphaltene particle diameter, μm (micrometer)
E_a	activation energy, kJ/kgmol
F	total number of moles per unit volume, lbmol/ft^3
F_i	number of moles of component i per unit volume, lbmol/ft^3
$\hat{f}_i^{\alpha}$	fugacity of component i in phase α
f_f	friction factor, dimensionless
f_l	liquid molar fraction
f_{ld}	liquid-dense molar fraction
f_s	solid molar fraction
f_v	vapor molar fraction
g_c	gravity constant
h	node (segment) depth/height, ft
$\vec{\vec{J}}$	Jacobian matrix
$\vec{\vec{k}}$	rock permeability tensor, mD
K_d	frequency factor, ft^2/s^2
K_i	equilibrium ratio of component i
K_t	transport coefficient, ft/s

K_t^+	dimensionless transport coefficient
k_{rocw}	oil relative permeability at connate water saturation
k_{rog}	oil relative permeability at actual gas saturation and connate water saturation
k_{row}	oil relative permeability at actual water saturation
$k_{r\alpha}$	relative permeability of phase α, dimensionless
L	length, ft
M_{w_i}	molecular weight of component i, lb/lbmol
M_w^α	molecular weight of phase α, lb/lbmol
$m_{asp_{wall}}$	mass of asphaltene deposited in the pipe wall, lb
$\dot{m}_{s/s}$	net mass rate from source/sink
N_{Re}	Reynolds Number
$\dot{n}_{asp_{wall}}$	asphaltene accretion rate, lbmol/ft^2/s
$\dot{n}_{i_{s/s}}$	net molar rate of component i from source/sink
$n_{asp_{wall}}$	moles of asphaltene deposited in the pipe wall, lbmol
$n_{COUP_{eq}}$	number of reservoir-network coupled equations
$n_{MSW_{eq}}$	number of multi-segment well equations
$n_{NET_{eq}}$	number of network equations
$n_{RES_{eq}}$	number of reservoir equations
n_{seg_w}	number of segments for well w
n_c	number of hydrocarbon components (or pseudocomponents)
$n_{gridblocks}$	number of reservoir gridblocks
n_{pipe}	number of network pipe segments
p	pressure, psia
p_{c_i}	critical pressure of component i, psia
p_{cgo}	gas-water capillary pressure, psi
p_{cow}	oil-water capillary pressure, psi
p_o	oil-phase pressure, psia

p_{oC}	central gridblock oil-phase pressure, psia
$p_{o\eta}$	neighbor gridblock oil-phase pressure, psia
p_{ref}	reference pressure, psia
p_{wf}	bottomhole flowing pressure for perforated gridblock, psia
$q_{ws/s}$	volumetric water rate from a well, ft^3/day
q_α	volumetric rate of phase α, STB/day, MSCF/day, or ft^3/day
R	gas constant, 10.7316 ft^3.psi/°R/lbmol or 8.31446 J/K/mol
$\vec{R}$	vector of residuals
R_{fug_i}	fugacity residual for component i
R_{HU}	hold-up residual
R_i	hydrocarbon component residual, lbmol/day
R_p	pressure drop residual, psi
R_{RR}	Rachford-Rice residual
R_{sat}	saturation (volume constraint) residual
R_w	water residual, lb/day
r_w	wellbore radius, ft
S	well skin, dimensionless
S_g	gas saturation, V/V fraction
S_o	oil saturation, V/V fraction
S_w	water saturation, V/V fraction
Sc	Schmidt Number
SP	sticking probability, dimensionless
$\mathcal{S}_i$	shift (translation) factor for component i
T	temperature, °F or R
T_{c_i}	critical temperature of component i, °F or R
T_K	temperature, K
T_η	interblock geometric transmissibility
t	time, day

t_p^+	dimensionless relaxation time (Stoke's stopping distance)
$\vec{u}_\alpha$	velocity of phase α, ft/s
u_m	fluid mixture velocity in segment or connection, ft/s
V	volume, STB or ft^3
$\vec{V}$	velocity, ft/s
$V_{asp_{wall}}$	volume of asphaltene deposited in the pipe wall, ft^3
V_b	gridblock rock bulk volume, ft^3
v_α	molar volume of phase α, ft^3/lbmol
W	mass of water per unit volume, lb/ft^3
W_{cut}	water cut, V/V fraction
WI_α	well index for phase α, lbmol/day/psi
WI_{geom}	well index geometric component
$\vec{x}$	vector of unknowns
x_i	liquid molar fraction of component i
y_i	vapor molar fraction of component i
y_α	hold-up of phase α, V/V fraction
Z_α	compressibility factor of phase α, dimensionless
z_i	total molar fraction of component i
z_C	central gridblock depth, ft
z_η	neighbor gridblock depth, ft
α_i	EOS parameter for component i
β	unit conversion factor
Δt	time-step size, day
Δx	gridblock size in x-direction
Δy	gridblock size in y-direction
Δz	gridblock size in z-direction
ε	error tolerance
ϵ	relative roughness, dimensionless

ζ_i viscosity parameter for component i

κ_B Boltzmann's constant, [1.3806×10^{-23} J/K]

κ_{ij} binary interaction coefficient between components i and j

$\lambda_{\alpha\eta}$ interblock phase α mobility

μ_i^* low pressure viscosity for component i, cP

μ_α viscosity of phase α, cP

μ_α^* viscosity of phase α at atmospheric pressure, cP

ν_p violation factor for constraint selection

ρ density, lb/ft^3

$\tilde{\rho}_{r_\alpha}$ reduced molar density of phase α, lbmol/ft^3

$\tilde{\rho}_\alpha$ molar density of phase α, lbmol/ft^3

ρ_p asphaltene particle density, lb/ft^3

ϕ rock porosity, V/V fraction

$\hat{\varphi}_i^\alpha$ fugacity coefficient of component i in phase α

Φ_α potential of phase α, psia

ω acentric factor EOS

Subscripts and superscripts

$asph$ asphaltene component

b bulk

B bottom gridblock

C central gridblock

C network pipe connection

$COUP$ reservoir-network coupled system

$downs$ downstream

E east gridblock

g gas phase

i component

$\vec{\imath}$ well segment index

$\vec{\imath}_c$	network pipe connection
$\vec{\imath}_p$	network pipe segment
l	liquid
ld	liquid-dense
MSW	multi-segment well system
N	north gridblock
NET	network system
n	time level
$n+1$	time level
$nwet$	non-wetting phase
o	oil phase
P	network pipe segment
RES	reservoir system
S	south gridblock
S	well segment (MSW context)
s/s	source/sink
SC	standard conditions (pressure and temperature)
T	top gridblock
ups	upstream
v	vapor
w	water phase
W	west gridblock
wet	wetting phase
α	phase (oil, gas, water)
η	neighbor (to central) gridblock
$'$	chord-slope

Units

acres	area (1 acre = 43,560 ft^2 = 4,046.86 m^2)
bbl	barrel at p & T, volume (1 bbl = 42 gal = 158.99 Liters)
STB	stock tank barrel, standard conditions 14.7 psia and 60 °F, volume
MMSTB	million standard barrel, volume (1 MMSTB = 10^6 STB)
cP	centi-Poise, viscosity (100 cP = 1 P = 0.1 kg/m/s)
ft	feet, length (1 ft = 0.3048 m)
in	inch, length (12 in = 1 ft = 0.3048 m)
SCF	standard cubic feet, volume (5.615 SCF = 1 STB = 158.99 Liters)
MSCF	thousand standard cubic feet, volume (1 MSCF = 10^3 SCF)
lbmol	pound-mole, quantity of substance
mD	milli-Darcy, permeability (1000 mD = 1 D = 9.869233×10^{-13} m^2)
psi	pound per square inch, pressure (1 psi = 6.8948 MPa)
°F	Fahrenheit degrees, temperature (°F = 32 + °C × 9/5)
R	Rankine degrees, temperature (R = K × 5/9)

TABLE OF CONTENTS

LIST OF FIGURES

Page

Page

Page

Page

Page

Page

LIST OF TABLES

Page

CHAPTER I
INTRODUCTION

The oil and gas industry has always recognized the importance of modeling pressure, temperature, and fluid phase behavior changes across the production system (reservoir, wellbore, and surface/subsea pipelines) to obtain more accurate performance forecasts and design proper asset management strategies.

Well deliverability depends on a wide variety of factors comprised in the three main components of the production system, namely reservoir, wellbore or production tubing, and pipeline networks laid on surface or subsea arrays. These three components interact under very complex relationships, and engineering design factors that can potentially improve or impair asset productivity must be identified to increase project profitability and safety.

Proper facilities and production system design become crucial in field developments were produced fluids are prone to solids deposition (asphaltenes, waxes, hydrates, etc.) or location conditions are challenging, e.g. offshore assets. Solids accretion in pipelines and equipment can severely reduce production rates by increasing pressure drops in the system; in addition, well cleanup and pigging operations to remove solids are costly and reducing their frequency can be the difference between profitable and non-profitable projects. Hence, accurate modeling of production forecast and selection of flow assurance strategies are essential to accomplish successful developments.

Multiple commercial and research simulation packages with capabilities for reservoir-network coupling are currently available. Integrated reservoir-network simulators are based on one of two general approaches, loosely- or tightly-coupling.

Loosely-coupled simulators solve reservoir and network in separate systems of equations and shared boundary conditions are explicitly exchanged through a coupling controller over an iteration process until specified convergence criteria are met. The main advantage of this approach is the ability to use already existing reservoir and network simulation models to develop an integrated study. Given its flexibility, this method is widely applied in the industry. Nonetheless, the explicit nature of the coupled solution can be prone to instability, oscillations, and material balance errors in problems involving complex fluid systems (gas condensate, volatile oil, solids precipitation, etc.) or sudden saturation changes in the nearwellbore region (water/gas injection and breakthrough).

Tightly-coupled simulators, conversely, solve reservoir and network in a single system of equations, ensuring mass conservation and more robust forecasts. In addition, it is expected to achieve more stable solutions and convergence applying tight coupling. Unfortunately, this approach involves considerable efforts from software developers, since the numerical solution for the system must be substantially modified from the stand-alone simulation method.

Independently of the coupling method used, the ability to perform flow assurance calculations in wellbore tubing and pipelines is required for complex fluid systems and offshore field developments. The most frequent problem faced under these scenarios is asphaltene, wax, and hydrate accretion in pipes. The usual industry approach to study solids deposition is to simulate the network stand-alone using boundary conditions provided by different sources, e.g. decline curve, material balance, reservoir simulation, among others, which does not allow to analyze the interdependence of reservoir and network. Furthermore, commercial packages offer limited capabilities for asphaltene deposition modeling in production pipelines and gathering systems.

On this research, a thermodynamically consistent integrated production system model is proposed based on a tightly-coupled approach. Reservoir and network governing

equations are solved simultaneously in a fully-implicit scheme for three-phase flow (oil, gas, and water) using a cubic equation of state (EOS) to calculate vapor/liquid equilibrium between hydrocarbon components. Subsequently, flow assurance analysis is performed on the network to calculate the potential of asphaltene precipitation through an EOS and vapor/liquid/liquid-dense equilibria (VLLE). Asphaltene transport to the pipeline wall (deposition or accretion) is then estimated through a mechanistic mathematical transport model based on asphaltene flux to the wall and empirical tuning parameters for the fraction of material that adheres to the pipe.

The proposed model was implemented in a new in-house simulator, allowing to study stand-alone reservoir and network models as well as reservoir-network integrated systems under the same platform. Multiple runs were performed to characterize asphaltene precipitation and deposition in the wellbore tubing and pipeline system for multiple production scenarios, including sensitivities on bottomhole flowing pressure, flowline temperature gradient, fluid composition, asphaltene inhibitor injection, and artificial gas-lift. In addition, reservoir-network coupled models were analyzed to assess the impact of asphaltene deposition in pipelines and remediation techniques. Resulting asphaltene precipitation and deposition calculations can be used to plan optimum flow assurance techniques, well cleanup interventions, pigging procedures, and necessary field operations leading to improved asset management strategies.

1.1 Objectives

The principal objectives of this research are to:

- Develop a robust tightly-coupled reservoir-network simulator for multi-phase compositional fluids using a rigorous thermodynamic model.
- Implement a consistent solid deposition numerical solution approach viable for asphaltene modeling in network pipelines. Formulation must be flexible for later development of additional solid deposits, e.g. hydrates and waxes.

- Study the impact of fluid composition, bottomhole pressure, network temperature profile, inhibitor injection, and artificial gas lift, on asphaltene deposition.

1.2 Definition of the Problem

Reliable modeling of oil, gas, and water flow through porous media and production pipelines has been a key objective for the oil and gas industry since its inception. Reservoir and production engineers often perform their forecasts using specialized software that does not consider mutual interactions between reservoir and network systems, leading to incomplete understanding of field operating conditions.

Integrated modeling of reservoir and network systems overcomes these limitations, enabling engineers to correctly assess the performance of production systems. The additional information generated allows making better informed decisions about development plans and asset management, often improving project effectiveness. This becomes a particularly important subject in fields that present solid deposition in the production system.

Current reservoir-network coupling techniques are classified in two main branches, loosely- and tightly-coupled formulations. Loosely-coupled formulations are used very frequently in the industry due to flexibility to simulate both, stand-alone and integrated cases using multiple software. However, equations are solved decoupled often leading to instability. On the other hand, tightly-coupled formulations are numerically robust, but do not allow flexibility in stand-alone runs and incorporating additional physics into the simulator.

This research is focused on developing a rigorous tightly-coupled reservoir-network approach to model integrated production systems. Reservoir and network will be solved fully-implicitly and simulations can be performed with stand-alone or coupled models. The application will include asphaltene modeling capabilities for network pipelines

through a sequential solution approach using a cubic EOS in VLLE calculation for asphaltene precipitation and a consistent transport equation for asphaltene deposition.

Flexibility of a sequential formulation for asphaltene precipitation and deposition will allow later development of hydrates and waxes modeling. This study also seeks modeling asphaltene inhibitor injection at bottomhole to mitigate solids deposition in pipelines and artificial gas lift impact on production performance due to asphaltene precipitation and deposition.

1.3 Relevance of the Study

Integrated production system analysis is an essential tool in oil and gas industry major capital projects. The ability to generate accurate production forecasts, plan field operations, minimize well interventions, and optimize field operating conditions, often dictates project success and profitability.

Reservoir-network coupled numerical solutions have been studied for more than four decades. Early days development on this approach was limited by deficiency in computational power. However, technology progress and improved knowledge in numerical techniques has enabled multiple implementations of coupling for black-oil and compositional fluid systems. The need for this modeling scheme is especially relevant in offshore fields and complex reservoir fluid systems (e.g. gas condensate, volatile oils, and asphaltene, hydrates, and waxes precipitation). Solid deposits can create severe blockage in pipelines and equipment, leading to operational problems and expensive cleanup procedures or equipment replacement.

Asphaltene deposition modeling with integrated production system analysis is intended to assist in the creation and application of asset management strategies to improve production performance and field operations. Production and pressure profiles can be forecasted to set better operating conditions as reservoir energy is drained. However, most commercial

software do not provide this modeling capability. Correct assessment of asphaltene buildup is used to design pressure maintenance methods, wellbore cleanup and pigging operations, and inhibitor injection. Fields with potential asphaltene precipitation problems can be evaluated for gas lift implementation, evaluating its impact on solid deposition.

1.4 Development Milestones

This section presents the general procedures and required milestones to accomplish research proposed objectives.

1. Program stand-alone reservoir and network compositional 3-phase (oil, gas, and water) simulators implementing a modified Young and Stephenson (1983) fully-implicit formulation.
2. Formulate transient reservoir and network calculations allowing fluid accumulation in gridblocks and pipe segments.
3. Code network system subroutines to allow input for explicit production pipeline temperature profiles. No heat transfer calculations are performed. Each pipe segment has a specified user-defined temperature.
4. Implement multiphase flow in pipelines based on no slippage between phases.
5. Program tightly-coupled reservoir-network simulator integrated in the same platform allowing stand-alone and coupled runs with the same base subroutines.
6. Solve phase equilibria calculations using Peng-Robinson cubic EOS with volume translation.
7. Solve VLE calculations using Newton-Raphson approach assuming no mutual dissolution between water and hydrocarbon components.
8. Develop VLLE scheme for asphaltene precipitation. Allow asphaltene component presence in liquid and solid phases only (Pedersen and Christensen 2006).
9. Implement a consistent solid transport equation to estimate asphaltene accretion to internal pipe walls.

10. Program inhibitor injection and artificial gas lift capabilities for the network system.
11. Study the effect of produced fluid composition, bottomhole pressure, network pipeline temperature profile, inhibitor injection, and artificial gas lift, on asphaltene deposition.

CHAPTER II
BACKGROUND RESEARCH

Reservoir simulation is one of the most important tools for petroleum engineers to study flow of oil, gas, and water across the porous media. Numerical simulation is used in all field development stages to assess performance, evaluate and rank production scenarios, well location, enhanced recovery processes, among other important design factors.

Multiple techniques and approaches have been developed in more than five decades to model specific problems in reservoir engineering (Rafiqul-Islam et al. 2010). Early simulators were tailored to study black-oil fluid systems, were fluid properties are only a function of pressure and phase composition was considered constant. More complex reservoir fluids, e.g. volatile oil and gas condensate, required additional thermodynamically robust calculations, which were enabled by advances in computational fluid dynamics and CPU power.

This chapter summarizes relevant information regarding compositional reservoir simulation, fluid flow in pipelines, reservoir-network coupled solution approaches, and asphaltene precipitation and deposition modeling.

2.1 Compositional Simulation

Fluids found in oil and gas reservoirs consist of mixtures of a wide variety of chemical components. Detailed description of fluid samples are obtained through gas chromatography and other laboratory experiments intended to characterize their volumetric and transport behavior. The detailed characterization contains tens or hundreds of components and computational cost of simulating such system is impractical. Fluid components are instead grouped, based on consistent criteria, into a smaller set (usually 5 to 10) of pseudo-components (Leibovici et al. 2000). Grouping criteria include mass balance, honoring physical restrictions, and ensuring predicted properties from grouped and detailed fluid descriptions are in agreement.

Several compositional simulation approaches have been developed to solve the highly non-linear behavior of the system of equations in a consistent, robust, stable, and efficient manner. The total number of unknown variables in the system are $3(number\ of\ components) + 15$ (**Table 2.1**), the expressions are solved based on constitutive equations (mass balance and momentum conservation) and auxiliary relationships (equation of state, well index, capillary pressure, viscosity, volume shift, relative permeabilities, rock compressibility, etc.). These secondary relationships are used to reduce the number of independent variables formulating a more efficient simulator.

Table 2.1—UNKNOWN VARIABLES PER GRIDBLOCK IN COMPOSITIONAL THREE-PHASE SIMULATION

Variable	Description	Number
z_i, x_i, y_i	Total and phase molar compositions	$3n_c$
p_α	Phase pressure	3
S_α	Phase saturation	3
ρ_α	Phase density	3
μ_α	Phase viscosity	3
k_α	Phase permeability	3
	$\boldsymbol{Total}$	$\boldsymbol{3n_c + 15}$

Compositional models can be divided into two fundamental methods, namely mass balance and volume balance methods. Both approaches model three-phase (oil, gas, and water) flow systems. The basic assumption that water and hydrocarbon mutual solubility is zero is made to simplify the system of equations, hence vapor/liquid equilibria (VLE) is only calculated amongst hydrocarbon components.

2.1.1 Mass Balance Method

The system of equations for this method is developed based on mass conservation of hydrocarbon components (or pseudo-components) and water. The hydraulic diffusivity equations for hydrocarbon component and water in differential form are presented in Eqs. (2.1) and (2.2).

$$\nabla \cdot \left[\vec{\vec{k}} A \left(x_i \frac{k_{ro}}{\mu_o} \nabla \Phi_o + y_i \frac{k_{rg}}{\mu_g} \nabla \Phi_g \right) \right] = V_b \frac{\partial}{\partial t} [\emptyset F_i] - \dot{n}_{i_{s/s}} \quad ; \quad i = 1 \; to \; n_c \quad \ldots\ldots (2.1)$$

$$\nabla \cdot \left[\vec{\vec{k}} A \frac{k_{rw}}{\mu_w} \nabla \Phi_w \right] = V_b \frac{\partial}{\partial t} [\emptyset W] - \dot{m}_{w_{s/s}} \quad \ldots\ldots\ldots\ldots\ldots\ldots\ldots\ldots\ldots\ldots\ldots\ldots\ldots\ldots\ldots\ldots\ldots\ldots\ldots\ldots\ldots\ldots (2.2)$$

Where,

$\vec{\vec{k}}$ is the permeability tensor

A is the area perpendicular to flow direction

x_i and y_i are liquid and vapor molar compositions of component i respectively

k_{ro}, k_{rg}, and k_{rw} are oil, gas, and water relative permeabilities

μ_o, μ_g, and μ_w are oil, gas, and water viscosities

Φ_o, Φ_g, and Φ_w are oil, gas, and water potentials

V_b is bulk rock volume

$\emptyset$ is rock porosity

F_i is number of moles of component i per unit volume

W is mass of water per unit volume

$\dot{n}_{i_{s/s}}$ is net molar rate of component i from sources and sinks

$\dot{m}_{w_{s/s}}$ is the net water mass rate from sinks and sources

n_c is the number of hydrocarbon components

Additional auxiliary equations are used to represent fluid phase behavior, porosity dependence on pressure, pore fluid saturations, well productivity/injectivity, etc. In Eq. (2.3) for fluid saturations, α indicates fluid phase (oil, gas, and water), n_p is the number of phases ($n_p = 3$ in this development), and S_o, S_g, S_w are oil, water and gas saturations correspondingly.

$$\sum_{\alpha=1}^{n_p} S_\alpha = S_o + S_g + S_w = 1 \quad \text{..... (2.3)}$$

There are multiple ways to solve the system of equations for compositional simulation by selecting different sets of primary independent and secondary variables. The most used approaches are briefly described in the following paragraphs.

Fussell and Fussell (1979) proposed a model in which n_c equations for phase equilibrium relationships and saturation constraint, i.e. summation of phase saturations equal unity, are used as primary equations. Corresponding primary variables are pressure, liquid molar fraction for hydrocarbon, and x_i or y_i (for $i = 2\ to\ n_c$, since summation of compositions equals unity); selection of liquid or vapor composition as independent variable depends on the dominant phase for the gridblock. The saturation equation is manipulated to have only pressure as independent variable, developing an IMPES (implicit in pressure and explicit in saturation) form.

Coats (1980) developed an approach using $n_c + 1$ equations corresponding to mass balance for each hydrocarbon component and water. Primary independent variables are chosen based on hydrocarbon phase existence in the cell as follows:

a. Oil and gas phases exist: pressure, S_o, S_g, and y_i, for $i = 3\ to\ n_c$
b. Only gas phase exists: pressure, S_g, and y_i, for $i = 1\ to\ n_c - 1$
c. Only oil phase exists: pressure, S_o, and x_i, for $i = 1\ to\ n_c - 1$

This method involves dynamically changing the selection of primary variables as phases appear and disappear in any given gridblock. The main advantage of this application is that mass balance equations can be easily written in terms of selected independent primary variables.

Young and Stephenson (1983) proposed a general solution based on individual phase compositions consisting of $3n_c + 4$ equations per every gridblock, which can be reduced depending on existing phases and assuming the vapor/liquid equilibrium ratios depend only on pressure and composition. The selected solution equations were water and hydrocarbon components mass balance, saturation constraint, and overall hydrocarbon balance. Independent primary variables included pressure, vapor phase molar fraction, overall hydrocarbon composition ($z_i \; for \; i = 1 \; to \; n_c - 1$), water mass per unit volume, and hydrocarbon mass per unit volume. This approach is independent of phase appearance and disappearance from gridblocks, hence change of primary variables is not required.

Several other investigators have proposed additional approaches and improvements to solving mass balance type of formulations for different applications (Abel et al. 1970; Chien et al. 1985; Coats 1982; Iranshahr et al. 2009; Nghiem et al. 1981). In general they all solve the same type of formulation with refined computational models and consistent selection of primary variables.

2.1.2 Volume Balance Method

Volume balance based method starts from a fundamentally different approach than mass balance formulations. Instead of departing from hydraulic diffusivity to describe mass transport between cells, the formulations are based on the physical principle of pore space being completely filled with fluids, hence the total pore volume of a cell must equal the summation of all phase volumes.

Since rock pore volume is only a function of pressure, assuming constant compressibility, an IMPES formulation can be developed setting the total fluid (oil, gas, and water) volume as a function of pressure and compositions. Analytical derivatives of volume with respect to pressure and compositions are calculated using different techniques. Some examples of this approach are presented by: Acs et al. (1985), Watts (1986), Wong et al. (1990), Liu (1997).

Given the IMPES nature of this method, reservoir models with drastic saturation and compositional changes, both in space and time, may present oscillations or limited time-step size, which could yield impractical simulation times.

2.2 Network Simulation

Network simulators model pressure and temperature variations in wellbore tubing and surface/subsea pipelines as oil, gas, and water are produced from the reservoir. Many commercial network simulators use explicit constant rate or pressure, inflow performance curves, or lookup tables as boundary conditions for well productivity. Pipelines are discretized into segments to perform mass, momentum, and energy balance calculations, similarly as reservoir simulators discretize the reservoir in smaller gridblock cells. The equations for each segment are usually solved, assuming steady-state flow for the given boundary conditions, applying non-linear solver techniques.

Conservation of component i and water in a pipe segment, including the accumulation term, can be expressed as follows:

$$\nabla \cdot \left[A\left(\mathcal{y}_o x_i \tilde{\rho}_o u_o + \mathcal{y}_g y_i \tilde{\rho}_g u_g\right)\right] = V_{seg}\frac{\partial}{\partial t}[F_i] - \dot{n}_{i_{s/s}} \quad ; \quad i = 1\ to\ n_c \quad \text{..... (2.4)}$$

$$\nabla \cdot [A\mathcal{y}_w \rho_w u_w] = V_{seg}\frac{\partial}{\partial t}[W] - \dot{m}_{w_{s/s}} \quad \text{..... (2.5)}$$

Where,

A is the segment connection area

$\mathcal{y}_o$, $\mathcal{y}_g$, and $\mathcal{y}_g$ are oil, gas, and water volumetric holdups

x_i and y_i are liquid and vapor molar compositions of component i respectively

$\tilde{\rho}_o$, and $\tilde{\rho}_g$ are oil and gas molar densities

ρ_w is water density

u_o, u_g, and u_g are oil, gas, and water superficial velocities

V_{seg} is segment volume

F_i is number of moles of component i per unit volume

W is mass of water per unit volume

$\dot{n}_{i_{s/s}}$ is net molar rate of component i from sources and sinks

$\dot{m}_{w_{s/s}}$ is the net water mass rate from sinks and sources

n_c is the number of hydrocarbon components

The steady-state approach assumes no fluid accumulation in the segments, hence the derivative with respect to time in Eqs. (2.4) and (2.5) are set to zero. The mechanical energy balance equation for a connection (momentum conservation ignoring heat transfer), R_p, can be described as a function of pressure (Δp), potential (Δp_{PE}), and friction (Δp_F) losses, as shown in Eqs. (2.6) through (2.9).

$$R_p = \Delta p + \Delta p_{PE} + \Delta p_F \quad \text{..... (2.6)}$$

$$\Delta p = p_{ups} - p_{downs} \quad \text{..... (2.7)}$$

$$\Delta p_{PE} = (\rho_m h)_{ups} - (\rho_m h)_{downs} \quad \text{..... (2.8)}$$

$$\Delta p_F = \frac{f_f \rho_m L u_m^2}{D} \quad \text{..... (2.9)}$$

With,

p as segment pressure

ρ_m as fluid mixture average density

h as segment height

f_f as friction factor

L as segment connection length

u_m as mixture average velocity

D as segment connection diameter

Note: Subscripts ups and $downs$ refer to upstream and downstream based on flow direction.

While steady state approach through non-linear solvers allows to study some aspects of multiphase flow and phase behavior of fluids during production, it does not properly incorporate the effects of transient flow phenomena and reservoir-network interdependence. Wylie et al. (1971) presented a formulation of transient pipeline modeling using a fully-implicit method for a simplified gas flow system. This approach was based on a centered finite-difference scheme for both time and space derivatives and allowed to simulate complex network layouts and connections with large time-step sizes.

Multiphase flow in pipelines includes complex transport and mass transfer mechanisms, challenging to model. The oil and gas industry uses semi-empirical correlations to estimate pressure drop in tubing and flowlines. Hagedorn and Brown (1965), Beggs and Brill (1973), Dukler et al. (1964), Duns and Ros (1963), Eaton et al. (1967), and Orkiszewski (1967) are among the ones used more frequently.

These correlations are based on mechanistic models and empirical laboratory observations of oil, gas, and water pipeline flow systems. The basic approach for pressure drop calculation on these methods is first predicting the flow regime in the pipe (bubble, slug, annular, stratified, wave, mist, etc.) based on phase velocities and flow regime maps. Subsequently, phase holdup, interfacial friction factor, and other properties are calculated. Finally, a pressure drop profile is calculated employing mechanistic models and previously estimated properties (Ellul et al. 2004).

2.3 Phase Equilibria Calculations

Phase equilibria calculations allow the estimation of fluid thermodynamic properties as a function of pressure, temperature, and composition. Using as example two-phase VLE, main properties of interest for reservoir and network simulation of compositional fluids are phase molar fractions (f_v and f_l), phase molar compositions (y_i and x_i), phase molecular weight (M_w^v and M_w^l), and phase molar densities ($\tilde{\rho}_v$ and $\tilde{\rho}_l$).

Fluid properties and phase fugacities in VLE calculations are based on an EOS, e.g. Peng-Robinson (PR-EOS) (Peng and Robinson 1976):

$$p = \frac{RT}{\mathcal{v} - b} - \frac{(a\alpha)}{\mathcal{v}^2 + 2\mathcal{v}b - b^2} \quad \text{..... (2.10)}$$

Or in its cubic form based on the compressibility factor, $Z = \frac{pV}{nRT}$:

$$Z^3 - (1 - B)Z^2 + (A - 3B^2 - 2B)Z - (AB - B^2 - B^3) = 0 \quad \text{..... (2.11)}$$

Thermodynamic equilibrium for a compositional fluid is reached when the phase fugacities for each component are equal, i.e. Eq. (2.12) is honored. Related to the chemical potential concept, this implies that for all components, the molecular transfer rate from liquid to vapor phase equals the molecular transfer rate from vapor to liquid phase, reaching equilibrium.

$$\hat{f}_i^l = \hat{f}_i^v \quad ; \quad i = 1 \; to \; n_c \quad \text{..... (2.12)}$$

The VLE or flash calculation can be performed using Newton-Raphson or successive substitution scheme. Appendix A details the VLE calculation procedure using PR-EOS.

2.4 Reservoir-Network Coupled Simulation

Integrated modeling of reservoir-network systems is not a new concept in the oil and gas industry. For several decades, the importance of coupled calculations has been recognized,

as it allows a better representation of the production system and more realistic forecasts. Coupled simulations enhance the understanding of well-network interactions, enables integrating multiple reservoirs and network (a condition often seen on the field), and promotes improved asset management.

Integrated models can be developed, in general, based on two different approaches loose or tight coupling. Following, a brief description of both approaches and a summary of previous work on reservoir-network coupling.

2.4.1 Loosely-Coupled Approach

Models based on loose coupling treat reservoir and network systems of equations separately, solving each system independently and then exchanging boundary conditions in an iterative process until convergence criteria are satisfied. In addition to reservoir and networks simulators, this approach requires a third software (usually called coupling controller) to manage simulation time-stepping, information exchange among simulators, and convergence evaluation.

Fig. 2.1 displays typical loosely-coupled simulation time-stepping. Coupled time-steps are performed using a fixed frequency (e.g. each simulation month), after which the reservoir stepping is solved using constant boundary conditions. A generic coupled step calculation starts with model initialization, followed by well IPR (inflow performance relationship) calculation in the reservoir simulator. The IPR is transferred, through the coupling controller, to the network simulator, which solves the network to determine the correct boundary conditions. Finally, boundary conditions are transferred back to the reservoir simulator to proceed with the solution.

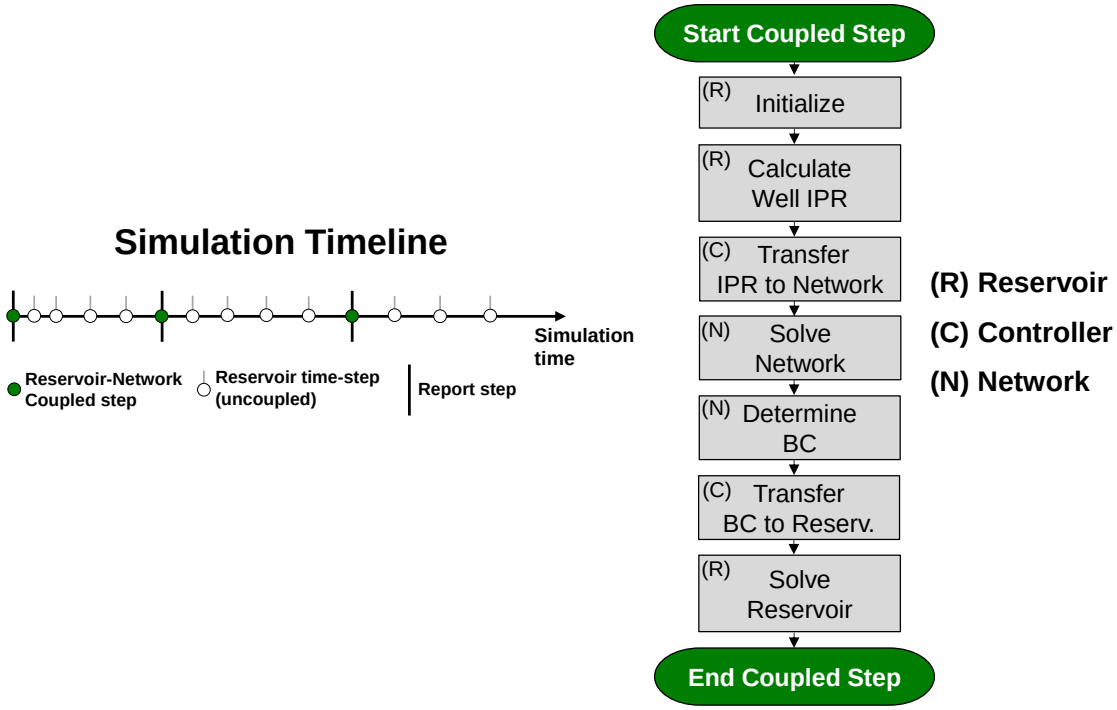

Fig. 2.1—Loosely-coupled simulation timeline and workflow. Coupled steps (green) are performed with a fixed frequency. Reservoir uncoupled steps (white) are solved with fixed network boundary conditions. Generic workflow for coupled step solution is presented on the right.

Dempsey et al. (1971) presented one of the earliest studies on reservoir-network. The loosely-coupled approach was developed for a black-oil gas field and proved a valuable tool for production forecast and engineering operations planning. The numerical technique involved a coupled global iteration scheme, which was divided into two sub-global iteration systems, one for the reservoir and one for the production network (wellbore tubing and pipelines).

This solution approach is common in the industry due to its convenience. Already existing reservoir and network simulators can be readily used to simulate coupled models, the only requirement is the development of the coupling controller. This allows reservoir and production engineers to create standalone models for specific or specialized purposes and then performing coupled runs for field studies.

However, the explicit nature of the coupled solution often leads to instability, oscillation, and even material balance errors, in models with rapid saturation changes near the wellbore region or complex fluid systems. Alternative solutions have been proposed to improve these cases. For example, implementing an iteratively-lagged solution, in which the coupled steps are performed at the Newton iteration level (**Fig. 2.2**). A fixed number of iterations is selected such that well conditions are relatively stable while boundary conditions are calculated.

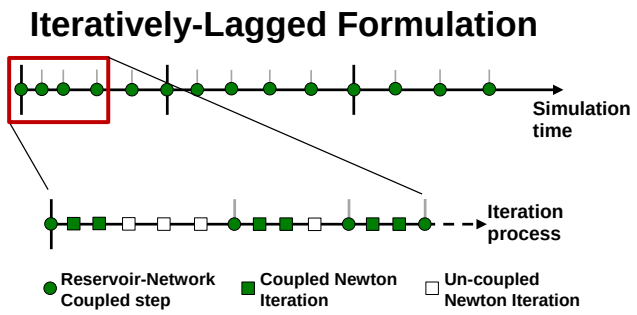

Fig. 2.2—Loosely-coupled simulation with iteratively-lagged formulation timeline. Coupled steps are performed on the Newton level for a fixed number of iterations.

Loosely-coupled simulations have also been expanded for multi-phase black-oil and compositional fluids (Al-Mutairi et al. 2010; Ghorayeb et al. 2003; Ghorayeb et al. 2008; Guyaguler et al. 2011). Additional innovative techniques to improve loosely-coupled simulations stability have been developed. Guyagüler et al. (2011) proposed a novel numerical technique by creating regions around wells and performing smaller simulations to calculate well IPR curves, leading to more consistent results.

2.4.2 Tightly-Coupled Approach

The tightly-coupled model takes advantage of advanced numerical methods and computer power to solve reservoir and network systems of equations simultaneously. This approach ensures mass conservation and allows larger time-steps without incurring in solution oscillations.

Multiple studies on black-oil fluids demonstrate the value of the tightly-coupled formulation. Litvak and Darlow (1995), Byers (2000), and Jiang (2007), among others, developed stable and functional integrated simulation using fully-implicit and adaptive-implicit approaches to accelerate simulation times. They also explored the use of pre-conditioners to solve the large system of equations resulting from coupled models. Coupling multiple reservoirs in a single production network also proved of importance, for both offshore and onshore fields, allowing optimization of the production system (Coats et al. 2003; Killough et al. 2013).

Surface facilities process simulations often require a detailed compositional description (>15 components) to properly model fluid flow and chemical reactions. Such a large number of components is restrictive for reservoir simulation given the large system of equations and associated computational time. Lumping and delumping schemes can be implemented in a fully-implicit formulation to allow fit-for-purpose reservoir and network fluid characterizations (Fleming and Wong 2013). This approach allows the reservoir to have a sufficient number of components for the required description of flow through porous media and a more detailed description for pipeline flow.

Field forecasts often are performed for several decades and simulation time-steps are large to reduce computational time. Usually, fluid throughput in the network for a large time-step is much greater than the fluid volume the network pipeline system can accumulate, in other terms, the residence time is very small. Most of previous studies assume steady-state network calculations (no fluid accumulation in pipes); this approach is convenient for long forecasts and large time-steps. However, it does not allow to analyze transient behavior during well startup and shutin. Implementation of a transient network formulation accounts for fluid accumulation in pipe segments when well operating conditions are changed.

2.5 Asphaltene Phase Behavior

Asphaltene deposition in porous media, pipelines, and equipment can negatively impact production performance, reducing permeability in the nearwellbore region and decreasing diameter size of pipes and equipment, causing additional pressure drops in the system. Components of petroleum reservoir fluids can be classified into four groups (Pedersen and Christensen 2006):

- Paraffins: Formed by chains of hydrocarbons connected by single bonds. Paraffins are often called alkenes.
- Naphtenes: Hydrocarbons connected by single bonds forming cyclic structures.
- Aromatics: Cyclic structures connected by aromatic double bonds.
- Asphaltenes and resins: Large and dense molecules composed of carbon and hydrogen with smaller contents of heteroatoms (sulfur, nitrogen, oxygen, etc.) and metallic components (e.g. mercury).

Distinction between asphaltene and resins is usually based on solubility properties at room temperature. Asphaltenes are insoluble in n-pentane and n-heptane, and are soluble in benzene and toluene. Resins are practically insoluble in propane. Physical and chemical description of these molecules is complex as they are not pure substances.

Asphaltene phase behavior describes the precipitation process from petroleum fluids under a defined pressure, temperature, and composition state. Precipitation mechanisms can be divided in two main theories for asphaltene stabilization, lyophobic and lyophilic (Li and Firoozabadi 2010b).

The lyophobic theory assumes asphaltene is insoluble in the oil mixture and it is stabilized by resins in its interface. Asphaltene precipitates due to resin desorption, which is a function of fluid state. The live oil can be characterized in two parts, asphaltic component with high boiling point and the rest of components in the crude oil that maintain asphaltene

solid particles in suspension (Civan 2000). This theory can be developed using the colloidal formulation (Leontaritis and Mansoori 1987) or the micellization approach (Pan and Firoozabadi 2000a).

The lyophilic theory models asphaltene precipitation based on solubility properties of asphaltene particles in live oil. Asphaltene is considered to be dissolved in the oil phase while onset precipitation state (pressure, temperature, and composition) is not reached. If precipitation conditions are found, asphaltene phase equilibrium can be evaluated through a variety of approaches, as following described.

2.5.1 Perturbed Chain Form of the Statistical Fluid Theory (PC-SAFT)

This approach uses nonpolar van der Waals interactions as fundamental mechanism for asphaltene phase behavior. Molecules are described as chain of bonded spheres of definite size, which dictates attraction forces between molecule groups (Gonzalez et al. 2007; Vargas et al. 2009). Downstream processes frequently use this method for its ability to predict interactions between molecules of different sizes. Nonetheless, Yan et al. (2011) mentioned that advanced fluid laboratory data is required to characterize heavy fractions and computational time of this formulation is expensive.

2.5.2 Cubic Plus Association EOS (CPA-EOS)

CPA-EOS associates conventional cubic EOS with statistical fluid theory (Li and Firoozabadi 2010a). Component characterization is performed with critical properties, analogous to conventional cubic EOS, and all component can be present in all phases (vapor, liquid, and solid). The final EOS is comprised of two parts, physical and association. The physical part is represented with the cubic EOS to model short-range repulsion and attractive forces, while the association term represents the polar/polar interactions for asphaltene and resin components. The association term is derived from the PC-SAFT approach, as has similar limitations in term of computational requirements and advanced laboratory fluid analyses.

2.5.3 Cubic EOS VLSE (Vapor/Liquid/Solid Equilibrium)

Formulated through vapor/liquid/solid equilibria calculations, this is the most common model used in reservoir simulators. The heavy fraction is split into a nonprecipitating heavy fraction and a precipitating fraction for solid asphaltene. Both fractions share same component description and critical properties. However, precipitating component has larger binary interaction coefficient (BIC) with light components.

Liquid and vapor fugacities are calculated with a cubic EOS and the solid fugacity is calculated as a function of pressure, temperature, asphaltene molar volume, and a reference solid fugacity at a predefined reference pressure (Gupta 1986; Thomas et al. 1992). Reference solid molar volume and fugacity must be defined at the reference pressure from laboratory experiments, which are difficult and costly.

2.5.4 Cubic EOS VLLE (Vapor/Liquid/Liquid-Dense Equilibrium)

The VLLE approach is based on a three-phase flash calculation assuming asphaltene component can be present dissolved in the liquid phase or precipitate as a liquid-dense phase. Computational time is reduced by treating the asphaltene liquid-dense phase as a pure component, in other works, precipitate phase only contains asphaltene (Pedersen and Christensen 2006). The heavy fraction may be split into a nonprecipitating component and a precipitating component (asphaltene). Both components are characterized by distinct critical properties and BIC.

Consistency in this model is provided by the rigorous three-phase flash performed using a cubic EOS, honoring thermodynamic principles. Gonzalez (2013) successfully implemented VLLE calculations for asphaltene modeling in petroleum reservoirs, demonstrating consistent and robust application of this method. Also, required computational time is drastically reduced in comparison with other methods.

2.6 Asphaltene Deposition in Pipelines

Thermodynamic state (pressure, temperature, and composition) of produced fluid in the pipeline system determines asphaltene precipitation as solid particles into the flow stream. Asphaltene deposition, or accretion, is the transport process of precipitated asphaltene from bulk fluid flow to the internal pipeline wall. Ignoring electrokinetic forces, deposition is dependent on three transport mechanisms: diffusion, inertia, and impaction. Dominant mechanism is selected based on flow velocity, pipe properties, fluid density and viscosity, asphaltene particle density and diameter, and the calculation of a transport coefficient. (Kern and Seaton 1959; Papavergos and Hedley 1984; Watkinson 1968)

Other approaches to model asphaltene deposition in pipelines have been developed assuming additional transport mechanisms, e.g. temperature gradient from center of the pipe to the wall considering heat transfer (Ramirez-Jaramillo et al. 2006). This model was developed for production networks using an iterative sequential method to calculate asphaltene layer thickness and pipe elongation due to temperature effects, considering internal pipe wall roughness change after asphaltene deposition.

Shirdel (2013) also studied asphaltene deposition in the production system through reservoir-network coupling. In this model, asphaltene can precipitate and deposit in reservoir rock pores and in network pipelines. A fully-implicit tightly-coupled formulation was developed, creating a robust numerical solution. However, the formed system of equations drastically increments in size when considering asphaltene deposition. Moreover, the formulation is not flexible to allow easy implementation of solids modeling other than asphaltene (e.g. hydrates or waxes). Independent variables for asphaltene calculation are fixed, making implementation of other models cumbersome.

An additional relevant phenomenon to study in flow assurance applications is asphaltene precipitation chemical inhibition. Pan and Firoozabadi (2000b) presented a thermodynamic model to quantify the effect of solvents (toluene and benzene) on

asphaltene precipitation. Chemical injection is a fundamental component of several producing fields to control solid deposition in pipelines and equipment.

2.7 Selection of Mathematical Formulation

Coupled simulation of reservoir-network systems with asphaltene modeling in pipelines involves multiple areas of knowledge for transport phenomena and phase behavior in porous media and production pipes. Representation in the production system through mathematical models was performed applying the following methods and assumptions:

a. Reservoir and network simulators are compositional 3-phase (oil, gas, and water) simulators implementing a modified Young and Stephenson (1983) fully-implicit formulation.
b. Reservoir and network calculations are performed through transient formulation to allow fluid accumulation in gridblocks and pipe segments.
c. Production network pipeline temperature profiles are explicitly specified. No heat transfer calculations are performed. Each pipe segment has a specified user-defined temperature.
d. Multiphase flow in pipelines based on no-slippage condition between phases.
e. Reservoir-network integrated simulator is developed using a tightly-coupled formulation. Stand-alone and coupled runs use same subroutine platform for calculations.
f. Phase equilibria calculations use three-parameter Peng-Robinson (PR) cubic EOS (with volume translation).
g. VLE calculations solved through Newton-Raphson approach assuming no mutual solubility between water and hydrocarbon components.
h. VLLE scheme for asphaltene precipitation modeling assumes asphaltene component presence in hydrocarbon liquid and liquid-dense phases only (Pedersen and Christensen 2006).

i. Solid transport equation to estimate asphaltene accretion to internal pipe walls is based on a mechanistic semi-empirical model (Kern and Seaton 1959; Papavergos and Hedley 1984). No asphaltene removal from wall as a function of shear forces is considered.
j. Asphaltene inhibitors are characterized by their critical properties and modeled using VLLE calculations with PR-EOS.
k. Artificial gas lift is performed by adding a source of compositional fluid injection at wellbore bottom. Gas-lift composition is user-defined.

CHAPTER III
RESERVOIR SIMULATOR FORMULATION

Numerical simulation is one of the most used technologies to study complex transport phenomena during production of oil, gas, and water from hydrocarbon-bearing reservoirs. Simulators are based on mass, momentum, and energy conservation laws, implemented in numerical formulations aimed to model pressure drop and phase behavior of fluids as they move through rock porous media. This chapter details the formulation of equations used in this study to develop the fully-implicit compositional reservoir simulator. The simulator was coded in MATLAB®.

3.1 Formulation Assumptions

The development of numerical reservoir simulator in this study is based on the following statements and assumptions:

- Finite differences spatial and time discretization.
- Block-centered grid geometry.
- Isothermal reservoir system.
- Equilibrium for each time-step is instantaneous.
- Darcy's law governs fluid flow mechanisms in porous media.
- Three-phase (oil, gas, and water) flow in porous media.
- Thermodynamic equilibrium of hydrocarbon components is represented by vapor/liquid equilibria (VLE) using Peng-Robinson equation of state (PR-EOS) with volume translation.
- There is no mutual dissolution between water and hydrocarbon components in VLE calculations.
- No-flow reservoir boundaries.
- Well productivity/injectivity is described by Peaceman's model.
- Rock has small and constant compressibility. Rock is immobile.
- No component chemical reactions or adsorption are considered.

- Multiphase flow in multi-segmented wells (MSW) is based on no-slippage condition between phases.
- MSW temperature profiles are explicitly defined. No heat transfer is calculated.

3.2 Fluid Flow in Porous Media

Governing or constitutive equations of multi-phase flow in porous media are derived from continuity equation (mass balance) and transport equation (momentum conservation). Auxiliary relationships (e.g. equation of state, relative permeability saturation functions, capillary pressure, well index, viscosity, rock and water compressibility) complement the expressions necessary to form a consistent system of equations.

3.2.1 The Continuity Equation

The continuity equation describes mass conservation as the relationship between inflow, outflow, and accumulation of material in a closed system, shown in Eq. (3.1). Accumulation is represented as the density change as a function of time ($\partial\rho/\partial t$), mass inflow and outflow in the control volume is given by the divergence of fluid density and velocity ($\nabla \cdot (\rho\vec{V})$), and $\dot{m}_{Vs/s}$ is the net mass rate from sinks and sources per unit volume.

$$\frac{\partial \rho}{\partial t} + \nabla \cdot (\rho\vec{V}) + \dot{m}_{Vs/s} = 0 \quad \text{..... (3.1)}$$

For convenience in compositional simulation, the previous equation can be also expressed for component moles conservation, see Eq. (3.2). The relationship between mass and moles of a substance is given by the molecular weight.

$$\frac{\partial \tilde{\rho}_i}{\partial t} + \nabla \cdot (\tilde{\rho}_i\vec{V}) + \dot{n}_{i_{Vs/s}} = 0 \quad \text{..... (3.2)}$$

Where,

ρ is fluid density, [lb/ft^3]

$\tilde{\rho}_i$ is molar density of component i ($\tilde{\rho}_i = \phi\left[x_i\tilde{\rho}_o S_o + y_i\tilde{\rho}_g S_g\right] = \phi F_i$), [lbmol/ft^3]

t is time, day

$\vec{V}$ is fluid velocity, [ft/day]

$\dot{m}_{Vs/s}$ is the net mass rate per unit volume from sinks and sources , [lb/day/ft^3]

$\dot{n}_{i_{Vs/s}}$ is net molar rate of component i per unit volume from sources and sinks, [lbmol/day/ft^3]

3.2.2 Transport Equation

The transport equation, or momentum conservation, used to describe pressure drop as fluid moves through the porous media is Darcy's law (Darcy 1856). Darcy fluid velocity is a function of fluid properties, rock permeability, and pressure potential. Eq. (3.3) displays the expression for velocity of phase α.

$$\vec{u}_\alpha = -\beta_c \frac{k_{r\alpha}}{\mu_\alpha} \vec{\vec{k}} (\nabla \Phi_\alpha) \quad \text{..... (3.3)}$$

With,

$\vec{u}_\alpha$ as Darcy velocity of phase α, [ft/day]

$k_{r\alpha}$ as relative permeability of phase α, [dimensionless]

μ_α as viscosity of phase α, [cP]

$\vec{\vec{k}}$ as rock permeability tensor, [mD]

Φ_α as potential of phase α, [psia]

$\beta_c = 0.00633$ as the conversion constant for field units

3.2.3 Water Hydraulic Diffusivity Equation

The differential form of the equation describing water flow in porous media is obtained by replacing Darcy's phase velocity, Eq. (3.3), into the continuity equation, Eq. (3.1), yielding:

$$\nabla \cdot \left[\beta_c \vec{\vec{k}} A \frac{k_{rw}}{\mu_w} \nabla \Phi_w \right] = V_b \frac{\partial}{\partial t} [\phi W] + \rho_w q_{w_{s/s}} \quad \text{..... (3.4)}$$

Where,

A is area perpendicular to flow direction, [ft^2]

V_b is gridblock rock bulk volume, [ft^3]

ϕ is rock porosity, [ft^3/ft^3]

W is mass of water per unit pore volume, [lb/ft^3]

$q_{w_{s/s}}$ is volumetric water rate from a well, [ft^3/day]

3.2.4 Hydrocarbon Components Hydraulic Diffusivity Equation

The differential form of the equation describing component flow in porous media is obtained by replacing Darcy's phase velocity, Eq. (3.3), into the moles conservation equation, shown in Eq. (3.2).

$$\nabla \cdot \left[\beta_c \vec{\vec{k}} A \left(x_i \frac{k_{ro}}{\mu_o} \nabla \Phi_o + y_i \frac{k_{rg}}{\mu_g} \nabla \Phi_g \right)\right] = V_b \frac{\partial}{\partial t}[\phi F_i] + \dot{n}_{i_{s/s}} \quad ; \quad i = 1 \; to \; n_c \quad \text{..... (3.5)}$$

Where,

x_i and y_i are liquid and vapor molar compositions of component i, [lbmol/lbmol]

F_i is number of moles of component i per unit pore volume, [lbmol/ft^3]

$\dot{n}_{i_{s/s}}$ is molar rate of component i from a well, [lbmol/day]

n_c is the number of hydrocarbon components (or pseudocomponents)

3.3 Equation of State

Fluid properties as a function of pressure, temperature, and composition are calculated from an equation of state (EOS). PR-EOS (Peng and Robinson 1976) is used to perform VLE calculations on hydrocarbon fluid properties in this study (shown below). Appendix A details the use of this approach to calculate equilibrium between liquid (oil) and vapor (gas) phases for a compositional fluid.

$$p = \frac{RT}{v - b} - \frac{(a\alpha)}{v^2 + 2vb - b^2} \quad \text{..... (3.6)}$$

Using pressure, temperature, and overall fluid composition as input, VLE provides phase molar fraction (f_α), phase molar compositions (x_i^α), and phase compressibility factor (Z_α). Fluid phase physical properties are then calculated from fundamental expressions:

$$M_w^\alpha = \sum_{i=1}^{n_c} x_i^\alpha M_{w_i} \quad \text{..... (3.7)}$$

$$\tilde{\rho}_\alpha = \frac{p}{Z_\alpha RT} \quad \text{..... (3.8)}$$

$$\upsilon_\alpha = \frac{1}{\tilde{\rho}_\alpha} \quad \text{..... (3.9)}$$

$$\upsilon = (1 - f_v)\upsilon_l + f_v\upsilon_v \quad \text{..... (3.10)}$$

Where,

M_w^α is the molecular weight of phase α, [lb/lbmol]

M_{w_i} is the molecular weight of component i, [lb/lbmol]

$\tilde{\rho}_\alpha$ is molar density of phase α, [lbmol/ft^3]

υ_α is molar volume of phase α, [ft^3/lbmol]

υ is fluid overall molar volume, [ft^3/lbmol]

T is absolute temperature, [R]

$R = 10.7316$ is the gas constant for field units, [psia.ft^3/R/lbmol]

Water physical properties are calculated assuming small and constant compressibility (McCain 1990). Water density and viscosity are input in tables as a function of pressure.

3.4 Selection of Reservoir Independent Variables

The system of equations developed in this study is based on moles/mass conservation of hydrocarbon components (or pseudo-components) and water. Selection of independent variables follows a modified Young and Stephenson (1983) formulation.

The system consists of $2n_c + 3$ independent variables for each reservoir model gridblock, see **Table 3.1**. The main advantage of this system is its independence from hydrocarbon phase existence in the gridblock, i.e. independent variables do not have to be changed as any particular hydrocarbon phase appears or disappears under reservoir dynamic conditions.

Table 3.1—INDEPENDENT VARIABLES FOR RESERVOIR GRIDBLOCK SYSTEM OF EQUATIONS

Variable	Description	Number
lnK_i	Natural logarithm of equilibrium ratio	n_c
p_o	Oil-phase pressure	1
F_i	Moles of component i per pore volume	n_c
W	Mass of water per pore volume	1
f_v	Vapor molar fraction	1
	Total	$\boldsymbol{2n_c + 3}$

Notice that these independent variables are represented by $2n_c + 3$ residual equations per gridblock, the additional $n_c + 12$ variables and equations required to complete the solution system of $3n_c + 15$ variables (introduced previously in Table 2.1) are developed applying auxiliary, or secondary, equations presented later in this chapter.

3.5 Reservoir Residual Equations

Residual form for hydraulic diffusivity equations of water and hydrocarbon components is obtained through finite difference approximation of partial differential equations presented previously. Residual equations for fluid phase behavior are developed from VLE calculations using PR-EOS. An additional residual, the saturation or volume constraint equation, ensures the pore volume is exactly filled by fluid phases with correct

saturations. Appendix A shows required steps to calculate VLE with PR-EOS. Appendix B details the discretization process for water and hydrocarbon components equations.

3.5.1 Hydraulic Diffusivity Equations (Water and Hydrocarbon Component)

Reservoir properties usually have significant lateral and vertical variations as a results of sedimentation and diagenesis processes. Characterization of reservoir petrophysical and fluid properties is performed by geoscientists and engineers, providing distribution maps of porosity, permeability, water saturation, fluid composition, among other properties, used in reservoir numerical models. The analytical differential expression for hydraulic diffusivity is discretized in space and time, enabling modeling heterogeneous and highly complex reservoir models.

Central difference is used for the 3-dimensional space discretization of convective flow terms in Eqs. (3.4) and (3.5) (refer to Appendix B for details). Applying block-centered geometry, each discretized element (gridblock) has constant properties and 6 possible flux surfaces (North, South, East, West, Bottom, and Top), as shown on **Fig. 3.1**. Following the continuity equation convention, flux leaving the gridblock is considered positive, and flux entering is negative.

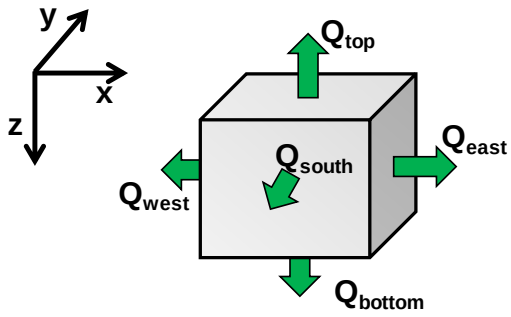

Fig. 3.1—Flux calculation for a gridblock. Flow across the face leaving the cell is calculated as positive and flow entering the cell is negative following this convention.

Time discretization is performed applying backward difference on the accumulation terms of Eqs. (3.4) and (3.5) (see details in Appendix B). This implementation yields a fully-implicit formulation for the system of equations, where all coefficients are calculated at the new time level $n+1$.

Eqs. (3.11) and (3.12) present the residual equations for water and hydrocarbon component hydraulic diffusivity in porous media after discretization.

$$R_w = \frac{V_b}{\Delta t}\left[W^n \phi'(p_{oC}^{n+1} - p_{oC}^n) + \phi^{n+1}(W^{n+1} - W^n)\right] - \sum_{\eta=1}^{6}\left[a_{w\eta}^{n+1}\left(\Delta p_{o\eta}^{n+1} - \gamma_{w\eta}^{n+1}\Delta z_\eta\right) - \frac{a_{w\eta}^{n+1} p_{cow_\eta}^{\prime\,(n+1)}}{\rho_{w\eta}^{n+1}}\Delta W_\eta^{n+1}\right] + WI_w^{n+1}\left(p_{oC}^{n+1} - p_{cow}^{n+1} - p_{wf}^{n+1}\right) \quad \text{..... (3.11)}$$

$$R_i = \frac{V_b}{\Delta t}\left[F_i^n \phi'(p_{oC}^{n+1} - p_{oC}^n) + \phi^{n+1}(F_i^{n+1} - F_i^n)\right] - \sum_{\eta=1}^{6}\left[a_{o\eta}^{n+1} x_i^{n+1}\left(\Delta p_{o\eta} - \gamma_{o\eta}^{n+1}\Delta z_\eta\right)\right] - \sum_{\eta=1}^{6}\left[a_{g\eta}^{n+1} y_i^{n+1}\left(\Delta p_{o\eta} - \gamma_{g\eta}^{n+1}\Delta z_\eta\right)\right] - \sum_{\eta=1}^{6}\left[\left(a_{g\eta} y_i p'_{cgo_\eta} S'_{g_\eta}\right)^{n+1}\Delta F_i\right] + WI_o^{n+1} x_i^{n+1}\left(p_{oC}^{n+1} - p_{wf}^{n+1}\right) + WI_g^{n+1} y_i^{n+1}\left(p_{oC}^{n+1} + p_{cgo}^{n+1} - p_{wf}^{n+1}\right) \quad \text{..... (3.12)}$$

Where,

R_w is water residual, [lb/day]

R_i is hydrocarbon component i residual, [lbmol/day]

Δt is the time-step size, [day]

ϕ' is porosity time chord-slope, [1/psi]

p_o is oil phase pressure, [psia]

$a_{\alpha\eta}$ is phase α transmissibility between central and neighbor η gridblocks, [lbmol/day/psi]

p_c' is capillary pressure spatial chord-slope, [psi]

S_g' is gas saturation spatial chord-slope, [fraction]

WI_α is phase α well index, [lbmol/day/psi]

p_{wf} is well flowing pressure at connecting gridblock center depth, [psia]

Superscripts n and $n+1$ indicate time level

Phase transmissibility (denoted by subscript α) results as the product of interblock geometric transmissibility T_η from Eq. (B.4), and phase mobility $\lambda_{\alpha\eta}$, which is a function of upstream phase relative permeability and interblock fluid properties. The following expression depicts phase transmissibility calculation between central gridblock and its neighbor in the η-direction.

$$a_{\alpha\eta} = T_\eta \lambda_{\alpha\eta} = T_\eta \left(k_{r\alpha} \frac{\tilde{\rho}_\alpha}{\mu_\alpha} \right)_\eta \quad for\ \eta = E, W, N, S, B, T \quad \text{..... (3.13)}$$

Spatial chord-slope of capillary pressure is calculated with respect to corresponding phase saturation (water for p'_{cow} and gas for p'_{cgo}), while saturation chord-slopes are performed with respect F_i. The following equation displays an example for gas-oil capillary pressure chord-slope between central gridblock (subscript C) and its neighbor (subscript η)

$$p'_{cgo_\eta} = \frac{p_{cgo_\eta} - p_{cgo_C}}{S_{g_\eta} - S_{g_C}} \quad \text{..... (3.14)}$$

3.5.2 Phase Equilibria Equations (Hydrocarbon Liquid and Vapor)

VLE residual equations are comprised of two fundamental concepts, component phase fugacity and molar vapor fraction equilibrium. Appendix A details the flash calculation process for compositional VLE.

Component fugacity residual is expressed as a function of component equilibrium ratio K_i, vapor fugacity coefficient $\hat{\varphi}_i^v$, and liquid fugacity coefficient $\hat{\varphi}_i^l$. Equilibrium is reached when R_{fug_i} (and R_{RR}) equals zero for all components, meaning that chemical potentials and fugacities of all components in vapor and liquid phases are balanced.

$$R_{fug_i} = lnK_i + ln\hat{\varphi}_i^v - \hat{\varphi}_i^l \quad ; \quad i = 1\ to\ n_c \quad \text{..... (3.15)}$$

Correct molar vapor fraction is assured by the Rachford-Rice (1952) residual in Eq. (3.16). This function is continuous and monotonic, avoiding trivial or local minima/maxima solutions, ideal for numerical applications.

$$R_{RR} = \sum_{i=1}^{n_c} \frac{z_i(K_i - 1)}{1 + f_v(K_i - 1)} \quad \text{..... (3.16)}$$

3.5.3 Saturation Constraint Equation

Fluids (oil, gas, and water) must entirely fill the available pore space in the rock, which is a function of pore pressure. The saturation, or volume, constrain residual, shown in Eq. (3.17), guarantees honoring this physical constraint, ensuring phase saturations add to unity and pore space is completely occupied by fluids.

$$R_{sat} = F\left[\frac{1 - f_v}{\tilde{\rho}_o} + \frac{f_v}{\tilde{\rho}_g}\right] + \frac{W}{\rho_w} - 1 \quad \text{..... (3.17)}$$

In the previous expression, F represents hydrocarbon moles per unit pore volume in the gridblock, calculated from hydrocarbon phases saturations and molar densities.

$$F = \tilde{\rho}_o S_o + \tilde{\rho}_g S_g \quad \text{..... (3.18)}$$

3.6 Auxiliary Equations

Constitutive equations form the main system solution; however, auxiliary (or secondary) equations are required to complement the solution. These additional relationships lead to more robust results and decrease the number of variables in the non-linear iterative process, reducing computational cost. The auxiliary equations presented next are jointly used with constitutive equations to create the fully-implicit numerical system solution.

3.6.1 Peaceman's Model (Well Treatment)

Fluid flow between well completions and reservoir gridblocks is represented by the well index, calculated with Peaceman's model (Peaceman 1978, 1983, 1990). The well index, similar to interblock transmissibility, consists of a geometric component WI_{geom} and a dynamic phase mobility component $\lambda_{\alpha C}$ for the gridblock in which the well is perforated.

$$WI_\alpha = WI_{geom}\lambda_{\alpha C} \quad \text{..... (3.19)}$$

The geometric component depends on static properties, hence it is constant. Eq. (3.20) presents the geometric well index calculation for a vertical well. Notice that other well geometries, i.e. horizontal wells, can be represented with this formulation by updating the appropriate spatial variables depending on well orientation.

$$WI_{geom} = 2\pi\beta_c \frac{\Delta z\sqrt{k_x k_y}}{ln\left(\frac{r_o}{r_w}\right) + S} \quad \text{..... (3.20)}$$

With,

$$r_o = 0.28 \frac{\left(\Delta x^2\sqrt{k_y/k_x} + \Delta y^2\sqrt{k_x/k_y}\right)^{1/2}}{\sqrt[4]{k_y/k_x} + \sqrt[4]{k_x/k_y}} \quad \text{..... (3.21)}$$

Where,

$\Delta x, \Delta y, \Delta z$ are gridblock dimensions, [ft]

k_x, k_y, k_z are permeability in each coordinate direction, [mD]

r_w is wellbore radius, [ft]

S is well skin, [dimensionless]

Producer wells phase mobility is calculated based on fluid properties and relative permeability of perforated gridblock, as shown in Eq. (3.22). For injection wells, injected phase mobility is calculated using the total fluid mobility (Schlumberger 2014).

$$\lambda_{\alpha C_{Producer}} = \left(k_{r\alpha}\frac{\tilde{\rho}_\alpha}{\mu_\alpha}\right)_C \quad \text{..... (3.22)}$$

$$\lambda_{\alpha C_{Injector}} = \left(\frac{k_{ro}}{\mu_o} + \frac{k_{rg}}{\mu_g} + \frac{k_{rw}}{\mu_w}\right)_C \tilde{\rho}_{\alpha C} \quad \text{..... (3.23)}$$

Finally, well water mass rate and hydrocarbon component molar rate for each gridblock well connection can be calculated from the following expressions:

$$\dot{m}_{w_{s/s}} = \rho_w \, q_{w_{s/s}} = WI_w\left(p_{oC} - p_{cow} - p_{wf}\right) \quad \text{..... (3.24)}$$

$$\dot{n}_{i_{s/s}} = WI_o x_i (p_{oC} - p_{wf}) + WI_g y_i \left(p_{oC} + p_{cgo} - p_{wf}\right) \quad \text{..... (3.25)}$$

3.6.2 Capillary Pressure

Capillary pressure describes the difference in pressure at the interface of two immiscible fluids, a wetting phase p_{wet} and a non-wetting phase p_{nwet}.

$$p_c = p_{nwet} - p_{wet} \quad \text{..... (3.26)}$$

In oil-water systems, water is usually considered the wetting phase. While in two-phase systems containing gas, gas is always considered the non-wetting phase. Since the purpose of using capillary pressures as auxiliary equations is to express oil pressure as independent variable, the following equations for oil-water and gas-oil capillary pressures can be applied.

$$\begin{aligned} p_{cow} &= p_o - p_w \\ p_{cgo} &= p_g - p_o \end{aligned} \quad \text{..... (3.27)}$$

3.6.3 Phase Potential

Phase potential Φ_α is defined by the pressure and gravitational forces acting on the fluid.

$$\Phi_\alpha = p_\alpha - \gamma_\alpha z = p_\alpha - g_c \rho_\alpha z \quad \text{..... (3.28)}$$

Where,

p_α is pressure of phase α, [psia]

ρ_α is density of phase α, [lb/ft^3]

z is depth, [ft]

g_c is the gravity constant

Interblock phase potential calculation between central and neighbor gridblocks (subscripts C and η respectively) must be calculated consistently. Eq. (3.29) presents an example of this calculation for water, including capillary pressure.

$$\begin{aligned} \Delta\Phi_{w\eta} &= \left(\Phi_{w\eta} - \Phi_{wC}\right) = \Delta p_{o\eta} - \Delta p_{cow_\eta} - \gamma_{w\eta}\Delta z_\eta \\ \Delta\Phi_{w\eta} &= \left(p_{o\eta} - p_{oC}\right) - \left(p_{cow_\eta} - p_{cow_C}\right) - g_c\left(\frac{\rho_{w\eta} + \rho_{wC}}{2}\right)\left(z_\eta - z_C\right) \end{aligned} \quad \text{..... (3.29)}$$

3.6.4 Relative Permeability (Saturation Functions)

Relative permeabilities are used in multiphase flow in porous media, as a dimensionless measure of the effective permeability of a phase in the presence of other phases. Numerically, is the ratio of phase effective permeability to absolute permeability.

For oil, gas, and water flow in porous media, relative permeability curves for each phase are created from laboratory tests as saturation functions. Laboratory experiments can be interpreted using multiple methods, Stone II (Stone 1973) is used on this study. This method assumes gas relative permeability is only a function of gas saturation and water relative permeability is only a function of water saturations, both independent of oil saturation. Oil relative permeability is then calculated as a function of absolute permeability, and gas and water relative permeabilities.

Stone did not specify the base for relative permeability calculation, i.e. absolute permeability to single phase or oil effective permeability at connate water saturation should be use as base for relative permeability ratio. Aziz and Settari (1979) proposed the use of connate water saturation as reference value and the expression below.

$$k_{ro} = k_{rocw}\left[\left(\frac{k_{row}}{k_{rocw}} + k_{rw}\right)\left(\frac{k_{rog}}{k_{rocw}} + k_{rg}\right) - k_{rw} - k_{rg}\right] \quad \text{..... (3.30)}$$

Where,

k_{ro} is oil relative permeability, $k_{ro}(S_w, S_g)$

k_{rocw} is oil relative permeability at connate water saturation, $k_{row}(S_o = 1 - S_{wc})$

k_{row} is oil relative permeability at actual water saturation, $k_{row}(S_o = 1 - S_w)$

k_{rog} is oil relative permeability at actual gas saturation and connate water saturation, $k_{rog}(S_o = 1 - S_g - S_{wc})$

k_{rw} is water relative permeability at actual water saturation, $k_{rw}(S_w)$

k_{rg} is gas relative permeability at actual gas saturation, $k_{rg}(S_g)$

Note that k_{ro} from previous equation can be negative, in which case it must be set to zero.

3.6.5 Rock Compressibility

Pore volume PV depends on overburden and fluid pore pressure. As pore pressure decreases, rock matrix expands causing the available pore volume to reduce. Conversely, when pressure increases, the pore volume increases accordingly. Both effects can be described with isothermal rock compressibility (Dake 1978).

$$PV|_p = PV|_{ref} \times e^{-c_{rock}(p_{ref}-p)} \quad \text{..... (3.31)}$$

The previous equation results from the integration of the isothermal compressibility. Note that the direct solution of this differential equation assumes constant compressibility for the range of pressures used, between p_{ref} and p.

$$c = -\frac{1}{V}\frac{\partial V}{\partial p}\bigg|_T \quad \text{..... (3.32)}$$

3.6.6 Volume Translation

Hydrocarbon phase volumetric properties (e.g. density, molar volume, etc.) are obtained from fundamental EOS definitions after VLE calculations have been performed. Often, calculated values do not match laboratory measurements and a correction is required. Improved volumetric properties estimation can be obtained by applying a volume translation method (Péneloux et al. 1982).

The volume translation method only corrects volumetric properties, it does not modify VLE calculations, making its application very practical and robust. The correction is performed by implementing a shift factor $\mathcal{S}_i$ for each component. The component correction factor c_i is calculated as the product of shift factor and b_i-parameter from the EOS, see Eq. (A.8) for calculation of this parameter for component i.

$$c_i = \mathcal{S}_i b_i \quad ; \quad i = 1 \; to \; n_c \quad \text{..... (3.33)}$$

Overall and phase correction factor is then calculated from compositions and c_i.

$$c = \sum_{i=1}^{n_c} c_i z_i \quad \text{..... (3.34)}$$

$$c_l = \sum_{i=1}^{n_c} c_i x_i \quad \text{..... (3.35)}$$

$$c_v = \sum_{i=1}^{n_c} c_i y_i \quad \text{..... (3.36)}$$

Finally, molar volume and Z-factor correction is applied as shown below. Corrected volumetric properties are then used for internal calculations in the numerical simulator.

$$\mathcal{v}_{shift} = \mathcal{v} - c \quad \text{..... (3.37)}$$

$$\mathcal{v}_{l_{shift}} = \mathcal{v} - c_l \quad \text{..... (3.38)}$$

$$\mathcal{v}_{v_{shift}} = \mathcal{v} - c_v \quad \text{..... (3.39)}$$

$$Z^{\alpha}_{shift} = \frac{p\mathcal{v}_{\alpha_{shift}}}{RT} \quad \text{..... (3.40)}$$

3.6.7 Hydrocarbon Phase Viscosity

Oil and gas viscosities are calculated after VLE and volume translation have been performed using an EOS. Lohrenz et al. (1964) proposed an empirical correlation based on theory of corresponding states and residual viscosity.

$$\mu_\alpha = \mu_\alpha^* + \frac{1}{\zeta_\alpha}\Big[\big(0.1023 + 0.023364\,\tilde{\rho}_{r_\alpha} + 0.058533\tilde{\rho}_{r_\alpha}^2 - 0.40758\tilde{\rho}_{r_\alpha}^3 + 0.0093324\tilde{\rho}_{r_\alpha}^4\big)^4 - 0.0001\Big] \quad \text{..... (3.41)}$$

Where,

μ_α is viscosity of phase α, [cP]

μ_α^* is viscosity of phase α at atmospheric pressure, [cP]

$\tilde{\rho}_{r_\alpha}$ is reduced molar density of phase α, [lbmol/ft^3]

The reduced molar density is the ratio of phase molar density $\tilde{\rho}_\alpha$ to phase pseudocritical molar density $\tilde{\rho}_{pc_\alpha}$ (a function of phase composition x_i^α and component critical molar volume v_{c_i}).

$$\tilde{\rho}_{r_\alpha} = \frac{\tilde{\rho}_\alpha}{\tilde{\rho}_{pc_\alpha}} \quad \text{..... (3.42)}$$

$$\tilde{\rho}_{pc_\alpha} = \frac{1}{\sum x_i^\alpha v_i} \quad \text{..... (3.43)}$$

The phase viscosity at low (atmospheric) pressure is calculated as a function of phase composition x_i^α (for liquid $x_i^l = x_i$ and for vapor $x_i^v = y_i$) and component low pressure viscosity μ_i^*.

$$\mu_\alpha^* = \frac{\sum x_i^\alpha \mu_i^* \sqrt{MW_i}}{\sum x_i^\alpha \sqrt{MW_i}} \quad \text{..... (3.44)}$$

$$\mu_i^* = \frac{0.00034 T_{ri}^{0.94}}{\zeta_i} \quad ; \quad T_{ri} \leq 1.5$$
$$\mu_i^* = \frac{0.0001778 (4.58 T_{ri} - 1.67)^{5/8}}{\zeta_i} \quad ; \quad T_{ri} > 1.5 \qquad \text{..... (3.45)}$$

T_{ri} and p_{ri} represent component i reduced temperature and pressure respectively. The component viscosity parameter ζ_i is then a function of components reduced properties and molecular weight.

$$T_{ri} = \frac{T}{T_{ci}} \qquad \text{..... (3.46)}$$

$$p_{ri} = \frac{p}{p_{ci}} \qquad \text{..... (3.47)}$$

$$\zeta_i = \beta_\gamma \frac{T_{ci}^{1/6}}{M_{w_i}^{1/2} p_{ci}^{2/3}} \qquad \text{..... (3.48)}$$

With,

T as fluid temperature, [R]

p as fluid pressure, [psia]

$\beta_\gamma = 5.4402$ conversion factor

Phase viscosity parameter ζ_α is calculated with an analogous expression to ζ_i, using instead phase pseudocritical properties, i.e. T_{pc_α} and p_{pc_α}

$$\zeta_\alpha = \beta_\gamma \frac{T_{pc_\alpha}^{1/6}}{(M_w^\alpha)^{1/2} p_{pc_\alpha}^{2/3}} \qquad \text{..... (3.49)}$$

$$T_{pc_\alpha} = \sum x_i^\alpha T_{ci} \quad \text{..... (3.50)}$$

$$p_{pc_\alpha} = \sum x_i^\alpha p_{ci} \quad \text{..... (3.51)}$$

$$M_w^\alpha = \sum x_i^\alpha M_{w_i} \quad \text{..... (3.52)}$$

3.7 Multi-Segment Wells

Fluid flow in wellbore tubulars near the perforated intervals is modeled with multi-segment wells (MSW). The numerical approach to perform pressure drop calculations and model multiphase fluid transport in MSW is analogous to reservoir equations, i.e. is based on constitutive and auxiliary equations. Continuity equation and EOS are the same as shown before, whereas the transport equation (momentum conservation) is now updated to model pressure drop in pipelines. Also, a new spatial discretization is required for pipeline geometry.

3.7.1 Selection of MSW Independent Variables

The MSW system consists of $2n_c + 4$ variables for each well segment (**Table 3.2**), this scheme is analogous to the one presented previously for reservoir gridblock. However, due to the highly non-linear behavior of fluid velocity with respect to pressure in pipelines ($\Delta p_{pipe} \propto \vec{u}_m^2$), this variable is added to the system.

Table 3.2—INDEPENDENT VARIABLES FOR WELL SEGMENT SYSTEM OF EQUATIONS

Variable	Description	Number
lnK_{i_S}	Natural logarithm of equilibrium ratio	n_c
p_S	Well segment pressure	1
F_{i_S}	Moles of component i per segment volume	n_c
W_S	Mass of water per segment volume	1
f_{v_S}	Vapor molar fraction	1
u_{m_S}	Fluid velocity	1
	$\boldsymbol{Total}$	$\boldsymbol{2n_c + 4}$

3.7.2 MSW Geometry Spatial Discretization

The wellbore is discretized into pipe segments, each with individual physical properties, e.g. diameter, length, roughness, etc. Pressure is evaluated at the bottom of each segment (the node), while velocity is evaluated at the top (end of the flowpath). The numbering convention implemented in this study starts at the top segment, which must be unique for any particular well. Numbers increase towards the well bottom (or toe), multiple branches are allowed with this approach (Holmes et al. 1998). Any segment, with the exception of the top segment, may be perforated such that flow between reservoir and well occurs. Bottomhole pressure (BHP) and reference depth are evaluated at the top of the first segment. **Fig. 3.2** illustrate the MSW geometry spatial discretization.

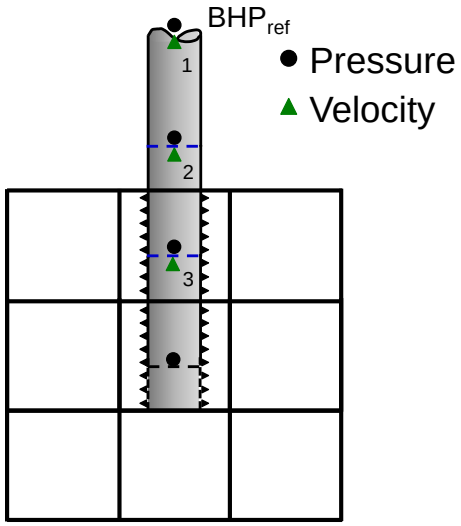

Fig. 3.2—Multi-segment well discretization. Segment pressure is evaluated at the bottom of each segment and velocity at the top. Numbering convention starts from top segment, bottomhole flowing pressure reference (BHP$_{ref}$).

3.7.3 MSW Residual Equations

Residual equations for fluid flow in MSW are obtained from water mass and hydrocarbon component moles conservation, mechanical energy balance, and EOS phase behavior fundamental relationships. Differential equations for flow in pipelines were previously presented, recall Eqs. (2.4) and (2.5).

Segment water and hydrocarbon component residuals, R_{w_S} and R_{i_S}, are comprised of three terms: accumulation, convection, and source/sink. The accumulation term is a function of mass (or moles) in the segment at time levels n and $n+1$. Convection accounts for the net flow in the segment, upstream properties are used to calculate mass/moles flux at each segment $\vec{\imath}$ (sign convention implies positive velocity for flow out of the segment). Finally, the source/sink term for segments perforated and connected to the reservoir is calculated from Peaceman's model presented previously.

$$\begin{aligned} R_{w_S} = \frac{A_{\vec{\imath}} L_{\vec{\imath}}}{\beta_t \Delta t} (W_S^{n+1} - W_S^n)_{\vec{\imath}} \\ + [(A \mathcal{y}_w \rho_w \vec{u}_w)_{\vec{\imath}} - (A \mathcal{y}_w \rho_w \vec{u}_w)_{\vec{\imath}+1}]^{n+1} \\ - \left[WI_w \left(p_{o_{res}} - p_{cow_{res}} - p_S\right)\right]_{\vec{\imath}}^{n+1} \end{aligned} \quad \text{..... (3.53)}$$

$$\begin{aligned} R_{i_S} = \frac{A_{\vec{\imath}} L_{\vec{\imath}}}{\beta_t \Delta t} \left(F_{i_S}^{n+1} - F_{i_S}^n\right)_{\vec{\imath}} \\ + \Big[A_{\vec{\imath}} \left(\mathcal{y}_o \tilde{\rho}_o x_i \vec{u}_o + \mathcal{y}_g \tilde{\rho}_g y_i \vec{u}_g\right)_{\vec{\imath}} \\ - A_{\vec{\imath}+1} \left(\mathcal{y}_o \tilde{\rho}_o x_i \vec{u}_o + \mathcal{y}_g \tilde{\rho}_g y_i \vec{u}_g\right)_{\vec{\imath}+1}\Big]^{n+1} \\ - \left[WI_o x_i \left(p_{o_{res}} - p_S\right)\right]_{\vec{\imath}}^{n+1} \\ - \left[WI_g y_i \left(p_{o_{res}} + p_{cgo_{res}} - p_S\right)\right]_{\vec{\imath}}^{n+1} \end{aligned} \quad \text{..... (3.54)}$$

Where,

R_{w_S} is segment water residual, [lb/day]

R_{i_S} is segment hydrocarbon component i residual, [lbmol/day]

W_S is segment mass of water per segment unit volume ($W_S = \mathcal{y}_w \rho_w$), [lb/ft^3]

F_{i_S} is number of moles of component i per segment unit volume, [lbmol/ft^3]

$A_{\vec{\imath}}$ is segment cross-sectional flow area, [ft^2]

$L_{\vec{\imath}}$ is segment length, [ft]

Δt is time-step size, [day]

$\mathcal{Y}_\alpha$ is phase holdup, [V/V]

ρ_w is water density, [lb/ft^3]

$\tilde{\rho}_o$ and $\tilde{\rho}_g$ are oil and gas molar densities, [lbmol/ft^3]

$\vec{u}_\alpha$ is phase (oil, gas, or water) velocity, [ft/s]

WI_α is phase well index, for water [lb/day/psi] and for hydrocarbons [lbmol/day/psi]

$p_{o_{res}}$ is oil phase gridblock pressure, [psia]

$p_{cow_{res}}$ is oil-water gridblock capillary pressure, [psia]

$p_{cgo_{res}}$ is gas-oil gridblock capillary pressure, [psia]

p_S is well-segment pressure, [psia]

$\beta_t = 86{,}400$ is time unit conversion factor

Phase velocities, flow regimes, and associated pressure drop in pipelines, are typically calculated from multiphase flow semi-empirical correlations (Beggs and Brill 1973; Dukler et al. 1964; Duns and Ros 1963; Eaton et al. 1967; Hagedorn and Brown 1965; Orkiszewski 1967). However, this study assumes the no-slip condition, in which fluid is fully mixed and all phases flow at the same velocity, represented by fluid mixture segment velocity $\vec{u}_{m_S}$.

$$\vec{u}_o = \vec{u}_g = \vec{u}_w = \vec{u}_{m_S} \quad \text{..... (3.55)}$$

The transport equation is derived from mechanical energy balance (momentum conservation neglecting heat transfer). Pressure drop across a well segment ($\Delta p_{\bar{i}}$), is a function of frictional ($\Delta p_{F_{\bar{i}}}$), potential ($\Delta p_{PE_{\bar{i}}}$), and acceleration ($\Delta p_{A_{\bar{i}}}$) pressure losses, as shown in the pressure drop residual equation $R_{p_{S_{\bar{i}}}}$.

$$R_{p_{S_{\bar{i}}}} = \Delta p_{\bar{i}} + \Delta p_{PE_{\bar{i}}} + \Delta p_{F_{\bar{i}}} + \Delta p_{A_{\bar{i}}} \quad \text{..... (3.56)}$$

$$\Delta p_{\vec{\imath}} = p_{S_{\vec{\imath}}} - p_{S_{\vec{\imath}-1}} \quad \text{..... (3.57)}$$

$$\Delta p_{PE_{\vec{\imath}}} = \frac{\rho_{m_{\vec{\imath}}}(h_{\vec{\imath}} - h_{\vec{\imath}-1})}{144} \quad \text{..... (3.58)}$$

$$\Delta p_{F_{\vec{\imath}}} = \beta_d \left(\frac{f_f \rho_m L \vec{u}_m^2}{D} \right)_{\vec{\imath}} \quad \text{..... (3.59)}$$

$$\Delta p_{A_{\vec{\imath}}} = \beta_{g_c} \frac{\left[(\dot{m}_w + \dot{m}_{HC})_{\vec{\imath}-1} \vec{u}_{m_{\vec{\imath}-1}} + (\dot{m}_w + \dot{m}_{HC})_{\vec{\imath}} \vec{u}_{m_{\vec{\imath}}} \right]}{A_{\vec{\imath}}} \quad \text{..... (3.60)}$$

Where,

$p_{S_{\vec{\imath}}}$ denotes segment $\vec{\imath}$ pressure, [psia]

$\rho_{m_{\vec{\imath}}}$ is segment $\vec{\imath}$ fluid mixture density, [lb/ft^3]

$h_{\vec{\imath}}$ is segment $\vec{\imath}$ node depth, [ft]

f_f is segment friction factor, [dimensionless]

$L_{\vec{\imath}}$ is segment length, [ft]

$\vec{u}_m$ is segment fluid mixture velocity, [ft/s]

D is segment diameter, [in]

$\dot{m}_w$ and $\dot{m}_{HC}$ are water and hydrocarbon mass rates, [lb/s]

$\beta_d = 24\beta_{g_c}$ is length conversion factor and gravity constant

$\beta_{g_c} = \frac{1}{32.174 \times 144}$ is length conversion factor and gravity constant

Notice that for the top segment ($\vec{\imath} = 1$) pressure residual, properties at location $\vec{\imath} - 1$ correspond to bottomhole pressure (BHP) and reference depth conditions. As an example of sign convention, for segment location index $\vec{\imath}$ in a producer, $\vec{\imath} + 1 = upstream$ and $\vec{\imath} - 1 = downstream$ directions. Also notice that the lower-most (toe) segment has zero

flux from upstream, that is, fluid does not enter/exit at the bottom of last segment; the acceleration pressure drop is included to correctly account this effect.

Fluid mixture density (ρ_m) and viscosity (μ_m) are calculated via volumetric phase averaging based of phase holdup.

$$\rho_m = \mathcal{y}_o\rho_o + \mathcal{y}_g\rho_g + \mathcal{y}_w\rho_w \quad \text{..... (3.61)}$$

$$\mu_m = \mathcal{y}_o\mu_o + \mathcal{y}_g\mu_g + \mathcal{y}_w\mu_w \quad \text{..... (3.62)}$$

Friction factor is calculated from Reynold's number, N_{Re}, for laminar flow ($N_{Re} \leq 2100$):

$$f_f = \frac{16}{N_{Re}} \quad \text{..... (3.63)}$$

For turbulent flow ($N_{Re} > 2100$), Chen's approximation of the Colebrook-White equation is used (Economides et al. 1993):

$$f_f = \left\{-4log\left\{\frac{\epsilon}{3.7065} - \frac{5.0452}{N_{Re}} log\left[\frac{\epsilon^{1.1098}}{2.8257} + \left(\frac{7.149}{N_{Re}}\right)^{0.8981}\right]\right\}\right\}^{-1/2} \quad \text{..... (3.64)}$$

With,

$$N_{Re} = \beta_{Re}\frac{\vec{u}_m\rho_m D}{\mu_m} \quad \text{..... (3.65)}$$

ϵ is segment's relative roughness, [dimensionless]

$\beta_{Re} = 124.01366$ is unit conversion factor for field units

Well segment EOS residuals $R_{fug_{i_S}}$ and R_{RR_S} are analogous to those presented previously for reservoir gridblocks. The holdup (phase volume) constraint R_{HU_S} is also analogous to reservoir's saturation constraint. Segment properties, denoted by subscript S are used for these residuals.

$$R_{fug_{i_S}} = lnK_{i_S} + ln\hat{\varphi}^{v}_{i_S} - \hat{\varphi}^{l}_{i_S} \quad ; \quad i = 1 \; to \; n_c \quad \text{..... (3.66)}$$

$$R_{RR_S} = \sum_{i=1}^{n_c} \frac{z_{i_S}\left(K_{i_S} - 1\right)}{1 + f_{v_S}\left(K_{i_S} - 1\right)} \quad \text{..... (3.67)}$$

$$R_{HU_S} = F_S \left[\frac{1 - f_{v_S}}{\tilde{\rho}_{o_S}} + \frac{f_{v_S}}{\tilde{\rho}_{g_S}}\right] + \frac{W_S}{\rho_{w_S}} - 1 \text{ ..... (3.68)}$$

A simplification of the system of equations can be performed for single-phase wells, i.e. water and gas injectors, by removing unnecessary independent variables and residuals for the appropriate single-phase segment.

3.7.4 MSW Boundary Conditions

Wells can be controlled either by rate or pressure constraints. Boundary condition is set at well's reference depth by substituting the pressure residual equation for the top segment with the constraint equation. For pressure constraint, Eq. (3.69) is applied to set the desired bottomhole target pressure. For rate constraint, Eq. (3.70) specifies the phase target volumetric rate $Q_{\alpha_{target}}$ at standard conditions, including phase density at standard conditions ($\rho_{\alpha_{SC}}$) and phase mass flux at the top segment velocity reference point.

$$R_{p_{S_1}} = p_{S_1} - BHP_{target} \text{ ..... (3.69)}$$

$$R_{p_{S_1}} = \dot{m}_{\alpha_1} - Q_{\alpha_{target}}\rho_{\alpha_{SC}} \text{ ..... (3.70)}$$

Often, multiple constraints (e.g. pressure and one or more phase rate constraints) for an individual well must be evaluated in order to determine the active boundary condition. This process is performed through the calculation of a violation factor (Watts et al. 2009) for each specified constraint.

Rate constraint violation factor ν_{Q_α} is represented by the absolute value of segment to target phase rate ratio. Pressure constraint violation factor ν_p for producers is calculated as the ratio of target BHP to top segment pressure and its reciprocal for injectors, shown in Eq. (3.72).

$$\nu_{Q_\alpha} = \left| \frac{Q_{\alpha_{segment\,1}}}{Q_{\alpha_{target}}} \right| \quad \text{..... (3.71)}$$

$$\nu_p = \frac{BHP_{min_{target}}}{p_{S_1}} \;\; for\ producers$$
$$\nu_p = \frac{p_{S_1}}{BHP_{max_{target}}} \;\; for\ injectors \quad \text{..... (3.72)}$$

The active boundary condition is selected from the largest calculated violation factor and used in the pressure residual equation for the top segment $R_{p_{S_1}}$.

3.8 Structure of Numerical Solution

The simulator consists of multiple subroutines performing calculations in a robust algorithm to model reservoir production performance under a wide variety of scenarios and conditions. The simulation workflow is summarized in **Fig. 3.3**.

Input data includes number of gridblock in all coordinate axis directions ($\vec{\imath}, \vec{\jmath}, \vec{k}$), gridblock size, porosity, permeabilities, and depth, rock and compositional fluid properties, saturation functions, well properties and production constraints, and finally, initial conditions for reservoir and MSW elements. Quality check (QC) is performed on input

data to ensure consistency in all parameters, including vector dimensions, normalized compositions, consistent relative permeability curves, etc. Miscellaneous calculations comprise geometric transmissibility and well index evaluation, computation of generic variables required for simulation, and parallel processing setup. The initialization routine consists on the calculation of independent variable values (F_i, W, lnK_i, f_v) from provided initial conditions ($p_{init}, z_{i_{init}}, S_{w_{init}}, y_{w_{init}}$). This process is performed based on EOS calculations and fundamental relationships. If the simulation restart option is used, the initialization routine assigns corresponding independent variable values from the restart file.

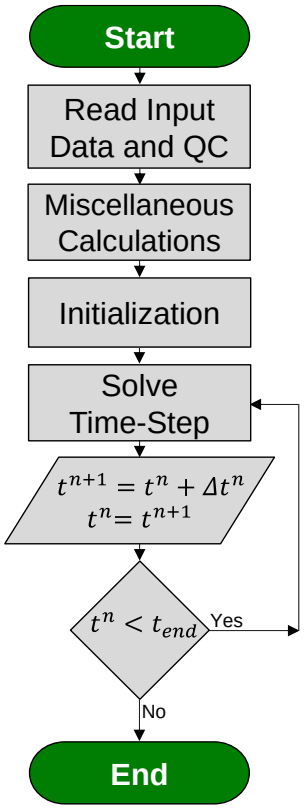

Fig. 3.3—Simulation workflow. Multiple subroutines performed required calculations for the numerical solutions. Input data is read and quality checked, miscellaneous calculations setup essential variables, independent variables are initialized, and time-step numerical system is solved until final simulation time.

3.8.1 Fully-Implicit Solution

Time-step solution involves a series of calculations within a Newton-Raphson iterative scheme applying a fully-implicit approach, see **Fig. 3.4**. The initial guess for independent variables is taken from previous time-step solution $\vec{x}^n$ to form the vector of unknowns $\vec{x}^k$. If the calculation is performed for the first time-step, initialization results are used as previous solution. The residual vector $\vec{R}$ is calculated based on independent variables values and application of boundary conditions. The Jacobian $\vec{\vec{J}}$ is computed numerically and the system of equations is solved using direct, conjugate gradient, generalized minimal residual, or biconjugate gradient stabilized method, implemented from MATLAB® libraries (MathWorks 2014).

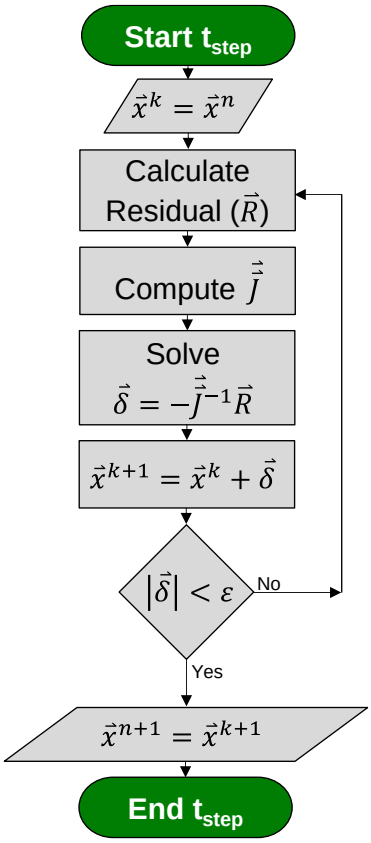

Fig. 3.4—Simulation time-step workflow. Independent variables initial guess is taken from previous step solution to calculate residuals. The Jacobian is calculated numerically and the system of equation is solved. Independent variables are updated and multiple convergence criteria are evaluated until desired tolerance is met.

Values for independent variables are updated to obtain new iteration values $\vec{x}^{k+1}$. This process is repeated for k-iterations until convergence criteria (detailed in Section 3.8.5) are met within specified tolerance ε. If convergence cannot be achieved within a specified maximum number of iterations, time-step size is reduced, initial guess is reset, and the iterative process is re-started. Once convergence is reached, the step solution is updated and results are saved, time-step size (Δt) is increased using a user-defined factor, and simulation continues until reaching final simulation time.

3.8.2 Vector of Unknowns

$\vec{x}$ is comprised of independent variables from reservoir gridblocks and well segments, ordered in increasing gridblock number cycling $\vec{\imath}$ first, $\vec{\jmath}$ second, and $\vec{k}$ last. Size of $\vec{x}$ ($n_{RES_{eq}} + n_{MSW_{eq}}$) is a function of number of reservoir model gridblocks ($n_{gridblocks}$), number of components (n_c), number of wells (n_{wells}), and corresponding number of segments per well (n_{seg_w}).

$$\vec{x} = \begin{bmatrix} \vec{x}_{RES} \\ \vec{x}_{MSW} \end{bmatrix} \quad ; \quad \vec{x}_{RES} = \begin{bmatrix} ln\vec{K}_i \\ p_o \\ \vec{F}_i \\ W \\ f_v \end{bmatrix}_{\forall(\vec{\imath},\vec{\jmath},\vec{k})} \quad ; \quad \vec{x}_{MSW} = \begin{bmatrix} ln\vec{K}_{i_S} \\ p_S \\ \vec{F}_{i_S} \\ W_S \\ f_{v_S} \\ u_{m_S} \end{bmatrix}_{\forall(\vec{\imath})} \quad \text{..... (3.73)}$$

$$size(\vec{x}_{RES}) = n_{RES_{eq}} = n_{gridblocks}(2n_c + 3) \quad \text{..... (3.74)}$$

$$size(\vec{x}_{MSW}) = n_{MSW_{eq}} = \sum_{w=1}^{n_{wells}} \left[n_{seg_w}(2n_c + 4) \right] \quad \text{..... (3.75)}$$

Notice that independent variables related to compositional values ($ln\vec{K}_i$ and $\vec{F}_i$) are vectors for $i = 1\ to\ n_c$, ordered as a column vector for each gridblock and well segment.

3.8.3 Vector of Residuals

Similarly to $\vec{x}$, the vector of residuals $\vec{R}$ is formed from reservoir and MSW residual equations for each discrete element, arranged in the order presented previously. The size of $\vec{R}$ also equals $n_{RES_{eq}} + n_{MSW_{eq}}$.

$$\vec{R} = \begin{bmatrix} \vec{R}_{RES} \\ \vec{R}_{MSW} \end{bmatrix} \quad ; \quad \vec{R}_{RES} = \begin{bmatrix} \vec{R}_{fug_i} \\ R_{sat} \\ \vec{R}_i \\ R_w \\ R_{RR} \end{bmatrix}_{\forall(\vec{\imath},\vec{\jmath},\vec{k})} \quad ; \quad \vec{R}_{MSW} = \begin{bmatrix} \vec{R}_{fug_{i_S}} \\ R_{HU_S} \\ \vec{R}_{i_S} \\ R_{w_S} \\ R_{RR_S} \\ R_{p_S} \end{bmatrix}_{\forall(\vec{\imath})} \quad \text{..... (3.76)}$$

3.8.4 Jacobian Calculation

The Jacobian represents the change of residual equations with respect to independent variables. In this study, the Jacobian is computed numerically by adding a small perturbation to each independent variable to calculate its respective derivative. The size of resulting Jacobian is $\left(n_{RES_{eq}} + n_{MSW_{eq}}\right) \times \left(n_{RES_{eq}} + n_{MSW_{eq}}\right)$.

$$\vec{\vec{J}} = \begin{bmatrix} \dfrac{\partial \vec{R}_{RES}}{\partial \vec{x}_{RES}} & \dfrac{\partial \vec{R}_{RES}}{\partial \vec{x}_{MSW}} \\ \dfrac{\partial \vec{R}_{MSW}}{\partial \vec{x}_{RES}} & \dfrac{\partial \vec{R}_{MSW}}{\partial \vec{x}_{MSW}} \end{bmatrix} \quad \text{..... (3.77)}$$

The template for a gridblock $(\vec{\imath}, \vec{\jmath}, \vec{k})$ Jacobian element of reservoir residuals with respect to reservoir independent variables is shown in Eq. (3.78). This template is repeated for all gridblocks and well segments to form the final Jacobian matrix.

$$\left[\frac{\partial \vec{R}_{RES}}{\partial \vec{x}_{RES}}\right]_{(\vec{i},\vec{j},\vec{k})} = \begin{bmatrix} \frac{\partial R_{fug_1}}{\partial lnK_1} & \cdots & \frac{\partial R_{fug_1}}{\partial lnK_{n_c}} & \frac{\partial R_{fug_1}}{\partial p_o} & \frac{\partial R_{fug_1}}{\partial F_1} & \cdots & \frac{\partial R_{fug_1}}{\partial F_{n_c}} & \frac{\partial R_{fug_1}}{\partial W} & \frac{\partial R_{fug_1}}{\partial f_v} \\ \vdots & \vdots & \vdots & \vdots & \vdots & \vdots & \vdots & \vdots & \vdots \\ \frac{\partial R_{fug_{n_c}}}{\partial lnK_1} & \cdots & \frac{\partial R_{fug_{n_c}}}{\partial lnK_{n_c}} & \frac{\partial R_{fug_{n_c}}}{\partial p_o} & \frac{\partial R_{fug_{n_c}}}{\partial F_1} & \cdots & \frac{\partial R_{fug_{n_c}}}{\partial F_{n_c}} & \frac{\partial R_{fug_{n_c}}}{\partial W} & \frac{\partial R_{fug_{n_c}}}{\partial f_v} \\ \frac{\partial R_{sat}}{\partial lnK_1} & \cdots & \frac{\partial R_{sat}}{\partial lnK_{n_c}} & \frac{\partial R_{sat}}{\partial p_o} & \frac{\partial R_{sat}}{\partial F_1} & \cdots & \frac{\partial R_{sat}}{\partial F_{n_c}} & \frac{\partial R_{sat}}{\partial W} & \frac{\partial R_{sat}}{\partial f_v} \\ \frac{\partial R_1}{\partial lnK_1} & \cdots & \frac{\partial R_1}{\partial lnK_{n_c}} & \frac{\partial R_1}{\partial p_o} & \frac{\partial R_1}{\partial F_1} & \cdots & \frac{\partial R_1}{\partial F_{n_c}} & \frac{\partial R_1}{\partial W} & \frac{\partial R_1}{\partial f_v} \\ \vdots & \cdots & \vdots & \vdots & \vdots & \cdots & \vdots & \vdots & \vdots \\ \frac{\partial R_{n_c}}{\partial lnK_1} & \cdots & \frac{\partial R_{n_c}}{\partial lnK_{n_c}} & \frac{\partial R_{n_c}}{\partial p_o} & \frac{\partial R_{n_c}}{\partial F_1} & \cdots & \frac{\partial R_{n_c}}{\partial F_{n_c}} & \frac{\partial R_{n_c}}{\partial W} & \frac{\partial R_{n_c}}{\partial f_v} \\ \frac{\partial R_w}{\partial lnK_1} & \cdots & \frac{\partial R_w}{\partial lnK_{n_c}} & \frac{\partial R_w}{\partial p_o} & \frac{\partial R_w}{\partial F_1} & \cdots & \frac{\partial R_w}{\partial F_{n_c}} & \frac{\partial R_w}{\partial W} & \frac{\partial R_w}{\partial f_v} \\ \frac{\partial R_{RR}}{\partial lnK_1} & \cdots & \frac{\partial R_{RR}}{\partial lnK_{n_c}} & \frac{\partial R_{RR}}{\partial p_o} & \frac{\partial R_{RR}}{\partial F_1} & \cdots & \frac{\partial R_{RR}}{\partial F_{n_c}} & \frac{\partial R_{RR}}{\partial W} & \frac{\partial R_{RR}}{\partial f_v} \end{bmatrix}_{(\vec{i},\vec{j},\vec{k})} \quad \text{..... (3.78)}$$

Fig. 3.5 displays a sample Jacobian for a 5x5x3 reservoir with 6-component fluid characterization. A producer and a water injector MSWs have 3 and 4 segments respectively. Notice that the number of equations is 1,181, a reduced system since only p_S and W_S variables are required for segments in the water injection well. The resulting Jacobian is a sparse matrix with 24,999 non-zero elements. Reservoir number of equations is 1,125, depicted by the gray shading in the figure. MSW is shown in pink, while derivative representing interaction between reservoir and MSW, i.e. perforated gridblocks, are shown in green shading (bottom and right rectangles).

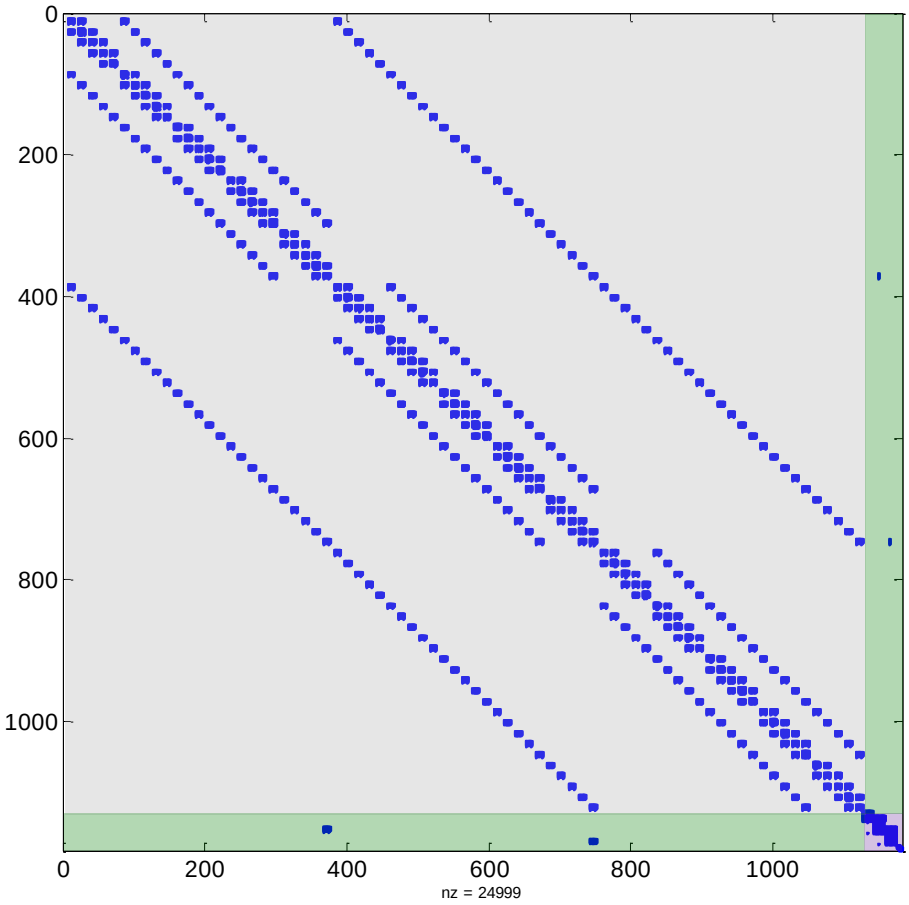

Fig. 3.5—Jacobian matrix sample for a 5x5x3 reservoir model with 6 components fluid description. Two multi-segment wells, a producer and a water injector, have 3 and 4 segments respectively. Total system size is 1,181x1,181 with 24,999 non-zero elements. Gray shading depicts reservoir derivatives, purple shade shows MSW, and green shade interaction between reservoir and MSW variables.

3.8.5 Convergence Criteria

The iteration updated solution $\vec{x}^{k+1}$ resulting from system of equation solver is tested for consistency. Multiple convergence criteria must be met before accepting iteration solution. Minimum criteria include solution is within physical limits (e.g. $p > 14.7\ psia$, $0 \leq S_\alpha \leq 1$, $0 \leq y_\alpha \leq 1$, etc.) and residuals are small, i.e. residual norm $\left\|\vec{R}\right\|_2 \to 0$.

In addition, maximum pressure and phase fugacity change within an iteration are also applied as convergence criteria (Schlumberger 2014). Liquid and vapor fugacities for each

component ($\hat{f}_i^l$ and $\hat{f}_i^v$) are calculated from fundamental relationships and EOS presented in Appendix A.

$$\|p^{k+1} - p^k\|_2 \leq \varepsilon_p \quad ; \quad \varepsilon_p = 1.47 \quad \text{..... (3.79)}$$

$$\left\|\hat{f}_i^{l\,k+1} - \hat{f}_i^{l\,k}\right\|_2 \leq \varepsilon_f \quad ; \quad \varepsilon_f = 0.001 \quad \text{..... (3.80)}$$

$$\left\|\hat{f}_i^{v\,k+1} - \hat{f}_i^{v\,k}\right\|_2 \leq \varepsilon_f \quad ; \quad \varepsilon_f = 0.001 \quad \text{..... (3.81)}$$

CHAPTER IV
NETWORK SIMULATOR FORMULATION

Network pipelines play a crucial role in oil and gas production, transporting produced fluids from wellbore tubing to wellhead and separator, downstream processing plants, and sales points. Accurate pipeline simulation is critical to forecast production trends accounting gathering system constraints. Successful implementation of flow assurance techniques is based on appropriate modeling of solid deposits (asphaltenes, hydrates, and waxes) along the production system, which can negatively impact production operations, pressure management, and field operations.

This chapter describes the compositional network simulator formulation based on an extension from multi-segment wells presented previously. Pipeline networks usually have a complex topology (diameter changes, branches, inline equipment, multiple connections, etc.), requiring a more flexible numerical discretization than well segments. Asphaltene precipitation and deposition modeling using vapor/liquid/liquid-dense equilibria with an equation of state (EOS) is also detailed. The implementation is aimed to forecast asphaltene accretion to pipeline under multiple conditions including natural depletion, artificial gas-lift, downhole inhibitor injection, and wellbore temperature gradients, among others.

4.1 Formulation Assumptions

The development of numerical network simulator in this study is based on the following statements and assumptions:

- Finite difference spatial and time discretization.
- Pipeline temperature profiles are explicitly defined. No heat transfer is calculated.
- Pipelines are incompressible and immobile.
- Three-phase (oil, gas, and water) flow in pipelines.
- Multiphase flow in pipelines is based on no-slippage condition between phases.

- Equilibrium for each time-step is instantaneous.
- Thermodynamic equilibrium of oil and gas hydrocarbon components is represented by vapor/liquid equilibria (VLE) using Peng-Robinson equation of state (PR-EOS) with volume translation.
- Asphaltene precipitation is represented by vapor/liquid/liquid-dense equilibria (VLLE) using PR-EOS with volume translation.
- Asphaltene deposition in pipelines is irreversible.
- There is no mutual solubility between water and hydrocarbon components in VLE nor VLLE calculations.
- No component chemical reactions are considered.

4.2 Fluid Flow in Pipelines

Multi-phase flow in pipelines is modeled in this study with an approach similar to the one presented previously for multi-segment wells (MSW). Governing and auxiliary equations for the network are used jointly to create a numerical solution. The spatial discretization developed for network pipelines differs from MSW to accommodate a more complex topology in the system and future implementation of inline equipment.

4.2.1 Primary and Auxiliary Equations

Required equations for network simulation have been presented previously in Chapters II and III. Primary equations are constituted by continuity (mass conservation in Eqs. (2.4) and (2.5)), mechanical energy balance (transport equation in Eq. (3.56)), and the EOS in Eq. (3.6). Auxiliary equations for fluid properties determination from VLE and EOS results, i.e. volume translation and hydrocarbon phase viscosity, can be found in Sections 3.6.6 and 3.6.7 respectively.

4.2.2 Network Geometry Spatial Discretization

Pipeline production systems consist of complex networks with diameter changes, pipe fittings, chokes, inline equipment, multiple connections, branches, etc. Numerical modeling of this type of topology requires a flexible spatial discretization for the pipelines.

The implemented spatial discretization is analogous to the block-centered approach, where pressure is evaluated at the center of the pipe segment, called the node, and velocities are evaluated at the pipe outlets or connections, as seen on **Fig. 4.1**. This approach allows robust modeling and convenient definition of networks including bottomhole, wellhead pipe fittings, pipe segments with multiple connections, diameter changes (specified at node location), and production separator.

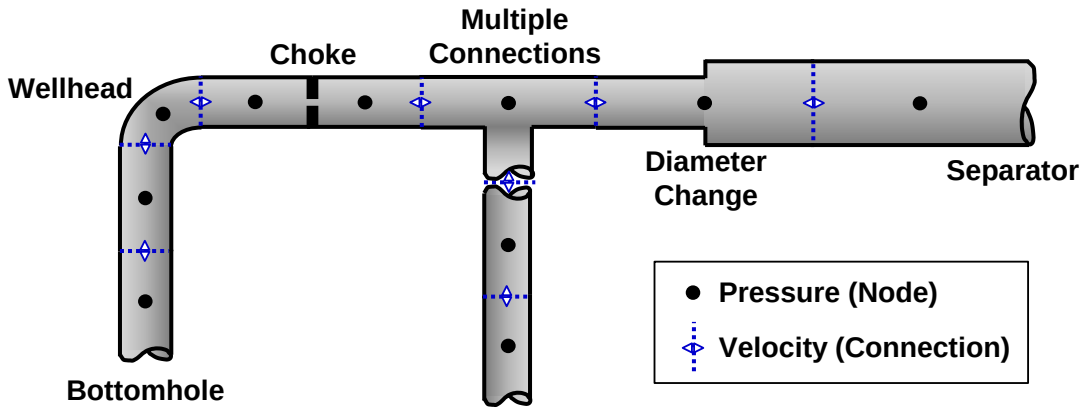

Fig. 4.1—Pipeline spatial discretization, network system sample layout. Discretization is based on pressure and velocity evaluation at node and connections respectively. Diameter changes occur at the nodes (center of pipe segment).

Flexibility of this formulation also facilitates later implementation of additional equipment such as multiphase choke modeling, compressors, pumps, and network loops, among others. Under this scenario, chokes are modeled as an additional pressure drop at the connection, while compressors and pumps are set as special equipment segments that perform a specified thermodynamic task on the fluid.

4.3 Selection of Network Independent Variables

The network system of equations consists, in general, of $2n_c + 4$ variables for each pipe segment, as displayed on **Table 4.1**. Fluid velocity is set as an independent variable due to its high non-linear behavior with respect to pressure drop.

Table 4.1—INDEPENDENT VARIABLES FOR NETWORK PIPE SEGMENT SYSTEM OF EQUATIONS

Variable	Description	Number
lnK_{i_P}	Natural logarithm of equilibrium ratio	n_c
p_P	Network pipe segment pressure	1
F_{i_P}	Moles of component i per segment volume	n_c
W_P	Mass of water per segment volume	1
f_{v_P}	Vapor molar fraction	1
u_{m_C}	Fluid velocity at connection	1
	$\boldsymbol{Total}$	$\boldsymbol{2n_c + 4}$

The final exact number of equations for the overall network system depends on the number of pipe segments n_{pipe}, number of components n_c, number of pipe connections n_{con}, number of inlets/outlets $n_{i/o}$, and type of boundary conditions. The impact of boundary conditions on the number of equations for connection fluid velocity ($n_{R_{p_C}}$) is detailed in Section 4.5.

4.4 Network Residual Equations

Residual equations for the network system are obtained from finite differences approximation of water and hydrocarbon conservation equations, mechanical energy balance, holdup constraint, and phase equilibria equations. Pressure and fluid properties are evaluated at pipe's node, while fluid velocity is evaluated at connections. Connections are comprised of pipe-to-pipe links and network inlets/outlets.

4.4.1 Water and Hydrocarbon Component Conservation Residuals

Pipe segment $\vec{\imath}_p$ water and hydrocarbon component residuals, R_{w_P} and R_{i_P}, are comprised of three terms: accumulation, convection, and source/sink. The accumulation term is a

function of mass (or moles) in the segment at time levels n and $n+1$. Convection accounts for the net flow in the segment from the total number of connections for the pipe n_{con}^{pipe}, upstream properties are used to calculate mass/moles flux at each connection $\vec{\imath}_c$ (sign convention implies positive velocity for flow out of the segment). Finally, the source/sink term is used for inflow from an external source, such as MSW connection, artificial gas lift systems, or bottomhole inhibitor injection.

$$R_{w_P} = \frac{V_{\vec{\imath}_p}}{\beta_t \Delta t}(W_P^{n+1} - W_P^n)_{\vec{\imath}_p} + \sum_{\vec{\imath}_c=1}^{n_{con}^{pipe}} \left[(A \mathcal{y}_w \rho_w \vec{u}_w)_{\vec{\imath}_c}\right]^{n+1} - \left(\dot{m}_{w_{s/s}}\right)_{\vec{\imath}_p}^{n+1} \quad \text{.... (4.1)}$$

$$\begin{aligned} R_{i_P} = {} & \frac{V_{\vec{\imath}_p}}{\beta_t \Delta t}\left(F_{i_P}^{n+1} - F_{i_P}^n\right)_{\vec{\imath}_p} \\ & + \sum_{\vec{\imath}_c=1}^{n_{con}^{pipe}} \left[A_{\vec{\imath}_c}\left(\mathcal{y}_o \tilde{\rho}_o x_i \vec{u}_o + \mathcal{y}_g \tilde{\rho}_g y_i \vec{u}_g\right)_{\vec{\imath}_c}\right]^{n+1} \quad \text{..... (4.2)} \\ & - \left(\dot{n}_{i_{s/s}}\right)_{\vec{\imath}_p}^{n+1} \end{aligned}$$

Where,

R_{w_P} is pipe segment water residual, [lb/day]

R_{i_P} is pipe segment hydrocarbon component residual, [lbmol/day]

W_P is pipe segment mass of water per pipe segment unit volume ($W_P = \mathcal{y}_w \rho_w$), [lb/ft^3]

F_{i_P} is number of moles of component i per pipe segment unit volume, [lbmol/ft^3]

$V_{\vec{\imath}_p}$ is pipe segment volume, [ft^3]

Δt is time-step size, [day]

$\mathcal{y}_\alpha$ is phase holdup, [V/V]

ρ_w is water density, [lb/ft^3]

$\tilde{\rho}_o$ and $\tilde{\rho}_g$ are oil and gas molar densities, [lbmol/ft^3]

$\vec{u}_\alpha$ is phase velocity, [ft/s]

$\dot{m}_{w_{s/s}}$ is water mass rate from source/sink, [lb/day]

$\dot{n}_{i_{s/s}}$ is hydrocarbon component molar rate from source/sink, [lbmol/day]

n_{con}^{pipe} is number of connections for the pipe segment, [natural number]

$\beta_t = 86{,}400$ is time unit conversion factor

Subscripts $\vec{\imath}_p$ and $\vec{\imath}_c$ indicate pipe and connection coordinate number respectively

The number of water residual equations equals the number of network pipe segments n_{pipe}, while the number of hydrocarbon component residual equations equal $n_c \times n_{pipe}$. Analogous to MSW formulation, common multi-phase flow correlations (Beggs and Brill 1973; Dukler et al. 1964; Duns and Ros 1963; Eaton et al. 1967; Hagedorn and Brown 1965; Orkiszewski 1967) are not required since no-slip condition between phases is assumed. All phases are assumed to flow at the same velocity, represented by fluid mixture segment velocity $\vec{u}_{m_C}$.

$$\vec{u}_o = \vec{u}_g = \vec{u}_w = \vec{u}_{m_C} \quad \text{..... (4.3)}$$

4.4.2 Holdup Constraint Residual

The holdup (phase volume) constraint R_{HU_P} is derived from the physical constraint of phase holdup summation equals unity, and numerically ensures the pipe segment volume is filled with fluids. This expression is equivalent to the saturation constraint residual presented in Section 3.5.3. There are n_{pipe} holdup constraint residual equations for the network system.

$$R_{HU_P} = F_P \left[\frac{1 - f_{v_P}}{\tilde{\rho}_{o_P}} + \frac{f_{v_P}}{\tilde{\rho}_{g_P}} \right] + \frac{W_P}{\rho_{w_P}} - 1 \quad \text{..... (4.4)}$$

4.4.3 Phase Equilibria Residuals

Network pipe segment EOS residuals $R_{fug_{i_P}}$ and R_{RR_P} are analogous to those presented previously for reservoir gridblocks (Section 3.5.2); the subscript *P* indicates network pipe segment. These expressions are derived from VLE fundamental relationships (see

Appendix A for details on flash calculation). The number of R_{RR_P} residual equations equals n_{pipe}, while the number of fugacity residual equations $R_{fug_{i_P}}$ equal $n_c \times n_{pipe}$.

$$R_{fug_{i_P}} = lnK_{i_P} + ln\hat{\varphi}^v_{i_P} - \hat{\varphi}^l_{i_P} \quad ; \quad i = 1\ to\ n_c \quad \text{..... (4.5)}$$

$$R_{RR_P} = \sum_{i=1}^{n_c} \frac{z_{i_P}(K_{i_P} - 1)}{1 + f_{v_P}(K_{i_P} - 1)} \quad \text{..... (4.6)}$$

4.4.4 Pressure Drop Residual

The pressure drop residual is obtained from mechanical energy balance (momentum conservation neglecting heat transfer). The pressure drop $\Delta p_{\vec{i}_c}$ at a connection is a function of frictional ($\Delta p_{F_{\vec{i}_c}}$), potential ($\Delta p_{PE_{\vec{i}_c}}$), and pipe fittings ($\Delta p_{PFit_{\vec{i}_c}}$) pressure losses, as presented in $R_{p_{C_{\vec{i}_c}}}$ residual equation.

$$R_{p_{C_{\vec{i}_c}}} = \Delta p_{\vec{i}_c} + \Delta p_{PE_{\vec{i}_c}} + \Delta p_{F_{\vec{i}_c}} + \Delta p_{PFit_{\vec{i}_c}} \quad \text{..... (4.7)}$$

$$\Delta p_{\vec{i}_c} = p_{\vec{i}_{p_{ups}}} - p_{\vec{i}_{p_{downs}}} \quad \text{..... (4.8)}$$

$$\Delta p_{PE_{\vec{i}_c}} = \frac{(\rho_m h)_{\vec{i}_{p_{ups}}} - (\rho_m h)_{\vec{i}_{p_{downs}}}}{144} \quad \text{..... (4.9)}$$

$$\Delta p_{F_{\vec{i}_c}} = \beta_d \left(\frac{f_f \rho_m L \vec{u}^2_{m_c}}{D} \right)_{\vec{i}_c} \quad \text{..... (4.10)}$$

Where,

$p_{\vec{i}_p}$ denotes network pipe segment $\vec{i}_p$ pressure, [psia]

$\rho_{m_{\vec{\imath}_p}}$ denotes network pipe segment $\vec{\imath}_p$ fluid mixture density, [lb/ft^3]

$h_{\vec{\imath}_p}$ denotes network pipe segment $\vec{\imath}_p$ node height, [ft]

$f_{f_{\vec{\imath}_c}}$ denotes network pipe connection friction factor, [dimensionless]

$\vec{u}_{m_C}$ denotes network pipe connection fluid mixture velocity, [ft/s]

$L_{\vec{\imath}_c}$ denotes network pipe connection length, [ft]

$D_{\vec{\imath}_c}$ denotes network pipe connection diameter, [in]

$\dot{m}_w$ and $\dot{m}_{HC}$ denote water and hydrocarbon mass rates, [lb/s]

$\beta_d = 24\beta_{g_c}$ is length conversion factor with gravity constant

$\beta_{g_c} = \frac{1}{32.174\times144}$ is length (diameter) conversion factor and gravity constant

Subscripts ups and $downs$ indicate upstream and downstream nodes

Pipe fittings $\Delta p_{PFit_{\vec{\imath}_c}}$ represents additional pressure losses caused by turbulence when fluids drastically change flow direction in pipe elbows, tees, valves, chokes, etc. This additional pressure drop is usually estimated as equivalent length in pipe diameters or mechanistic models (Economides et al. 1993).

Network pipe segment fluid mixture density and viscosity are calculated via volumetric phase averaging based of phase holdup.

$$\rho_{m_{\vec{\imath}_p}} = \left(\mathcal{Y}_o\rho_o + \mathcal{Y}_g\rho_g + \mathcal{Y}_w\rho_w\right)_{\vec{\imath}_p} \quad \text{..... (4.11)}$$

$$\mu_{m_{\vec{\imath}_p}} = \left(\mathcal{Y}_o\mu_o + \mathcal{Y}_g\mu_g + \mathcal{Y}_w\mu_w\right)_{\vec{\imath}_p} \quad \text{..... (4.12)}$$

Connection fluid properties are averaged based on upstream and downstream pipe segment fluid property values and segment volume V. The following expression for a generic property ξ applies to connection phase holdup, density, viscosity, etc.

$$\xi_{\vec{\imath}_c} = \frac{(\xi V)_{\vec{\imath}_{p_{ups}}} + (\xi V)_{\vec{\imath}_{p_{downs}}}}{V_{\vec{\imath}_{p_{ups}}} + V_{\vec{\imath}_{p_{downs}}}} \quad \text{..... (4.13)}$$

Connection friction factor is calculated from Reynold's number, N_{Re}, for laminar flow ($N_{Re} \leq 2100$):

$$f_{f_{\vec{\imath}_c}} = \frac{16}{N_{Re_{\vec{\imath}_c}}} \quad \text{..... (4.14)}$$

For turbulent flow ($N_{Re} > 2100$), Chen's approximation of the Colebrook-White equation is used (Economides et al. 1993):

$$f_{f_{\vec{\imath}_c}} = \left\{ -4log\left\{ \frac{\epsilon_{\vec{\imath}_c}}{3.7065} - \frac{5.0452}{N_{Re_{\vec{\imath}_c}}} log\left[\frac{\epsilon_{\vec{\imath}_c}^{1.1098}}{2.8257} + \left(\frac{7.149}{N_{Re_{\vec{\imath}_c}}} \right)^{0.8981} \right] \right\} \right\}^{-1/2} \quad \text{..... (4.15)}$$

With,

$$N_{Re_{\vec{\imath}_c}} = \beta_{Re} \left(\frac{\vec{u}_m \rho_m D}{\mu_m} \right)_{\vec{\imath}_c} \quad \text{..... (4.16)}$$

$\epsilon_{\vec{\imath}_c}$ is network connection relative roughness, [dimensionless]

$\beta_{Re} = 124.01366$ is unit conversion factor for field units

Recall that in the network pipeline discretization, a connection is the link between pipe node segments. In general, there is a pressure drop residual for each connection n_{con} (excluding network inlets/outlets). However, if rate constraint boundary conditions are specified, the number of $R_{p_{C_{\vec{\imath}_c}}}$ equations could increase, as described in Section 4.5.

4.5 Network Boundary Conditions

Network pipeline systems commonly have multiple inlets and outlets, and boundary conditions (BC) have to be specified for each one of them. Hence, $n_{i/o}$ corresponds to the number of boundary conditions required to define the numerical system of equations.

Pressure or rate constraints can be established to control network production. For the system to be well-defined, appropriate conditions must be set. For example, in a network with one inlet and one outlet, two BC are required. Allowed BC combinations are pressure-pressure, pressure-rate, or rate-pressure; rate-rate is not allowed because it makes an ill-conditioned system. In case both, pressure and rate, constraints are specified for the same segment, the active BC can be identified applying the violation factor approach presented in Section 3.7.4.

For stand-alone network models, water cut and hydrocarbon composition must be also specified as BC. This is not a requirement for coupled models since the reservoir dictates produced composition and water cut.

4.5.1 Pressure Constraint

Pressure BC is specified by replacing the R_{HU_P} residual equation for the pipe segment in which the constraint is desired, e.g. $\vec{i}_p$. The updated residual is a function of pipe segment pressure and target pressure.

$$R_{HU_{P_{\vec{i}_p}}} = p_{\vec{i}_p} - p_{target} \quad \text{..... (4.17)}$$

4.5.2 Rate Constraint

Rate BC is specified by adding a R_{p_C} residual equation for the inlet/outlet connection in which the constraint is desired, e.g. $\vec{i}_c$. Rate control is specified for the desired phase (oil, gas, or water) evaluated at standard conditions $Q_{\alpha_{target}}$ and phase density $\rho_{\alpha_{SC}}$ (evaluated

from EOS). $\dot{m}_{\alpha\vec{i}_c}$ represents the connection mass rate for phase α, which is a function of phase velocity, holdup, and density at connection pressure and temperature.

$$R_{p_{C\vec{i}_c}} = \dot{m}_{\alpha\vec{i}_c} - Q_{\alpha_{target}}\rho_{\alpha_{SC}} \quad \text{..... (4.18)}$$

The final number of R_{p_C} equations for the network system depends on number of connections n_{con}, inlets/outlets, and number of rate BC specified ($n_{Q_{BC}}$) for them.

$$n_{R_{p_C}} = n_{con} + n_{Q_{BC}} \quad \text{..... (4.19)}$$

4.5.3 Water Cut Constraint

Water cut BC is specified by replacing the R_{w_P} residual equation for the pipe segment in which the constraint is desired, e.g. $\vec{i}_p$. The updated residual is a function of pipe segment water cut calculated at standard conditions ($\mathcal{Y}^{SC}_{w_{\vec{i}_p}}$) and target water cut ($W_{cut_{target}}$). Calculation of $\mathcal{Y}^{SC}_{w_{\vec{i}_p}}$ involves flashing fluids from pipe segment conditions to standard conditions to calculate water ratio in the segment at surface conditions.

$$R_{w_{P_{\vec{i}_p}}} = \mathcal{Y}^{SC}_{w_{\vec{i}_p}} - W_{cut_{target}} \quad \text{..... (4.20)}$$

4.5.4 Hydrocarbon Composition Constraint

Hydrocarbon composition BC is specified by replacing the R_{i_P} residual equations for the pipe segment in which the constraint is desired, e.g. $\vec{i}_p$. The updated residual is a function of pipe segment composition and target composition.

$$R_{i_{P_{\vec{i}_p}}} = z_{i_{\vec{i}_p}} - z_{i_{target}} \quad ; \quad i = 1 \; to \; n_c \quad \text{..... (4.21)}$$

4.6 Structure of Network Numerical Solution

The network simulator consists of multiple subroutines performing calculations in a robust algorithm to model production performance of network system, from bottomhole to

separator, under a wide variety of scenarios and conditions. The network simulation workflow follows the same structure as the reservoir simulator, summarized in Fig. 3.3.

Input data includes number of network pipe segments and connections, segment geometry (length, connection diameters, depth, relative roughness), compositional fluid properties, and production constraints, and finally, initial pressure, velocity, composition, and water holdup for each segment. Quality check (QC) is performed on input data to ensure consistency in all parameters, including vector dimensions, normalized compositions, consistent length/depth relationships, etc. Miscellaneous calculations comprise computation of generic variables required for simulation and parallel processing setup. The initialization routine is in charge of calculating independent variable values ($F_{i_P}, W_P, lnK_{i_P}, f_{v_P}$) from provided initial conditions ($p_{P_{init}}, z_{i_{init}}, y_{w_{P_{init}}}$). This process is performed based on EOS calculations and fundamental relationships. If the simulation restart option is used, the initialization routine assigns corresponding independent variable values from the restart file.

4.6.1 Fully-Implicit Solution

Solution for the system of equations in a time-step is performed in a fully-implicit scheme (similar as shown in Fig. 3.4). A Newton-Raphson iterative process allows calculating new time values for the vector of unknowns $\vec{x}_{NET}^{k}$. The residual vector $\vec{R}_{NET}$ is calculated based on independent variables values and application of boundary conditions. The Jacobian $\vec{\vec{J}}_{NET}$ is computed numerically and the system of equations is solved using direct, conjugate gradient, generalized minimal residual, or biconjugate gradient stabilized method, implemented from MATLAB® libraries (MathWorks 2014). Updated values are obtained for $\vec{x}_{NET}^{k+1}$ and the iteration process is performed until a specified number of iterations or until convergence. If convergence is not reached, time-step size is reduced, independent variable values are reset, and iteration process is resumed. When convergence is achieved, solution vector is updated and saved, time-step size is increased by a user-defined factor, and simulation continues until final desired time.

4.6.2 Vector of Network Unknowns

Vector of unknowns is formed by independent variables in the system. Node variables for all network segments are arranged first and connection velocities are left at the end of the vector. Main reason for this approach is to facilitate tracking the arrangement of variables, since number of R_{p_C} equations depends on specified boundary conditions, which can change during the simulation. Notice that independent variables related to compositional values ($ln\vec{K}_{i_P}$ and $\vec{F}_{i_P}$) are vectors for $i = 1\ to\ n_c$, ordered as a column vector for each network segment.

$$\vec{x}_{NET} = \begin{bmatrix} \vec{x}_{pipe} \\ \vec{x}_{con} \end{bmatrix} \quad ; \quad \vec{x}_{pipe} = \begin{bmatrix} ln\vec{K}_{i_P} \\ p_P \\ \vec{F}_{i_P} \\ W_P \\ f_{v_P} \end{bmatrix}_{\forall(\vec{\imath}_p)} \quad ; \quad \vec{x}_{con} = \left[\vec{u}_{m_C}\right]_{\forall(\vec{\imath}_c)} \qquad \text{..... (4.22)}$$

The size of network vector of unknowns is a function of number of pipe segments n_{pipe}, number of components n_c, and number of R_{p_C} equations ($n_{R_{p_C}}$).

$$size(\vec{x}_{NET}) = n_{NET_{eq}} = n_{pipe}(2n_c + 3) + n_{R_{p_C}} \text{ ..... (4.23)}$$

4.6.3 Vector of Network Residuals

Analogously to the vector of unknowns, vector of network residuals $\vec{R}_{NET}$ is formed by pipe segment residual equations, followed by R_{p_C} residuals for all connections. The size of $\vec{R}_{NET}$ equals $n_{NET_{eq}}$.

$$\vec{R}_{NET} = \begin{bmatrix} \vec{R}_{pipe} \\ \vec{R}_{con} \end{bmatrix} \quad ; \quad \vec{R}_{pipe} = \begin{bmatrix} \vec{R}_{fug_{i_P}} \\ R_{HU_P} \\ \vec{R}_{i_P} \\ R_{w_P} \\ R_{RR_P} \end{bmatrix}_{\forall(\vec{\imath}_p)} \quad ; \quad \vec{R}_{con} = \left[R_{p_C}\right]_{\forall(\vec{\imath}_c)} \text{ ..... (4.24)}$$

4.6.4 Network Jacobian Calculation

The Jacobian represents the change of residual equations with respect to independent variables. In this study, the Jacobian is computed numerically by adding a small perturbation to each independent variable to calculate its respective derivative. The size of resulting Jacobian is $n_{NET_{eq}} \times n_{NET_{eq}}$.

$$\vec{\vec{J}} = \left[\frac{\partial \vec{R}_{NET}}{\partial \vec{x}_{NET}}\right] = \begin{bmatrix} \frac{\partial \vec{R}_{pipe}}{\partial \vec{x}_{pipe}} & \frac{\partial \vec{R}_{pipe}}{\partial \vec{x}_{con}} \\ \frac{\partial \vec{R}_{con}}{\partial \vec{x}_{pipe}} & \frac{\partial \vec{R}_{con}}{\partial \vec{x}_{con}} \end{bmatrix} \quad \text{..... (4.25)}$$

A sample template of the Jacobian for a reservoir gridblock was presented previously in Eq. (3.78). Network Jacobian elements can be arranged following a similar approach.

Fig. 4.2 displays a sample Jacobian for a network model from bottomhole to separator. The production system has 23 pipe segments, 22 connections, 1 inlet and 1 outlet, and 8 components fluid description. Boundary conditions are defined as bottomhole flowing pressure (at pipe segment $\vec{\imath}_p = 1$) and separator oil rate (at outlet connection $\vec{\imath}_c = 24$). Given that no rate BC was defined at inlet connection ($\vec{\imath}_c = 1$), this equation is removed from the solution. For this network example, $n_{NET_{eq}} = 460$, with $n_{R_{p_C}} = 23$. Total number of non-zero elements in the Jacobian is 14,717. Gray shading depicts pipe segment derivatives, pink denotes connection derivatives, and green interactions between segment and connection elements.

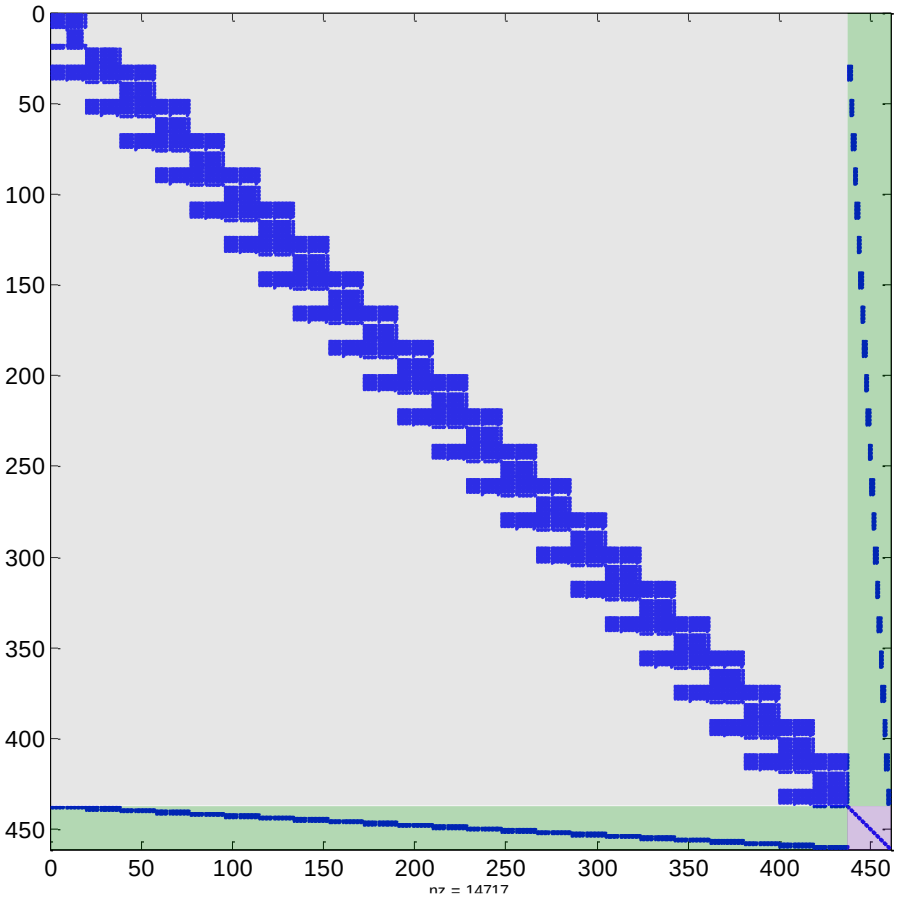

Fig. 4.2—Jacobian matrix sample for a network system with 23 segments, 22 connections, 2 inlet/outlet, and 8 components fluid description. Bottomhole flowing pressure and separator oil rate are specified as boundary conditions. Total system size is 460x460 with 14,717 non-zero elements. Gray shading depicts pipe segment derivatives, purple shade shows connection derivatives, and green shade interaction between pipe segments and connection variables.

4.6.5 Convergence Criteria

Consistency test in the solution for the network system of equations is performed using same criteria presented for reservoir and MSW (Section 3.8.5). Physical limits are checked for pressure and phase holdups ($p_P > 14.7\ psia$ and $0 \leq y_{\alpha_P} \leq 1$). Residuals norm must be small $\left\|\vec{R}_{NET}\right\|_2 \rightarrow 0$.

Finally, pressure and phase fugacity changes within iterations must satisfy the following constraints (Schlumberger 2014). Liquid and vapor fugacities for each component ($\hat{f}_i^l$ and $\hat{f}_i^v$) are calculated from fundamental relationships and EOS, see Appendix A for details.

$$\left\| p_P^{k+1} - p_P^k \right\|_2 \leq \varepsilon_p \quad ; \quad \varepsilon_p = 1.47 \quad \text{..... (4.26)}$$

$$\left\| \hat{f}_{i_P}^{l\,k+1} - \hat{f}_{i_P}^{l\,k} \right\|_2 \leq \varepsilon_f \quad ; \quad \varepsilon_f = 0.001 \quad \text{..... (4.27)}$$

$$\left\| \hat{f}_{i_P}^{v\,k+1} - \hat{f}_{i_P}^{v\,k} \right\|_2 \leq \varepsilon_f \quad ; \quad \varepsilon_f = 0.001 \quad \text{..... (4.28)}$$

4.7 Pipeline Asphaltene Modeling

Asphaltene precipitation and deposition in the network system is performed in a sequential process after convergence has been reached for the time-step. The fully-implicit numerical solution is completed through the Newton-Raphson iterative process, followed by asphaltene deposition modeling evaluation (**Fig. 4.3**). During the iteration process, the fluid properties are calculated using the VLE calculation, assuming asphaltene is dissolved in the hydrocarbon liquid phase. For the asphaltene deposition model, a rigorous vapor/liquid/liquid-dense (VLLE) calculation is performed with PR-EOS to determine asphaltene precipitation and phase properties. A material balance assessment certifies consistency of the deposition process by evaluating mass inlet, outlet, accumulated, and asphaltene deposited during the time-step. If the material balance error criterion is satisfied, the simulation proceeds to the new time-step, otherwise the iterative process is resumed.

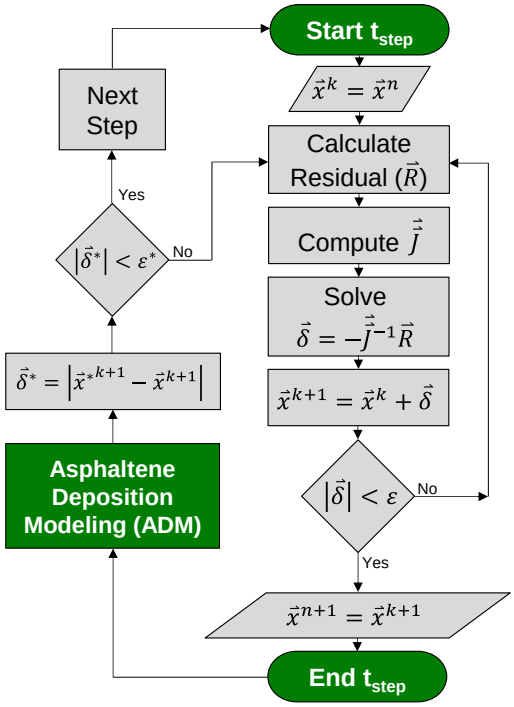

Fig. 4.3—Asphaltene modeling sequential approach. Fully-implicit network solution is followed by asphaltene deposition evaluation. Material balance assessment is checked to ensure consistency before proceeding to new time-step.

The Asphaltene Deposition Modeling (ADM) routine, shown in **Fig. 4.4**, is comprised of three general procedures. First, three-phase VLLE using PR-EOS is calculated to assess if asphaltene precipitates and quantify asphaltene molar fraction, concentration, and amount of material precipitated. Next, asphaltene accretion to the pipe wall is calculated with a mechanistic transport model based of asphaltene concentration, fluid velocity, pipe connection properties, temperature, etc. Finally, independent variables are updated based on new fluid compositions resulting after solid asphaltene deposition.

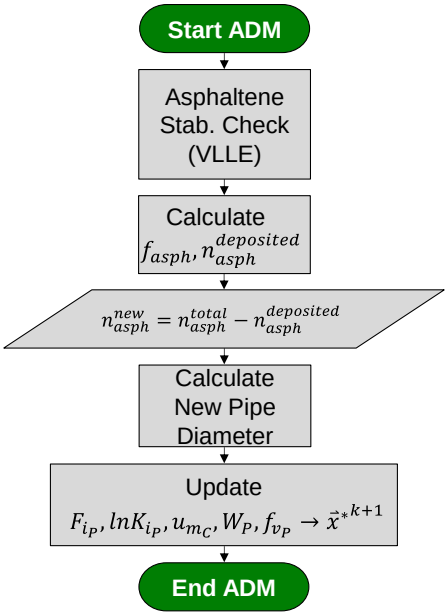

Fig. 4.4—Asphaltene Deposition Modeling (ADM) routine workflow. Asphaltene stability check is performed via VLLE (3-phase flash). Asphaltene deposit is calculated with a mechanistic transport model and pipe segment diameter and fluid properties are updated.

The total amount of asphaltene (n_{asph}^{total}) consists of asphaltene still dissolved in the liquid hydrocarbon and the precipitated portion. Only a fraction of the precipitated asphaltene ultimately deposits onto the pipe wall ($n_{asph}^{deposited}$). The remaining asphaltene (n_{asph}^{new}) continues flowing with the oil. For purposes of the new time-step iteration process, it is assumed to redissolve in the liquid hydrocarbon phase.

4.7.1 Asphaltene Three-Phase Flash (Precipitation)

The VLLE approach is based on a three-phase flash using PR-EOS. The asphaltene component is present dissolved in the hydrocarbon liquid phase or as a precipitate forming a liquid-dense phase. The liquid-dense phase is assumed to be composed only by asphaltene (Pedersen and Christensen 2006).

Equilibrium calculations require component fugacities of all phases to be equal. The VLLE method assumes asphaltene component is not present in the vapor phase, hence

only liquid and liquid-dense phases fugacities must reach equilibrium for the asphaltene component.

$$\begin{matrix} \hat{f}_i^l = \hat{f}_i^v & for & i \neq asphaltene \\ \hat{f}_i^l = f_i^{ld} & for & i = asphaltene \end{matrix} \quad \text{..... (4.29)}$$

Material balance for the system is satisfied by phase molar fractions (f_α) summing to unity, overall molar composition (z_i), and phase molar compositions (x_i and y_i).

$$f_v + f_l + f_{ld} = 1 \quad \text{..... (4.30)}$$

$$z_i = \begin{cases} f_v y_i + f_l x_i & for \quad i \neq asphaltene \\ f_l x_i + f_s & for \quad i = asphaltene \end{cases} \quad \text{..... (4.31)}$$

The general procedure to solve the VLLE flash with asphaltene precipitation is displayed in **Fig. 4.5**, adapted from Gonzalez (2013). Pressure, temperature, and fluid overall composition are used to calculate a conventional VLE (assuming two-phase equilibrium). Three possible scenarios exist: 100% vapor, two-phase liquid/vapor, and 100% liquid. If the fluid is in vapor phase only, no asphaltene precipitates from the mixture and calculation is complete.

The other two scenarios, resulting liquid phase (single or two-phase) existence require a second stability test to assess if conditions to trigger asphaltene precipitate exist, evaluated with Eq. (4.32). If asphaltene is found to precipitate, a new overall composition for asphaltene component still dissolved in the liquid is calculated with Eq. (4.33), the composition is renormalized, and the iterative process continues until equilibrium criterion in Eq. (4.34) is satisfied. Typically, $\varepsilon_{asph} = 1 \times 10^{-10}$.

$$\hat{f}_{asph}^l > f_{asph}^{ld} \rightarrow Asphaltene\ Precipitates \quad \text{..... (4.32)}$$

$$z_{asph}^{k+1} = z_{asph}^{k} \frac{f_{asph}^{ld}}{\hat{f}_{asph}^{l}} \quad \text{..... (4.33)}$$

$$\left| ln\left(\frac{\hat{f}_{asph}^{l}}{f_{asph}^{ld}} \right) \right| < \varepsilon_{asph} \rightarrow Asphaltene\ in\ Equilibrium \quad \text{..... (4.34)}$$

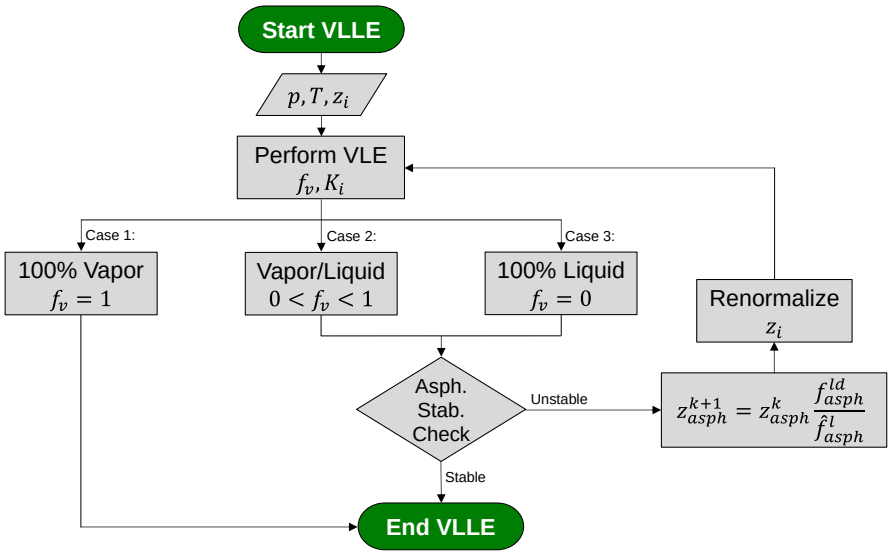

Fig. 4.5—Vapor/liquid/liquid-dense three-phase flash for asphaltene precipitation workflow. With pressure, temperature, and composition as input, a VLE flash determines presence of liquid and vapor phases. A secondary stability analysis is performed to assess asphaltene precipitation from liquid phase. (Adapted from Gonzalez (2013))

Finally, the liquid-dense phase molar fraction is estimated with the new and original overall asphaltene molar composition, as shown in Eq. (4.35). The final liquid molar fraction is updated accounting the asphaltene precipitate fraction from the original liquid molar fraction with Eq. (4.36). The original composition, and liquid molar fraction, corresponds to the unaltered composition used as input.

$$f_{ld} = \frac{z_{asph}^{new} - z_{asph}^{orig}}{z_{asph}^{new} - 1} \quad \text{..... (4.35)}$$

$$f_l^{new} = f_l^{orig}(1 - f_{ld}) \quad \text{..... (4.36)}$$

4.7.2 Asphaltene Transport Model (Deposition)

Asphaltene deposition, or accretion, in the internal pipeline wall (ignoring electrokinetic forces) depends on three transport mechanisms: diffusion, inertia, and impaction. Selection of dominant mechanism is based on flow velocity, pipe properties (e.g. diameter, relative roughness, etc.), fluid density and viscosity, and asphaltene particle density and diameter, used in the transport coefficient calculation.

The asphaltene accretion rate can be expressed in terms of sticking probability, transport coefficient, and asphaltene molar concentration gradient (Kern and Seaton 1959).

$$\dot{n}_{asp_{wall}} = SP\, K_t \left(\tilde{C}_b - \tilde{C}_{wall}\right) \quad \text{..... (4.37)}$$

Where,

$\dot{n}_{asp_{wall}}$ is asphaltene accretion rate, [lbmol/ft^2/s]

SP is sticking probability, [dimensionless]

K_t is transport coefficient, [ft/s]

$\tilde{C}_b$ is bulk fluid precipitated asphaltene molar concentration, [lbmol/ft^3]

$\tilde{C}_{wall}$ is deposited asphaltene molar concentration, [lbmol/ft^3]

Asphaltene accretion to the internal pipe wall is assumed irreversible, i.e. once asphaltene is deposited it is considered part of the tubular and it is no longer in equilibrium with the fluid. Under this assumption, the asphaltene concentration at the wall is zero at the end of the ADM calculation.

The sticking parameter is defined as an Arrhenius-type correlation based on adhesion and drag forces, and two tunable parameters (K_d and E_a) that can be used to match laboratory and field data (Watkinson 1968). Activation energy refers to the minimum necessary

energy for the asphaltene particle transport from bulk to wall, while the frequency factor is related to incidence of molecule collisions.

$$SP = K_d \frac{e^{-E_a RT_K}}{u_{m_C}^2} \quad \text{..... (4.38)}$$

With,

K_d as frequency factor constant, [ft^2/s^2]

E_a as activation energy, [kJ/kgmol]

T_K as absolute temperature, [K]

u_{m_C} as pipe connection fluid velocity, [ft/s]

$R = 8.31446$ as gas constant, [J/K/mol]

The transport coefficient K_t accounts for particle velocity from the fluid bulk to the wall as a function of fluid velocity, friction factor, and the dimensionless transport coefficient K_t^+ (Papavergos and Hedley 1984).

$$K_t = K_t^+ u_{m_C} \sqrt{f_f/2} \quad \text{..... (4.39)}$$

$$K_t^+ = \begin{cases} 0.07Sc^{-2/3} & for \quad t_p^+ < 0.2 \\ 0.00035\left(t_p^+\right)^2 & for \quad 0.2 \le t_p^+ \le 10 \\ 0.18 & for \quad 10 < t_p^+ \end{cases} \quad \text{..... (4.40)}$$

The identification and selection criteria for the three main transport mechanisms, namely diffusion ($t_p^+ < 0.2$), inertia ($0.2 \le t_p^+ \le 10$), and impaction ($10 < t_p^+$), are based on Stoke's stopping distance, or dimensionless relaxation time, t_p^+.

$$t_p^+ = \beta_{t_p} \frac{\rho_p d_p^2}{18} \frac{\rho_m u_{m_C}^2 f_f/2}{\mu_m^2} \quad \text{..... (4.41)}$$

With the Schmidt number Sc representing the ratio of viscous to mass diffusivity as a function of fluid properties and Brownian diffusivity, D_B.

$$Sc = \beta_{Sc} \frac{\mu_m}{\rho_m D_B} \quad \text{..... (4.42)}$$

The Brownian diffusivity can be calculated from the Stokes-Einstein equation (Bird et al. 2002):

$$D_B = \beta_{D_B} \frac{\kappa_B T_K}{3\pi \mu_m d_p} \quad \text{..... (4.43)}$$

Where,

ρ_p is asphaltene particle density, [lb/ft^3]

d_p is asphaltene particle diameter, [µm (micrometer)]

ρ_m is fluid mixture density, [lb/ft^3]

μ_m is fluid mixture viscosity, [cP]

$\kappa_B = 1.3806 \times 10^{-23}$ is Boltzmann's constant, [J/K]

$\beta_{t_p} = 2.3838 \times 10^{-5}$ is unit conversion constant for relaxation time equation

$\beta_{Sc} = 6.7197 \times 10^{-4}$ is unit conversion constant for Schmidt number equation

$\beta_{D_B} = 1.0764 \times 10^{10}$ is unit conversion constant for Brownian diffusivity equation

This model for solids transport is calculated and applied at each network pipe connection, where velocities are evaluated. A connection is formed by the union of upstream and downstream half pipe segments and connection fluid properties must be used in the calculations. An advantage of using this discretization and evaluation approach is that pipe diameter changes occur at the node location, leaving connection diameter equal for the upstream and downstream half segments, making more consistent the diameter reduction calculation due to asphaltene deposition.

Finally, moles, mass, and volume of asphaltene deposited in the pipeline wall are calculated from the asphaltene accretion rate, flux area perpendicular to solid particle trajectory, and the time-step size.

$$n_{asp_{wall}} = \beta_{n_a} \dot{n}_{asp_{wall}} \pi D L \Delta t \quad \text{..... (4.44)}$$

$$m_{asp_{wall}} = n_{asp_{wall}} M_{w_{asph}} \quad \text{..... (4.45)}$$

$$V_{asp_{wall}} = \frac{n_{asp_{wall}}}{\tilde{\rho}_{asph}} \quad \text{..... (4.46)}$$

Where,

$n_{asp_{wall}}$ is moles of asphaltene deposited in the pipe wall, [lbmol]

$m_{asp_{wall}}$ is mass of asphaltene deposited in the pipe wall, [lb]

$V_{asp_{wall}}$ is volume of asphaltene deposited in the pipe wall, [ft^3]

$M_{w_{asph}}$ is molecular weight of asphaltene component, [lb/lbmol]

D is pipe connection diameter, [in]

L is pipe connection length, [ft]

Δt is time-step size, [day]

$V_{asp_{wall}}$ is volume of asphaltene deposited in the pipe wall, [ft^3]

$\beta_{n_a} = 7{,}200$ is the unit conversion constant

4.7.3 Variables Update

Asphaltene accretion to the pipe wall results in flow area reduction and relative roughness change due to surface properties of asphaltene layer. In addition, it is assumed that after the asphaltene fraction is deposited, it is no longer flowing with hydrocarbons in the pipeline, thus altering overall flowing fluid composition.

The first variable to be updated is network pipe connection diameter. Diameter reduction due to asphaltene deposition is a function of previous time level connection volume ($V_{i_c}^n$) and asphaltene deposit volume. Relative roughness for connections where asphaltene deposits is also updated. Pipe segment upstream and downstream diameters are updated based on new connection diameter calculation. Properties are left unchanged if no asphaltene precipitates, or deposits, in the connection.

$$D_{i_c}^{n+1} = 24\sqrt{\left(\frac{V^n - V_{asp_{wall}}}{\pi L}\right)_{i_c}} \quad \text{..... (4.47)}$$

Fluid composition update is performed in a serial process following fluid direction, starting a bottomhole (first network pipe connection) and ending at the separator. The total molar flow entering the connection during the time-step is calculated for each component.

$$n_{i_{i_c}}^{in} = 86{,}400\left(u_{m_c} A(1 - \not{y}_w)\tilde{\rho}_{HC} z_i\right)_{i_c} \Delta t \quad ; \quad i = 1 \; to \; n_c \quad \text{..... (4.48)}$$

The outlet moles of asphaltene for the time-step are estimated by subtracting the moles of asphaltene deposited from the inlet flow. The average composition is then calculated at the connection outlet to serve as inlet composition for the downstream connection.

$$n_{i_{i_c}}^{out} = \begin{cases} n_{i_{i_c}}^{in} & for \quad i \neq asphaltene \\ n_{i_{i_c}}^{in} - n_{asp_{wall i_c}} & for \quad i = asphaltene \end{cases} \quad \text{..... (4.49)}$$

Next, the updated compositions for each connection are flashed at pipe pressure and temperature to determine the new equilibrium ratios ($lnK_{i_P}^{n+1}$) and vapor fraction ($f_{v_P}^{n+1}$). Fluid velocity (u_{mC}^{n+1}) is also recalculated solving Eq. (4.48) with average hydrocarbon throughput and the new flow area, considering asphaltene deposit. Finally, hydrocarbon component mole ($F_{i_P}^{n+1}$) and water mass (W_P^{n+1}) contents are updated accounting the

remaining moles of each component after asphaltene is deposited and the new pipe volume after diameter reduction.

New independent variable values are used as input for the next time-step iteration process in the Newton-Raphson scheme.

CHAPTER V
COUPLED RESERVOIR-NETWORK SIMULATOR

Integrated asset modeling, coupling reservoir and network systems, provides better means to forecast production performance. Well productivity is constraint by reservoir and network conditions, which highlights the importance of characterizing interaction mechanisms in reservoir-well-network, multiple reservoirs producing to a single surface network, and flow assurance evaluation for solid deposition (asphaltene, hydrates, and waxes). Understanding such mechanisms facilitates the development of improved asset management strategies.

This chapter describes the formulation of reservoir-network tightly-coupled system implementing a fully-implicit solution method. The system of equations is comprised of reservoir, multi-segment wells, and network variables and residuals, solved simultaneously in a robust and stable scheme. Fluid compositional delumping from reservoir to network is performed to reduce computational cost while maintaining an accurate fluid description for pipeline asphaltene modeling.

5.1 Reservoir-Network Tightly-Coupled Formulation

The system of equations for reservoir and network systems are solved simultaneously, developing a tightly-coupled formulation. In addition, implementation of a fully-implicit solution method (Fig. 3.4) yields stable results during the simulation. The vector of independent variables, vector of residuals, and Jacobian array, are constructed by assembling reservoir, multi-segment wells (MSW), and network variables and equations.

Proper establishment of boundary conditions between the three components allows a simultaneous solution. The reservoir is connected to the MSWs via perforated intervals in the wellbore, while the upper-most well segment is connected to the network pipeline system. If the MSW system describes the entire wellbore, the connection is established at

the wellhead. More frequently, however, the connection is located at bottomhole reference depth to allow the implementation of especial network features such as artificial gas-lift, downhole chemical injection, asphaltene modeling, etc.

5.2 Selection of Coupled System Independent Variables

The coupled system independent variables is a collection of reservoir, MSW, and network components variables, displayed on **Table 5.1**. The total number of variables in the coupled system ($n_{COUP_{eq}}$) is the summation of variables from each component.

$$n_{COUP_{eq}} = n_{RES_{eq}} + n_{MSW_{eq}} + n_{NET_{eq}} \quad \text{..... (5.1)}$$

Table 5.1—INDEPENDENT VARIABLES FOR COUPLED SYSTEM OF EQUATIONS

System	Variable	Description
Reservoir	lnK_i	Natural logarithm of equilibrium ratio
	p_o	Oil-phase pressure
	F_i	Moles of component i per pore volume
	W	Mass of water per pore volume
	f_v	Vapor molar fraction
MSW	lnK_{i_S}	Natural logarithm of equilibrium ratio
	p_S	Well segment pressure
	F_{i_S}	Moles of component i per segment volume
	W_S	Mass of water per segment volume
	f_{v_S}	Vapor molar fraction
	u_{m_S}	Fluid velocity
Network	lnK_{i_P}	Natural logarithm of equilibrium ratio
	p_P	Network pipe segment pressure
	F_{i_P}	Moles of component i per segment volume
	W_P	Mass of water per segment volume
	f_{v_P}	Vapor molar fraction
	u_{m_C}	Fluid velocity at connection

5.3 Coupled System Boundary Conditions

The coupled system is usually controlled by wellbore and surface network constraints, e.g. target production rates, maximum water cut or gas-oil-ratio handling capacity, choke size,

system backpressure, etc. For a closed reservoir model, boundary conditions are set with well controls, or with MSW constraints, as developed on this study.

In coupled systems, MSW's top segment is connected to the network and the boundary condition must be set in the network wellhead, separator, or injection manifold. In addition, a consistent mathematical relationship must be established in the MSW-network link to ensure material balance and energy conservation when transferring produced fluids.

Mass transfer between MSW's top segment and connected network segment (subscripts MSW_1 and $NET_{\tilde{\imath}_p}$ respectively) is performed through sink/source terms in the conservation equations of well and network segment, as shown below. For a production well, water mass and hydrocarbon molar rate at MSW's top segment are calculated using convection terms presented in Eqs. (3.53) and (3.54). Calculated values are allocated to network segment source/sink terms in residual Eqs. (4.1) and (4.2).

$$\left(\dot{m}_{w_{s/s}}\right)_{NET_{\tilde{\imath}_p}} = (A\mathcal{Y}_w\rho_w\vec{u}_w)_{MSW_1} \quad \text{..... (5.2)}$$

$$\left(\dot{n}_{i_{s/s}}\right)_{NET_{\tilde{\imath}_p}} = A_{MSW_1}\left(\mathcal{Y}_o\tilde{\rho}_o x_i\vec{u}_o + \mathcal{Y}_g\tilde{\rho}_g y_i\vec{u}_g\right)_{MSW_1} \quad ; \quad i = 1\ to\ n_c \quad \text{..... (5.3)}$$

Mechanical energy balance at the link is provided by pressure (R_p) residuals. Following the previous example of a producer, the pressure residual for the top MSW segment is set to match the network connected segment pressure. Well-network connection depth (usually well's bottomhole reference depth) must equal both well and network segment depth to ensure conservation. A similar approach is performed for coupled injection wells, setting the network variables as upstream values transferring into the well segment.

$$R_{p_{MSW_1}} = p_{MSW_1} - p_{NET_{\tilde{\imath}_p}} \quad \text{..... (5.4)}$$

The network boundary condition at surface can be set as pressure or phase rate (presented in Section 4.5). Hydrocarbon composition constraint in coupled models is only required for compositional injection networks, since produced fluid composition is governed by reservoir and network thermodynamics. Multiple constraints can be specified along the network system, in such scenario, the active constraint is identified applying the violation factor approach presented in Section 3.7.4.

Compositional delumping at well-network link can be performed to reduce computational costs. Network fluid description is usually more detailed (larger number of components or pseudocomponents) than reservoir description to allow better modeling of complex phase behavior in surface facilities equipment. This method is particularly relevant when modeling asphaltene precipitation and deposition in the pipeline system, where accurate fluid characterization is crucial for accurate forecasts.

Component mapping is used in this study to lump (injection networks) or delump (production networks) fluid characterization at the well-network link. A split fraction, ranging from zero to one, is set for each reservoir and network component, providing a map for component relationships. This application is presented in the Results Chapter.

5.4 Vector of Coupled System Unknowns

The vector of independent variables $\vec{x}$ for the coupled system is constructed from reservoir, MSW, and network independent variables from Eqs. (3.73) and (4.22). The variables are arranged as a column vector, see below. The size of the vector of unknowns is $n_{COUP_{eq}}$.

$$\vec{x} = \begin{bmatrix} \vec{x}_{RES} \\ \vec{x}_{MSW} \\ \vec{x}_{NET} \end{bmatrix} \quad \text{..... (5.5)}$$

5.5 Vector of Coupled System Residuals

Similarly to $\vec{x}$, the vector of residuals $\vec{R}$ is formed from reservoir, MSW, and network residual equations for each discrete element, arranged in the order presented previously. The size of $\vec{R}$ also equals $n_{COUP_{eq}}$.

$$\vec{R} = \begin{bmatrix} \vec{R}_{RES} \\ \vec{R}_{MSW} \\ \vec{R}_{NET} \end{bmatrix} \quad \text{..... (5.6)}$$

5.6 Coupled System Jacobian Calculation

The change of residual equations with respect to independent variables is represented by the Jacobian matrix. Following the same approach of reservoir and network stand-alone formulations, the Jacobian is computed numerically by adding a small perturbation to each independent variable to calculate its respective derivative. The size of resulting Jacobian is $n_{COUP_{eq}} \times n_{COUP_{eq}}$.

$$\vec{\vec{J}} = \left[\frac{\partial \vec{R}}{\partial \vec{x}}\right] = \begin{bmatrix} \frac{\partial \vec{R}_{RES}}{\partial \vec{x}_{RES}} & \frac{\partial \vec{R}_{RES}}{\partial \vec{x}_{MSW}} & \frac{\partial \vec{R}_{RES}}{\partial \vec{x}_{NET}} \\ \frac{\partial \vec{R}_{MSW}}{\partial \vec{x}_{RES}} & \frac{\partial \vec{R}_{MSW}}{\partial \vec{x}_{MSW}} & \frac{\partial \vec{R}_{MSW}}{\partial \vec{x}_{NET}} \\ \frac{\partial \vec{R}_{NET}}{\partial \vec{x}_{RES}} & \frac{\partial \vec{R}_{NET}}{\partial \vec{x}_{MSW}} & \frac{\partial \vec{R}_{NET}}{\partial \vec{x}_{NET}} \end{bmatrix} = \begin{bmatrix} \frac{\partial \vec{R}_{RES}}{\partial \vec{x}_{RES}} & \frac{\partial \vec{R}_{RES}}{\partial \vec{x}_{MSW}} & 0 \\ \frac{\partial \vec{R}_{MSW}}{\partial \vec{x}_{RES}} & \frac{\partial \vec{R}_{MSW}}{\partial \vec{x}_{MSW}} & \frac{\partial \vec{R}_{MSW}}{\partial \vec{x}_{NET}} \\ 0 & \frac{\partial \vec{R}_{NET}}{\partial \vec{x}_{MSW}} & \frac{\partial \vec{R}_{NET}}{\partial \vec{x}_{NET}} \end{bmatrix} \quad \text{..... (5.7)}$$

The Jacobian characterizes the derivatives of residual equations with respect to independent variables for the following nine interacting systems:

- <u>*Reservoir-Reservoir*</u> ($\partial \vec{R}_{RES}/\partial \vec{x}_{RES}$): Matrix location (1,1) within Jacobian. Square matrix size $n_{RES_{eq}} \times n_{RES_{eq}}$.
- <u>*Reservoir-MSW*</u> ($\partial \vec{R}_{RES}/\partial \vec{x}_{MSW}$): Matrix location (1,2) within Jacobian. Rectangular matrix size $n_{RES_{eq}} \times n_{MSW_{eq}}$.

- *Reservoir-Network* ($\partial\vec{R}_{RES}/\partial\vec{x}_{NET}$): Matrix location (1,3) within Jacobian. Rectangular matrix size $n_{RES_{eq}} \times n_{NET_{eq}}$. All elements are zero since there is no direct link between reservoir and network elements.
- *MSW-Reservoir* ($\partial\vec{R}_{MSW}/\partial\vec{x}_{RES}$): Matrix location (2,1) within Jacobian. Rectangular matrix size $n_{MSW_{eq}} \times n_{RES_{eq}}$.
- *MSW-MSW* ($\partial\vec{R}_{MSW}/\partial\vec{x}_{MSW}$): Matrix location (2,2) within Jacobian. Square matrix size $n_{MSW_{eq}} \times n_{MSW_{eq}}$.
- *MSW-Network* ($\partial\vec{R}_{MSW}/\partial\vec{x}_{NET}$): Matrix location (2,3) within Jacobian. Rectangular matrix size $n_{MSW_{eq}} \times n_{NET_{eq}}$.
- *Network-Reservoir* ($\partial\vec{R}_{NET}/\partial\vec{x}_{RES}$): Matrix location (3,1) within Jacobian. Rectangular matrix size $n_{NET_{eq}} \times n_{RES_{eq}}$. All elements are zero since there is no direct link between reservoir and network elements.
- *Network-MSW* ($\partial\vec{R}_{NET}/\partial\vec{x}_{MSW}$): Matrix location (3,2) within Jacobian. Rectangular matrix size $n_{NET_{eq}} \times n_{MSW_{eq}}$.
- *Network-Network* ($\partial\vec{R}_{NET}/\partial\vec{x}_{NET}$): Matrix location (3,3) within Jacobian. Square matrix size $n_{NET_{eq}} \times n_{NET_{eq}}$.

Fig. 5.1 displays a sample Jacobian for a coupled system including reservoir, MSW, and network components. The reservoir model is 10x10x3 gridblocks with six components ($n_{RES_{eq}} = 4{,}500$). One producer MSW with 3 segments is defined ($n_{MSW_{eq}} = 48$). The production network has 23 pipe segments, 22 connections, and 1 outlet, with a 8-component fluid description. Boundary condition is defined as separator pressure, at pipe segment $\vec{\imath}_p = 23$ ($n_{NET_{eq}} = 459$). The total number of independent variables in the coupled solution are $n_{COUP_{eq}} = 5{,}007$. Color shadings depict each of the nine matrix components previously detailed.

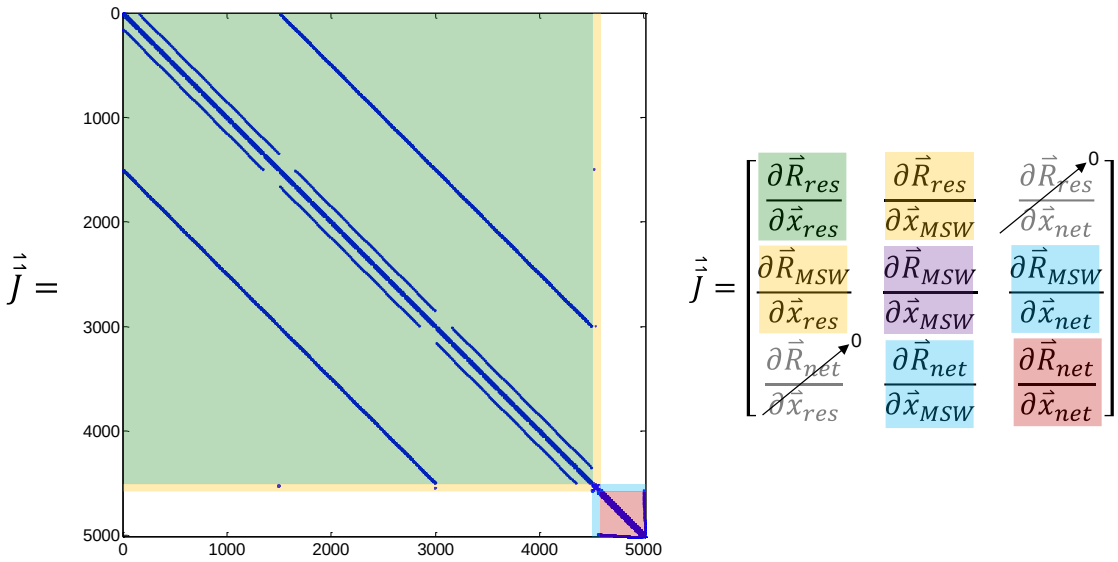

Fig. 5.1—Coupled system Jacobian matrix sample. Reservoir model with 10x10x3 gridblocks with 6-component fluid. Producer MSW with 3 segments. Network system with 23 segments, 22 connections, 1 outlet, and 8 components fluid description. Separator pressure specified as boundary condition. Total system size is 5,007x5,007 elements. Green shading depicts reservoir derivatives, purple shade shows MSW derivatives, and pink shade network derivatives. Yellow and cyan shades depict interactions between reservoir-MSW and MSW-network respectively. White rectangular matrices depict reservoir-network with no direct linkage, represented by all-zero elements.

5.7 Coupled System Convergence Criteria

Convergence criteria for the coupled system is comprised of reservoir, MSW, and network elements (Sections 3.8.5 and 4.6.5). Pressure, fugacity, and physical ranges are honored for all elements in the system.

CHAPTER VI
DESCRIPTION OF SIMULATION MODELS

The development of proposed new simulator allows modeling a wide variety of scenarios forecasting production performance and impact of asphaltene deposition in network pipelines. This chapter details reservoir and network models created to analyze key mechanisms involved in flow assurance evaluations. Description includes reservoir static model, multi-segment wells (MSW) properties, network topology and pipe segment properties, and fluid equation of state (EOS) characterization.

6.1 Reservoir Model Description

A synthetic reservoir model with heterogeneous and anisotropic permeability distribution represents the base case of study for the simulation sensitivities. **Fig. 6.1** shows the dimensions of the reservoir model, a 40-acre area representing a quarter of an inverted five-spot pattern with a thickness of 90 ft. The model is spatially discretized in 15x15x3 gridblocks of equal dimensions, length and width of 88 ft and thickness of 30 ft respectively, as summarized in **Table 6.1**.

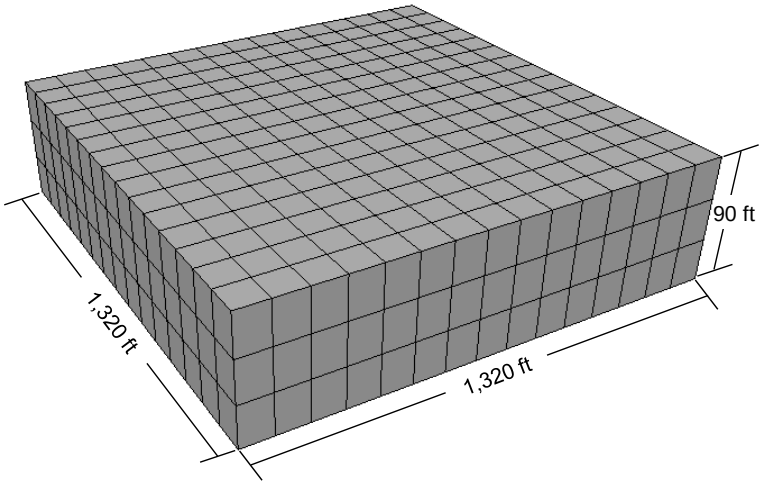

Fig. 6.1—Reservoir model dimensions. Areal extension of the reservoir is 40 acres and the thickness is 90 ft

Table 6.1—RESERVOIR MODEL DIMENSIONS AND GRIDBLOCK DISCRETIZATION

Property	Value
Length, ft	1,320
Width, ft	1,320
Thickness, ft	90
Grid size x-direction, ft	88
Grid size y-direction, ft	88
Grid size z-direction, ft	30
Gridblocks in x direction	15
Gridblocks in y direction	15
Gridblocks in z direction	3

6.1.1 Reservoir Static Properties

The top of the reservoir is located at 2,665 ft TVD (true vertical depth). Initial pressure of 8,868 psia, porosity of 20%, and water saturation of 35% are set for all gridblocks. Reservoir temperature is 200 °F. The high value of initial pressure, for the given reservoir depth, is set to study the effect of depletion process on asphaltene deposition in network pipelines.

Fig. 6.2 displays well locations and the heterogeneous and anisotropic horizontal permeability distribution, with minimum value of 59.04 mD, geometric mean of 400.24 mD, and maximum of 3,246.00 mD. Each layer displays the same property distribution (Appendix C shows permeability values for each gridblock). Vertical to horizontal permeability ratio is 0.1. **Table 6.2** summarizes reservoir properties including water density at standard conditions (SC), rock compressibility at reference pressure, well locations, and fluids in place, for a simulation time of 365 days.

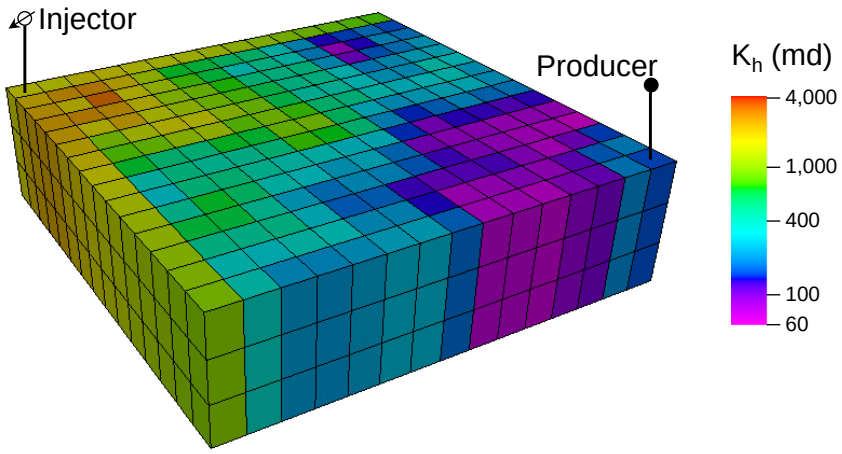

Fig. 6.2—Reservoir model heterogeneous and anisotropic permeability map. All three layers display the same property distribution. Injection and production wells are located at gridblock (1,1) and (15,15) respectively.

Table 6.2—RESERVOIR MODEL PROPERTIES

Property	Value
Reservoir top depth, ft	2,665
Porosity, fraction	0.2
k_h Geometric mean, mD	400.2
k_v/k_h, fraction	0.1
Initial water saturation, fraction	0.35
Initial gas saturation, fraction	0
Initial pressure, psia	8,868
Temperature, °F	200
Water density at SC, lb/ft^3	63.0
Rock compressibility, psia^{-1}	4x10^{-6}
Reference pressure, psia	5,868
Injector location	(1,1)
Producer location	(15,15)
Oil in place, MMSTB	3.30
Gas in place, MMSCF	929.48
Water in place, MMSTB	1.94
Simulated time, days	365

6.1.2 Saturation Functions

Relative permeability curves describe multiphase flow in porous media as a function of phase saturation. **Fig. 6.3** shows oil-water and oil-gas relative permeability curves. Oil-water system assumes gas saturation is zero, while oil-gas system measurements are taken

at connate water saturation ($S_{wc} = 0.16$). Three-phase relative permeabilities are calculated using Stone II method (Stone 1973), as previously described in Chapter III.

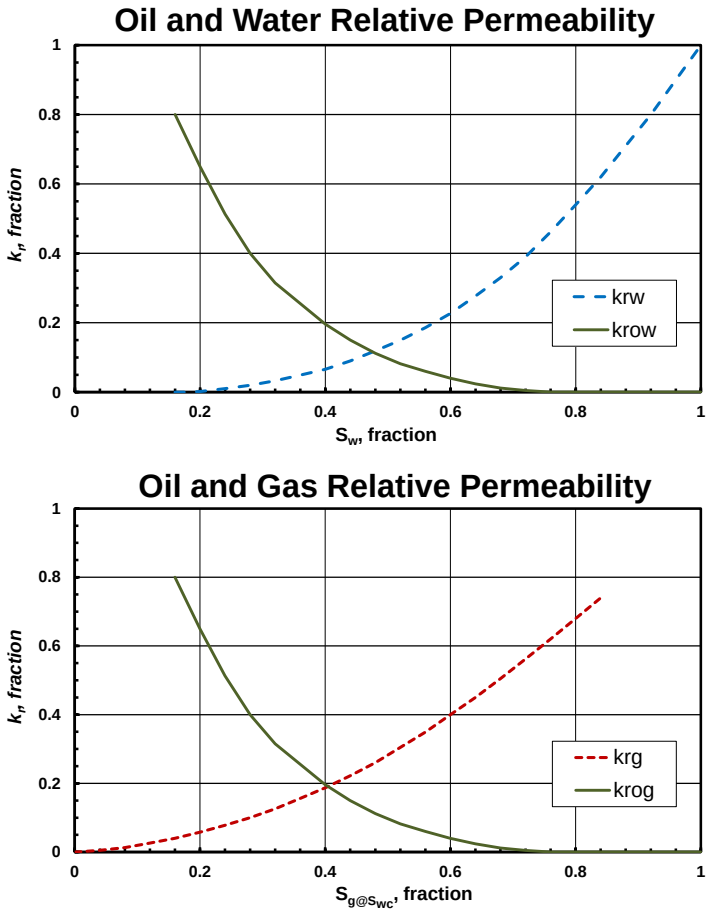

Fig. 6.3—Relative permeability curves for oil-water (top) and oil-gas (bottom) systems. Oil-water system assumes no gas saturation, while oil-gas system is measured at connate water saturation. Three-phase relative permeability is calculated using Stone II method.

Fig. 6.4 presents capillary pressure values for oil-water and gas-oil systems as a function of water saturation and gas saturation respectively. Tabulated values for saturation function are provided in Appendix C.

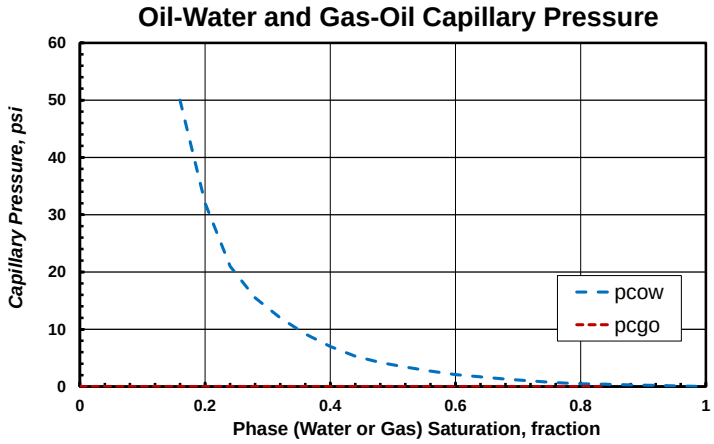

Fig. 6.4—Oil-water and gas-oil capillary pressure curves. Oil-gas capillary pressure is assumed zero for this conventional reservoir system.

6.1.3 MSW Properties

The reservoir model has two wells, a water injector defined in in gridblock (1,1) and a producer in gridblock (15,15). The injection well is perforated and completed through the entire reservoir thickness, while the producer is completed only in the top two layers (**Fig. 6.5**). Number of segments in each well is different, the injector is defined with four segments and the producer with three.

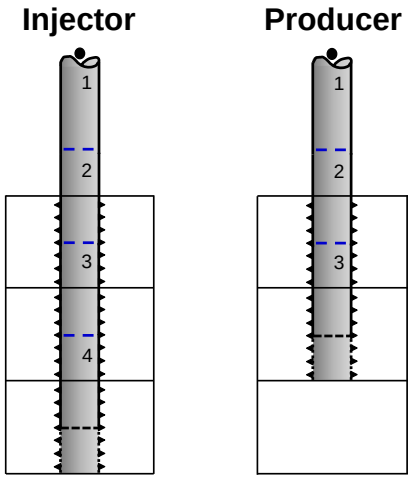

Fig. 6.5—Injector and producer MSW description. Injection well is perforated through the entire reservoir thickness, while the producer is completed in the top two layers. Injector is modeled with four segments and producer with three.

Table 6.3 provides additional properties for MSW description, including bottomhole reference depth, wellbore radius, segment dimensions and relative roughness, etc. Segments are oriented vertically and temperature of produced fluids is assumed to equal reservoir temperature of 200 °F while flowing though MSWs near the perforated region.

Table 6.3—INJECTOR AND PRODUCER MSW PROPERTIES

Property	Value
Reference depth, ft	2,625
Skin, dimensionless	0
Wellbore radius, ft	0.3
Top segment length, ft	25
Lower segments length, ft	30
Relative roughness, fraction	$5x10^{-4}$
Segment diameter, ft	0.6
Segment temperature, °F	200
Orientation	Vertical

6.2 Network Model Description

The network model is comprised of wellbore tubing and surface pipeline spanning from well bottomhole reference depth to production separator. Only the production network is modeled for the analyzed cases in this study.

6.2.1 Network Topology and Segment Properties

The production network, displayed in **Fig. 6.6**, is discretized in 23 segments and 24 connections to model flow from bottomhole reference depth of 2,625 ft (located at nodal point of segment #1) to wellhead (node segment #11) and separator (node segment #23). Wellbore section is vertical and surface pipeline horizontal.

Network pipe segments are 250 ft long. Internal diameter of wellbore tubing is 3 in (connections $\#1^c$-11^c), while surface pipeline is 4 in (connections $\#12^c$-24^c). Total network pipeline volume is 402 ft^3. Internal wall relative roughness is modified for segments where asphaltene deposits. Clean pipe and asphaltene accretion roughness values are provided in **Table 6.4**, along with network segment properties.

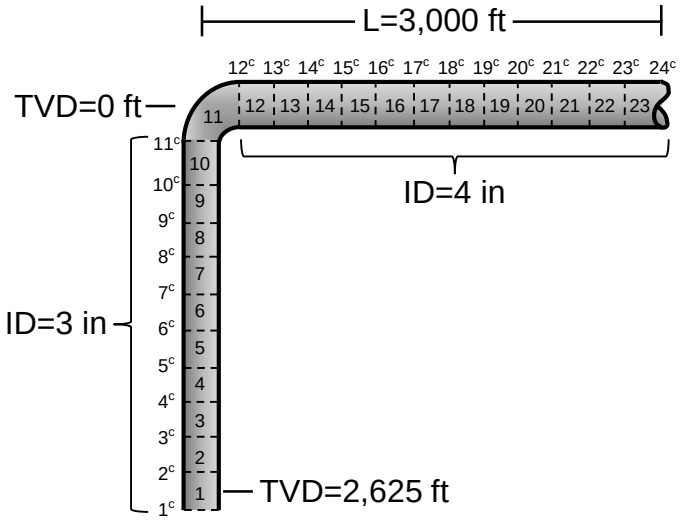

Fig. 6.6—Production network topology. Pipeline is discretized with 23 segments and 24 connections spanning from bottomhole reference depth to separator. A pipeline diameter change is located at wellhead (connection #12^c).

Table 6.4—NETWORK PIPELINE SEGMENT PROPERTIES

Property	Value
Segment length, ft	250
Tubing diameter (#1^c-11^c), in	3
Pipeline diameter (#12^c-24^c), in	4
Relative roughness, fraction	1.25×10^{-4}
Asphaltene rel. roughness, fraction	1.00×10^{-3}

6.2.2 Temperature Profile

Temperature variations along wellbore and surface pipeline are explicitly defined in this study, since heat transfer calculations are not incorporated in the numerical model. Temperature profiles can be calculated using a commercial software as a pre-process step. Sensitivities on temperature profile are performed in Chapter VII to assess the influence of this variable on asphaltene deposition profiles. The base case scenario for temperature profile has a linear temperature drop from bottomhole (200 °F) to wellhead (110 °F) with a gradient of 0.036 °F/ft (note that this value correspond to the internal tubing temperature gradient, not the geothermal gradient). From wellhead to separator the temperature gradient is 0.0018 °F/ft, yielding a separator temperature of 105 °F. **Fig. 6.7** illustrates the

network temperature vs. distance profile for the base case scenario. Temperature values are specified at the nodal point for each segment.

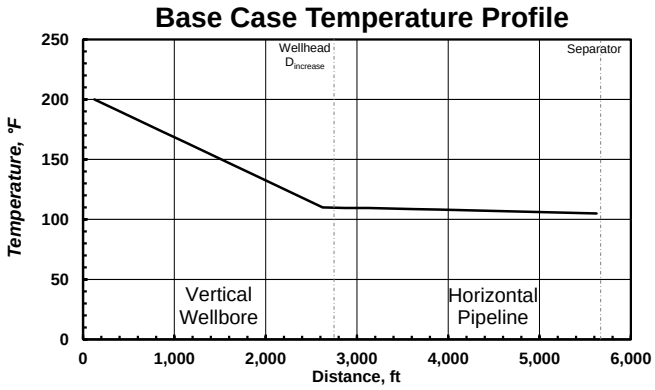

Fig. 6.7—Network temperature profile for base case scenario. Temperatures are specified at nodal point (center) of each segment. Bottomhole, wellhead, and separator temperatures are 200, 110, and 105 °F respectively. Linear temperature gradients in wellbore and surface are 0.036 and 0.0018 °F/ft respectively.

6.3 Fluid Description

Modeling complex fluid phase behavior, e.g. asphaltene precipitation, requires a good description and characterization of hydrocarbon components. The fluid description used in the simulation cases was first described with 12 components (or pseudocomponents) (Burke et al. 1990). Later, Gonzalez (2013) created a consistent 8-component description to enhance computational performance in reservoir simulation with asphaltene deposition modeling. The latter is used in this study to model fluid phase behavior in the network system.

All PVT analyses in this section were performed using in-house developed software in the Petroleum Engineering Department of Texas A&M University.

6.3.1 Hydrocarbon Fluid 8-Components Characterization

Complete compositional description for the 8-component fluid is provided in **Table 6.5 and Table 6.6**, detailing molecular weight, critical pressure and temperature, acentric

factor, critical compressibility factor (for viscosity calculation), volume translation factor, composition, and binary interaction coefficients (BIC).

Table 6.5—COMPOSITIONAL FLUID PROPERTIES FOR 8-COMPONENT EOS CHARACTERIZATION

Component	M_{w_i}	p_c (psia)	T_c (°F)	ω	Z_{crit}	δ_{shift}	z_i
CO_2	44.01	1,070.20	87.60	0.22500	0.27435	-0.01313	0.02460
C_1-N_2	16.23	664.70	-118.69	0.00849	0.28848	-0.09426	0.36940
C_2-C_3	37.59	658.63	152.12	0.12708	0.28510	-0.07819	0.07520
C_4	58.10	544.54	295.98	0.18780	0.27711	-0.01798	0.01930
C_5	72.20	490.21	377.48	0.23969	0.27048	-0.00501	0.01570
C_6	86.00	477.20	453.50	0.27500	0.28818	-0.02941	0.01620
C_{7+}	320.00	180.80	1,089.00	1.02200	0.28290	0.00974	0.47145
Asphaltene	800.00	178.30	2,105.00	1.44100	0.39341	0.01648	0.00815

Table 6.6—BINARY INTERACTION COEFFICIENTS FOR 8-COMPONENT FLUID EOS CHARACTERIZATION

BIC	CO_2	C_1-N_2	C_2-C_3	C_4	C_5	C_6	C_{7+}	Asph.
CO_2	0							
C_1-N_2	0	0						
C_2-C_3	0	0	0					
C_4	0	0	0	0				
C_5	0	0	0	0	0			
C_6	0	0	0	0	0	0		
C_{7+}	0	0.053	0	0	0	0	0	
Asph.	0	0.135	0.135	0.135	0.135	0	0	0

The 8-component fluid model was used in the production network system for a more accurate representation of fluid phase behavior. **Fig. 6.8** displays the saturation envelope and asphaltene precipitation envelop for this fluid. Both, pressure and temperature conditions, exhibit considerable changes along the network as fluids are produced. These conditions, combined with fluid compositional changes, trigger asphaltene precipitation and deposition in pipes, highlighting the importance of proper fluid analysis. Maximum asphaltene precipitation is located near the saturation envelope.

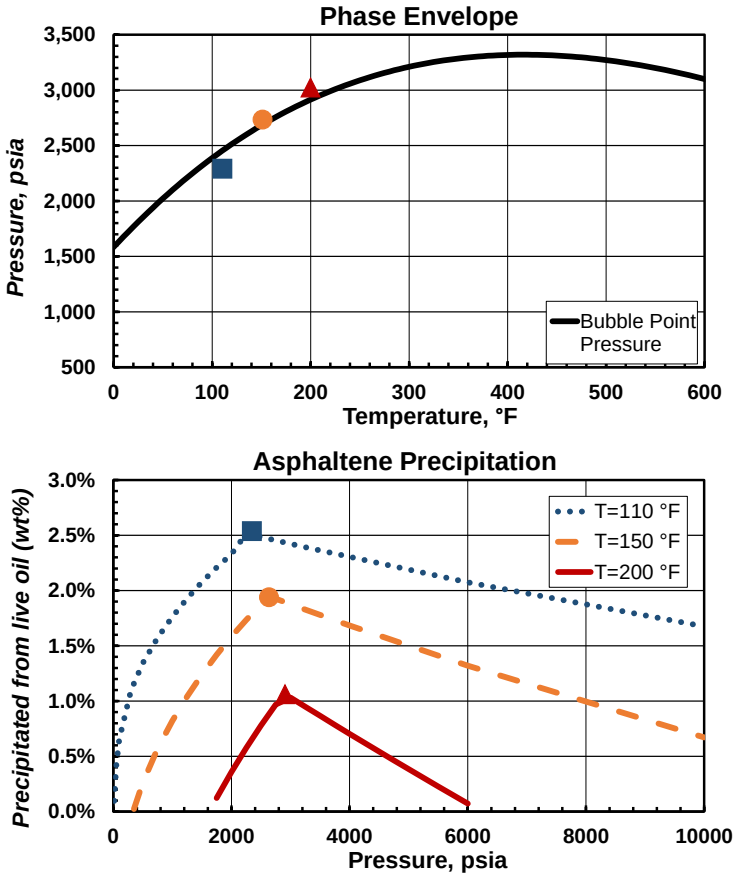

Fig. 6.8—Saturation pressure (top) and asphaltene precipitation (bottom) envelopes for 8-component fluid description. Asphaltene precipitation analysis at multiple temperatures is required in network system where pressure and temperature change drastically. Maximum onset asphaltene precipitation points are located close to the saturation pressure.

6.3.2 Hydrocarbon Fluid 6-Components Characterization

The 8-component fluid description was further grouped to create a 6-component characterization for the reservoir model. Grouping was performed by combining CO_2 with C_2-C_3 and the heavy fraction C_{7+} with Asphaltene components. This process aimed reducing computational cost while maintaining accurate description of fluid phase behavior at reservoir conditions, demonstrated in the following section. A detailed compositional description for the 6-component fluid is provided in **Table 6.7 and Table 6.8**.

Table 6.7—COMPOSITIONAL FLUID PROPERTIES FOR 6-COMPONENT EOS CHARACTERIZATION

Component	M_{w_i}	p_c (psia)	T_c (°F)	ω	Z_{crit}	δ_{shift}	z_i
C_1-N_2	16.23	664.70	-118.69	0.00849	0.28848	-0.09426	0.36940
C_2-C_3-CO_2	39.18	760.08	136.22	0.15122	0.28245	-0.02202	0.09980
C_4	58.10	544.54	295.98	0.18780	0.27711	-0.01798	0.01930
C_5	72.20	490.21	377.48	0.23969	0.27048	-0.00501	0.01570
C_6	86.00	477.20	453.50	0.27500	0.28818	-0.02941	0.01620
C_{7+}-Asph.	328.16	180.76	1,106.27	1.02912	0.28628	0.00885	0.47960

Table 6.8—BINARY INTERACTION COEFFICIENTS FOR 6-COMPONENT FLUID EOS CHARACTERIZATION

BIC	C_1-N_2	C_2-C_3-CO_2	C_4	C_5	C_6	C_{7+}-Asph.
C_1-N_2	0					
C_2-C_3-CO_2	0	0				
C_4	0	0	0			
C_5	0	0	0	0		
C_6	0	0	0	0	0	
C_{7+}-Asph.	0.058900	0.003700	0.002294	0.002294	0	0

The 6-component fluid description is only used in the reservoir system, where no asphaltene modeling is performed. **Fig. 6.9** shows the phase envelope for this fluid.

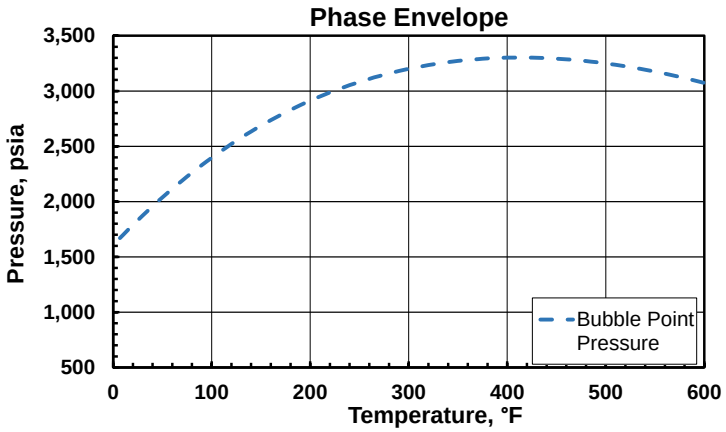

Fig. 6.9—Saturation envelope for 6-component fluid description. This fluid is used in the reservoir system where asphaltene modeling is not performed.

6.3.3 Compositional Lumping Validation

The grouping process to create the 6-component fluid description was evaluated through a set of rigorous tests to ensure material balance and the ability to predict fluid properties correctly. The compositional mapping between 8- and 6-component fluid descriptions is provided in **Table 6.9**, through use of splitting factors.

Fig. 6.10 displays the phase envelope comparison for the two fluids, an excellent match is demonstrated by an average difference of 0.5% in the evaluated pressure/temperature intervals, and a 0.05% difference in saturation pressure at reservoir temperature of 200 °F.

Table 6.9—COMPOSITIONAL LUMPING/DELUMPING TABLE

8-Comp. Fluid	6-Comp. Fluid	Split Factor
CO_2	C_2-C_3-CO_2	0.246493
C_1-N_2	C_1-N_2	1
C_2-C_3	C_2-C_3-CO_2	0.753507
C_4	C_4	1
C_5	C_5	1
C_6	C_6	1
C_{7+}	C_{7+}-Asph.	0.983007
Asphaltene	C_{7+}-Asph.	0.016993

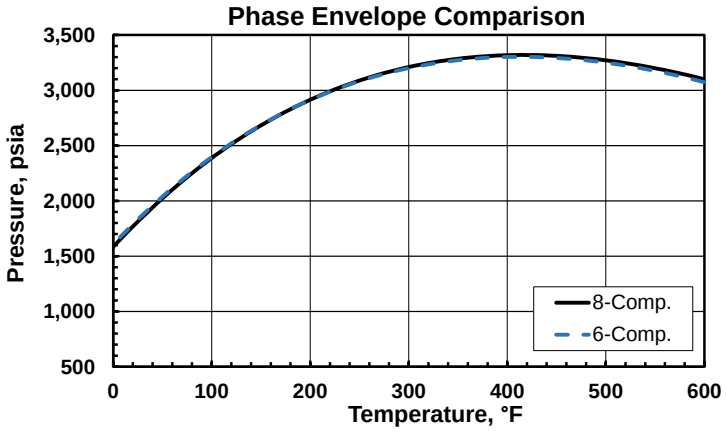

Fig. 6.10—Comparison of saturation envelopes for 8- and 6-component fluids. Excellent match is confirmed by an average difference of 0.5% between curves.

In addition, **Fig. 6.11 and Fig. 6.12** validate consistency of the fluid description by matching liquid and vapor molar volumes and viscosity of the two fluids at reservoir temperature. Average difference between the two fluid systems is 0.06% and 0.07% for liquid and vapor molar volumes, and 0.32% and 0.91% for liquid and vapor viscosities respectively.

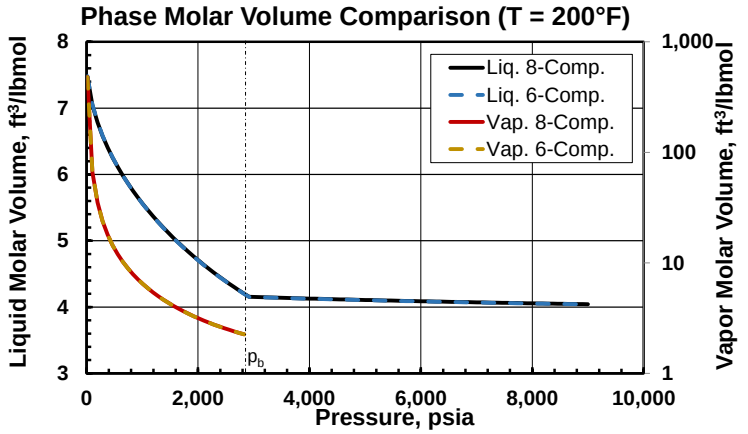

Fig. 6.11—Comparison of liquid and vapor molar volumes for 8- and 6-component fluids. Liquid and vapor molar volumes match within 0.06% and 0.07% respectively.

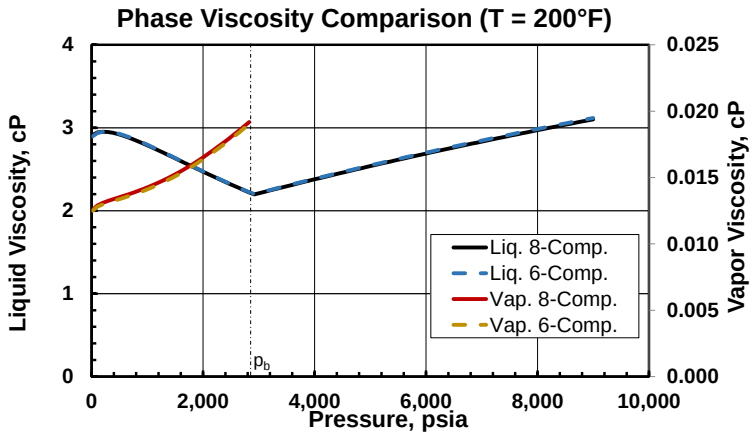

Fig. 6.12—Comparison of liquid and vapor viscosities for 8- and 6-component fluids. Liquid and vapor viscosities match within 0.32% and 0.91% respectively.

6.3.4 Asphaltene Particle and Transport Properties

Asphaltene precipitation and volumetric properties are estimated from three-phase VLLE and PR-EOS. In addition, the mechanistic transport model that describes asphaltene particle movement from bulk fluid to pipe wall requires further parameters, i.e. asphaltene particle diameter, activation energy, and frequency factor (Geng and Liao 2002; Shirdel 2013). **Table 6.10** presents base values for these parameters and asphaltene relative roughness after depositing in the pipe wall. Sensitivities on frequency factor constant are shown in the Chapter VII.

Table 6.10—ASPHALTENE PARTICLE AND TRANSPORT PROPERTIES

Property	Value
Particle diameter (d_p), μm	0.5
Activation energy (E_a), kJ/kgmol	65.3
Frequency factor (K_d), ft^2/s^2	3.23x10^2
Asphaltene rel. roughness, fraction	1.00x10^{-3}

6.3.5 Water Properties

Water properties are calculated from compressibility (c_w), reference pressure (p_{ref}), volumetric factor ($B_{w_{ref}}$), and viscosity ($\mu_{w_{ref}}$), shown in **Table 6.11**. The expressions below (Schlumberger 2014) were used to compute water volumetric factor and viscosity as a function of pressure. Calculated values are input in the simulator in tabular form, Appendix C displays table values for the simulation model.

Table 6.11—WATER REFERENCE VOLUMETRIC PROPERTIES

Property	Value
Reference pressure, psia	5,868
Water compressibility, psia^{-1}	3x10^{-6}
Reference $B_{w_{ref}}$, bbl/STB	1.029
Reference $\mu_{w_{ref}}$, cP	0.31

$$B_w = \frac{B_{w_{ref}}}{1 + \chi + \frac{\chi^2}{2}} \quad \text{..... (6.1)}$$

$$\mu_w = \frac{\mu_{w_{ref}}}{1 + \chi + \frac{\chi^2}{2}} \quad \text{..... (6.2)}$$

$$\chi = c_w(p - p_{ref}) \quad \text{..... (6.3)}$$

CHAPTER VII
RESULTS AND ANALYSIS OF SIMULATION CASES

Multiple production scenarios, including analysis of stand-alone reservoir models and reservoir-network coupled systems, are presented in this chapter to validate the development of the new numerical simulator and demonstrate the impact of asphaltene deposition in pipelines on production performance. Additional sensitivities on pipeline temperature profile, fluid composition, artificial gas-lift, and asphaltene inhibitor injection, are performed on the stand-alone network model to develop better understanding of important thermodynamic and transport mechanisms observed in pipelines during constant pressure or rate boundary conditions.

7.1 Reservoir Stand-Alone Validation

Validation of the reservoir simulator is performed through a waterflooding case using multi-segment wells (MSW). The objective of analyzing the stand-alone reservoir model, Case 1, is to verify results with an established commercial software, e.g. Eclipse (ECL) (Schlumberger 2014), and to validate the compositional lumping method by comparing the 8- and 6-component fluid characterizations.

7.1.1 Case 1—Reservoir Waterflooding

Reservoir and MSW in the model were described in Chapter VI. Wells were controlled by phase rates and bottomhole flowing pressure limits, shown in **Table 7.1**. Case 1 is comprised of three tests runs: 8- and 6-component fluid characterizations (both with new developed simulator) and a 6-component run performed with a commercial software (ECL).

Excellent match between new simulator and commercial software verify consistency in mathematical approach for a three-phase waterflooding process, as shown in **Fig. 7.1**. In

addition, matching results for the two fluid characterizations validate the compositional lumping approach.

Table 7.1—CASE 1 MSW CONTROL FOR STAND-ALONE RESERVOIR MODEL

Condition	Value
Max. oil production rate, STB/day	2,000
Max. water injection rate, STB/day	10,000
Producer BHP_{min}, psia	2,000
Injector BHP_{max}, psia	6,000
Start of water injection, day	145

Further analysis of simulation results reveal a difficult mathematical scenario where gravity segregation plays an important role in the model, allowing to test consistency of the simulator development due to complexity in thermodynamic and transport mechanisms. **Fig. 7.2** shows reservoir gas saturation at 145 days of primary depletion, the point at which water injection starts. Gas is mainly located at the top of the reservoir and close to the production well, where local gridblock pressure is lower. The average reservoir pressure at this stage is 2,622 psia.

Reservoir water saturation at the end of the synthetic forecast (365 days of simulation) is presented in **Fig. 7.3**. Average reservoir water saturation reaches 44% and reservoir pressure is restored to 5,744 psia. Higher water saturation is observed in bottom layers due to gravity segregation, creating preferential channels for breakthrough to the producer.

The main objective of modeling the reservoir fluid with a 6-component fluid description is reducing computational cost. Previous results verified that the compositional lumping process is robust and results match those of the 8-component simulation. **Table 7.2** displays CPU times for both cases, performed in the new simulator. A reduction of 28.6% is achieved by using the 6-component fluid characterization, without compromising quality of results.

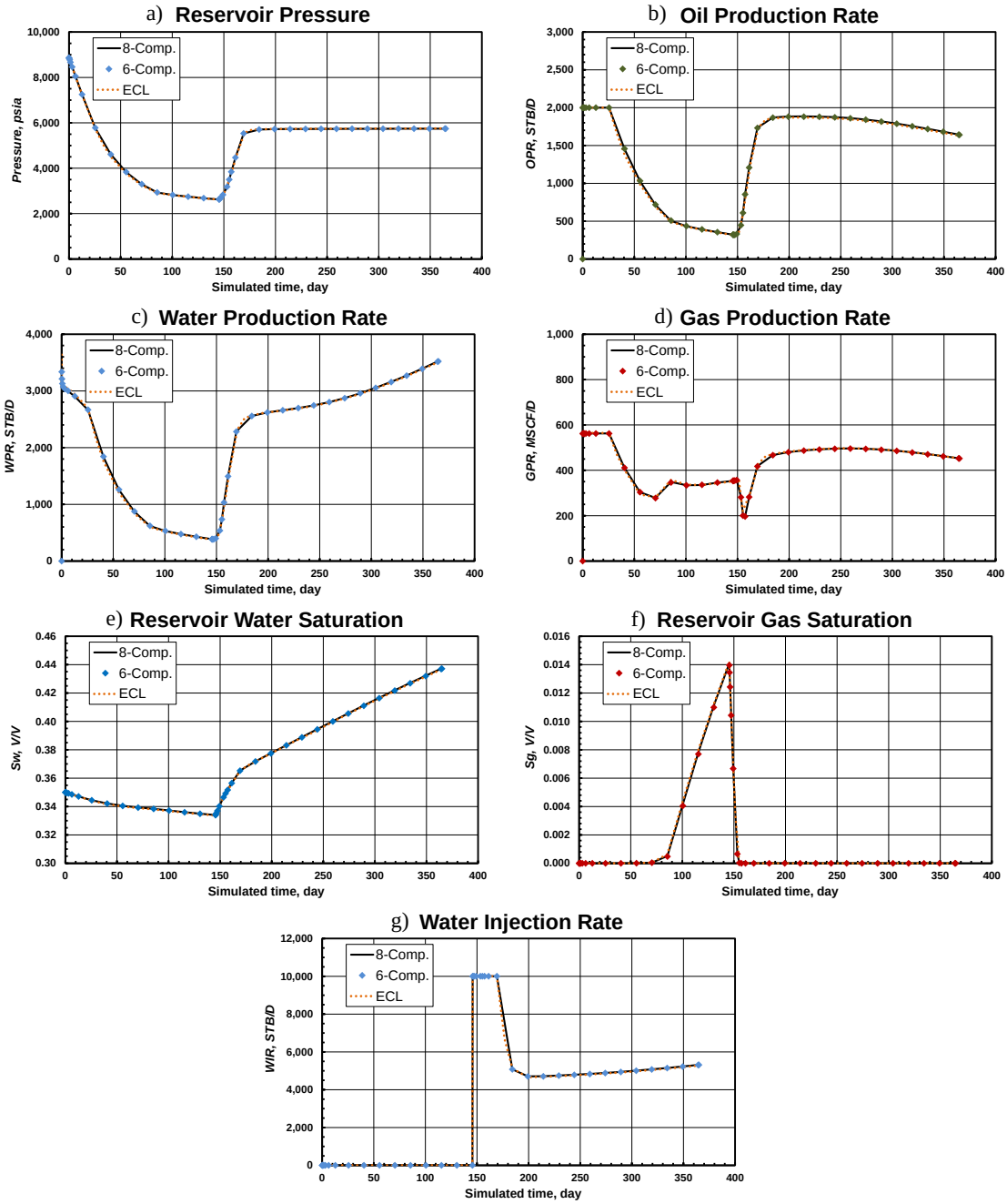

Fig. 7.1—Case 1 comparison of key reservoir parameters. Excellent agreement between new simulator (8- and 6-component cases) and commercial software (ECL) verify the waterflooding synthetic case forecast. Outstanding match between 8- and 6-component fluid systems validate the hydrocarbon characterization approach.

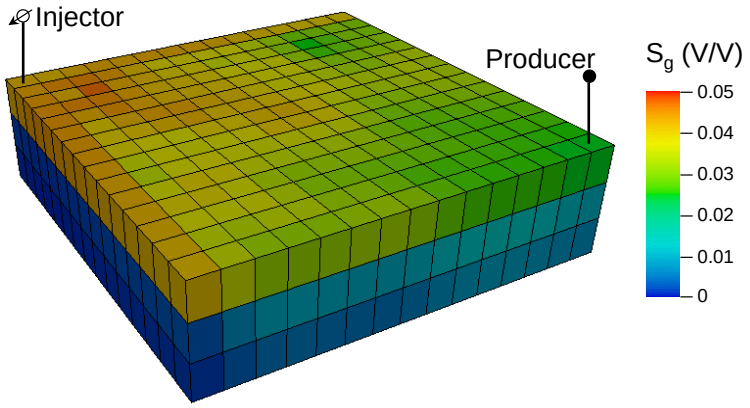

Fig. 7.2—Case 1 reservoir gas saturation at 145 days of production (start of water injection), with average reservoir pressure of 2,622 psia. Gas is located at the top layer and close to the producer.

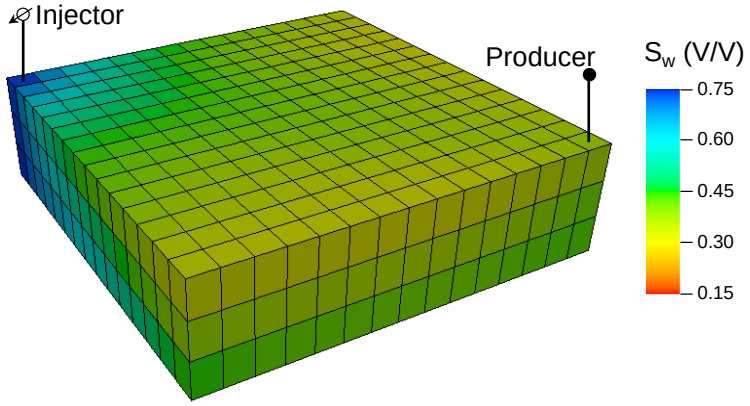

Fig. 7.3—Case 1 reservoir water saturation at 365 days of simulation (end of forecast), with average reservoir of 5,744 psia and water saturation of 44%. Water breakthrough occurs primarily through bottom layers.

Table 7.2—CASE 1 CPU REDUCTION FROM COMPOSITIONAL LUMPING

Case	CPU, s
8-Component Fluid	27,214
6-Component Fluid	19,440
CPU Reduction	**28.6%**

7.2 Coupled Reservoir-Network

Integrated analysis of reservoir-network production systems provides more realistic forecasts and better understanding of key mechanisms governing field production. The reservoir-network coupled cases following analyzed highlight the impact of asphaltene deposition in pipelines during primary depletion of a reservoir system. Network and reservoir models used in this section were described in Chapter VI.

7.2.1 Case 2—Compositional Delumping Validation

The reservoir model fluid is described by a 6-component characterization since asphaltene modeling is not performed in porous media in this study. However, the 8-component fluid description is required in the network system to accurately model asphaltene precipitation and deposition in production pipelines. Case 2 is hereby analyzed to validate the compositional delumping method when reservoir fluids are transferred to network.

Two scenarios are tested, the first one having the 8-component fluid description both in reservoir and network (R8-N8) where no delumping is required, and the second with 6-components in the reservoir and 8-components in the network (R6-N8) with compositional delumping. In both cases the boundary condition is set for the network separator (segment #23) to a constant pressure of 150 psia. Asphaltene modeling in pipelines is not activated in this test to allow a proper comparison of the delumping process. Compositional delumping is performed according to Table 6.9, presented previously.

Fig. 7.4 illustrates a strong match in key engineering performance parameters (reservoir pressure, phase rates, saturation, and well bottomhole flowing pressure) between scenarios with and without compositional delumping requirement. Furthermore, a reduction of 24.2% in CPU time is achieved by modeling the reservoir system with 6 components and the network with 8 components (**Table 7.3**). These results validate the delumping method implemented and the use of 6-to-8 component modeling between reservoir and network.

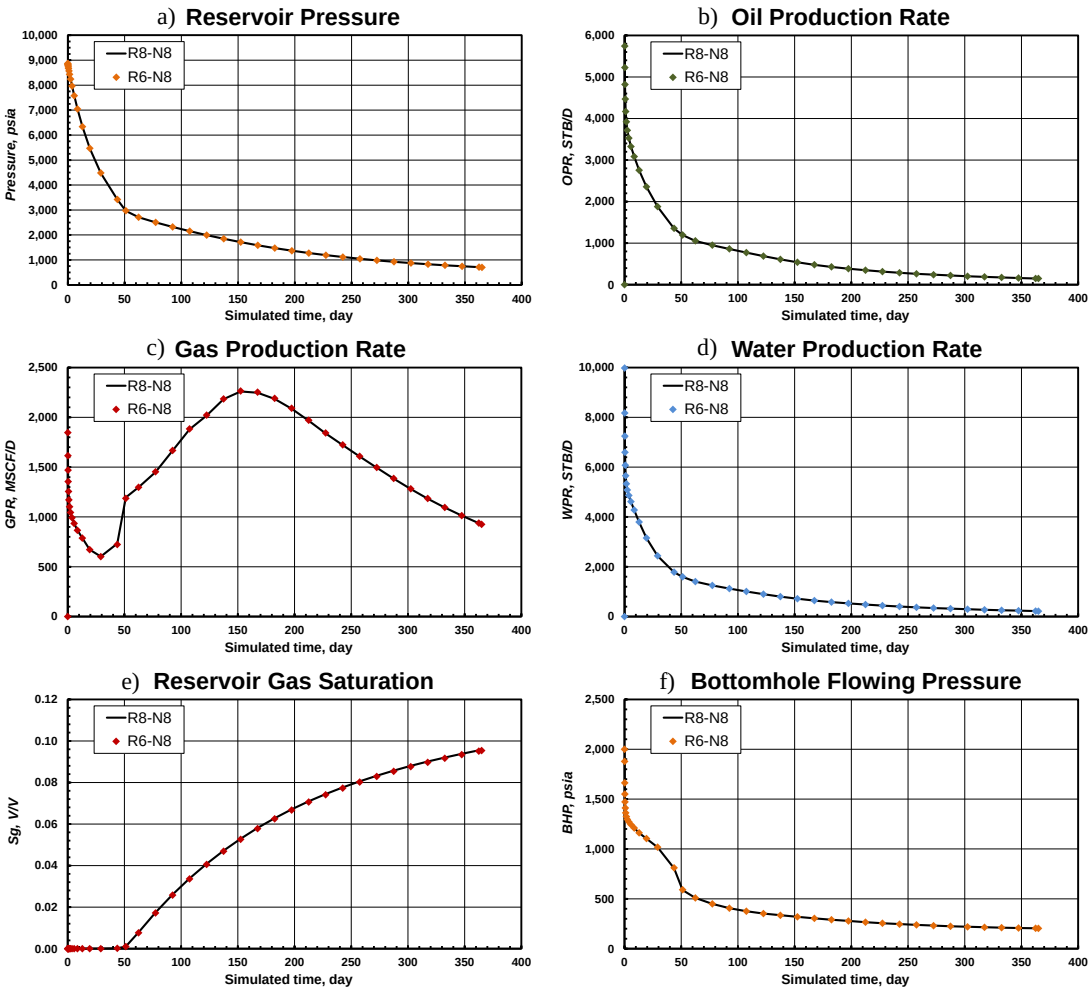

Fig. 7.4—Case 2 comparison of key reservoir parameters for two simulation scenarios. Excellent match between fluid descriptions R8-N8 (8 components in reservoir and network) and R6-N8 (6 components in reservoir and 8 in network) validates the compositional delumping method.

Table 7.3—CASE 2 CPU REDUCTION FROM COMPOSITIONAL DELUMPING BETWEEN RESERVOIR AND NETWORK SYSTEMS

Case	CPU, s
R8-N8	39,215
R6-N8	29,713
CPU Reduction	**24.2%**

7.2.2 Case 3—Asphaltene Deposition Impact on Production Performance

Network system conditions, i.e. pressure, temperature, and fluid composition, may trigger asphaltene precipitation and deposition in pipelines. Case 3 demonstrates the impact of asphaltene accretion on production performance by establishing a comparison of a primary depletion scenario with and without asphaltene modeling. The coupled case in study is Case 2 (R6-N8), previously analyzed. Fluid characterization in reservoir and network is 6 and 8 components respectively, with compositional delumping. Separator boundary condition is set at 150 psia. Asphaltene particle diameter, activation energy, frequency factor, and relative roughness, are those shown in Table 6.10.

Fig. 7.5 shows asphaltene deposition, diameter reduction, fluid velocity, and pressure profiles as a function of distance and simulation time. This information enables analyzing location of asphaltene major accumulation and conditions that trigger this phenomenon. Asphaltene deposit thickness along production pipelines increases with time, causing a maximum pipeline diameter reduction of 44% at the wellhead (Fig. 7.5 a and b), where pipe diameter is increased from 3-in tubing to 4-in surface pipeline. High deposition at this location is caused by the velocity reduction due to diameter increase (Fig. 7.5 e).

Additional analysis also allows to identify three major deposition regions with different behaviors. The first region extends from bottomhole up to 750 ft distance, where flow conditions (pressure, temperature, and fluid composition) do not trigger asphaltene precipitation. The second, spans the vertical wellbore section from 750 to 2,750 ft (wellhead) distance, where rapid pressure and temperature drops cause accelerated asphaltene precipitation and deposition. The third region corresponds to the surface pipeline from wellhead to separator, pressure and temperature changes are less severe and deposition is slower.

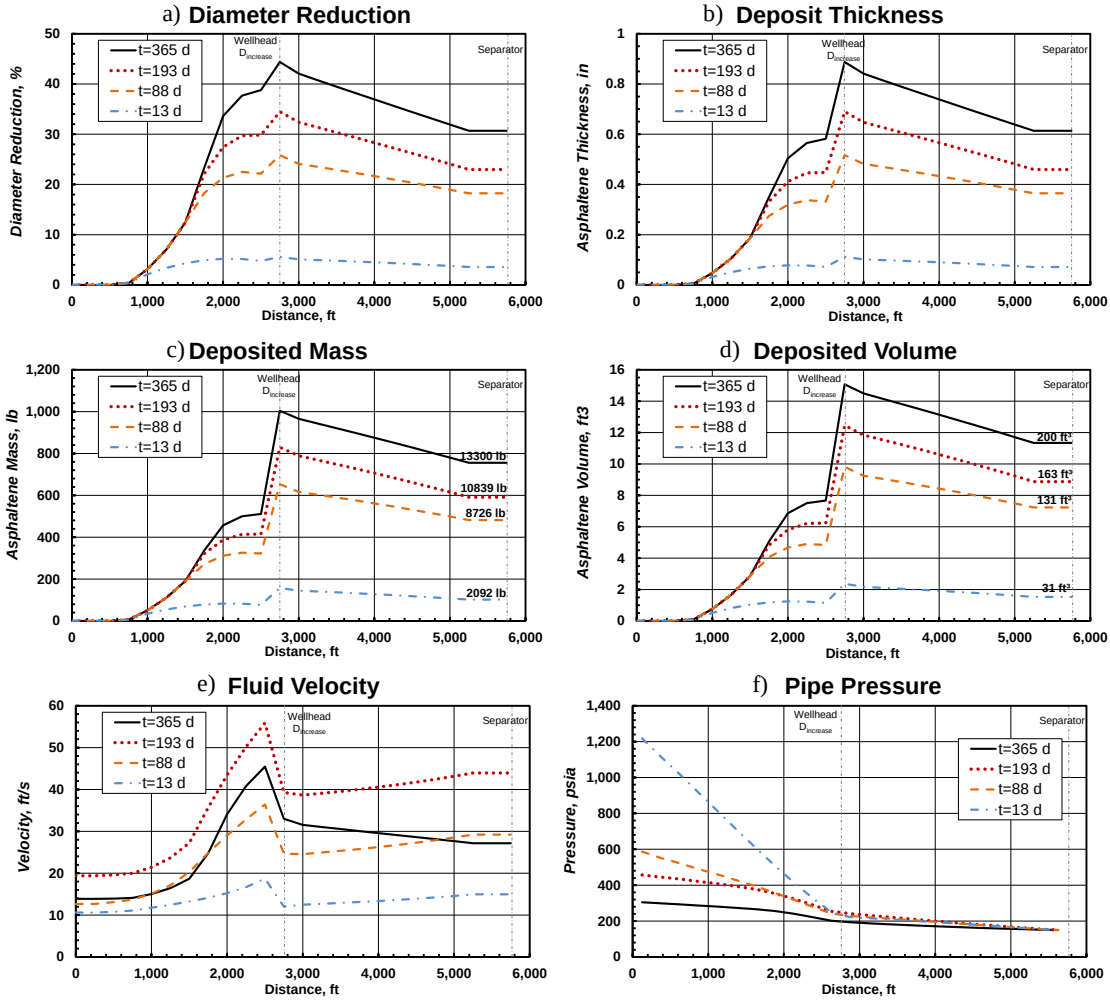

Fig. 7.5—Case 3 network asphaltene accretion and velocity profiles vs. distance for multiple simulation times. Asphaltene layer thickness continuously increases with time (b), causing a maximum pipeline diameter reduction (a) of 44% at the wellhead, where pipeline diameter is increased from 3-in tubing to 4-in pipe. The velocity reduction at the wellhead (e) increases deposition. Profiles of deposited asphaltene mass (c) and volume (d) show 13,300 lb of material block half of the 400 ft^3 entire pipe volume.

Fig. 7.5 (c and d) illustrate accumulated asphaltene mass and volume along the pipe. A total mass of 13,300 lb of material block half of the pipeline volume (402 ft^3). These profiles can be used to design cleaning operations, properly planning location and amount of material to be removed from the system. This is particularly important in offshore deepwater applications where design is constrained by equipment accessibility and available space or location size.

In addition to asphaltene accumulation profiles, coupled modeling presents a significant advantage allowing to study the impact of solid deposition on production performance. **Fig. 7.6** displays basic performance parameters for Case 3 with and without asphaltene modeling.

Required bottomhole flowing pressure (BHP) to meet separator pressure target is underestimated, by 160 psi in average, when asphaltene deposition is neglected (Fig. 7.6 g). Additional pressure losses, caused by pipeline diameter reduction, require higher BHP when asphaltene accretion in considered. The higher production BHP results in lower oil, gas, and water production rates (Fig. 7.6 c, e, and f), creating a slower depletion of reservoir pressure and smaller gas saturation (observed in Fig. 7.6 a and b).

Furthermore, neglecting impact of asphaltene deposits in this case, results in a cumulative oil production overestimation of 7%, or 16,500 STB (Fig. 7.6 d) and 10%, or 56,000 SCF, in gas production, during the first year of primary depletion.

Under this setting it is recommended to analyze asphaltene inhibitor injection to mitigate asphaltene deposition in pipelines and increase productivity. Downhole inhibitor injection for the coupled system will be evaluated in Section 7.2.4.

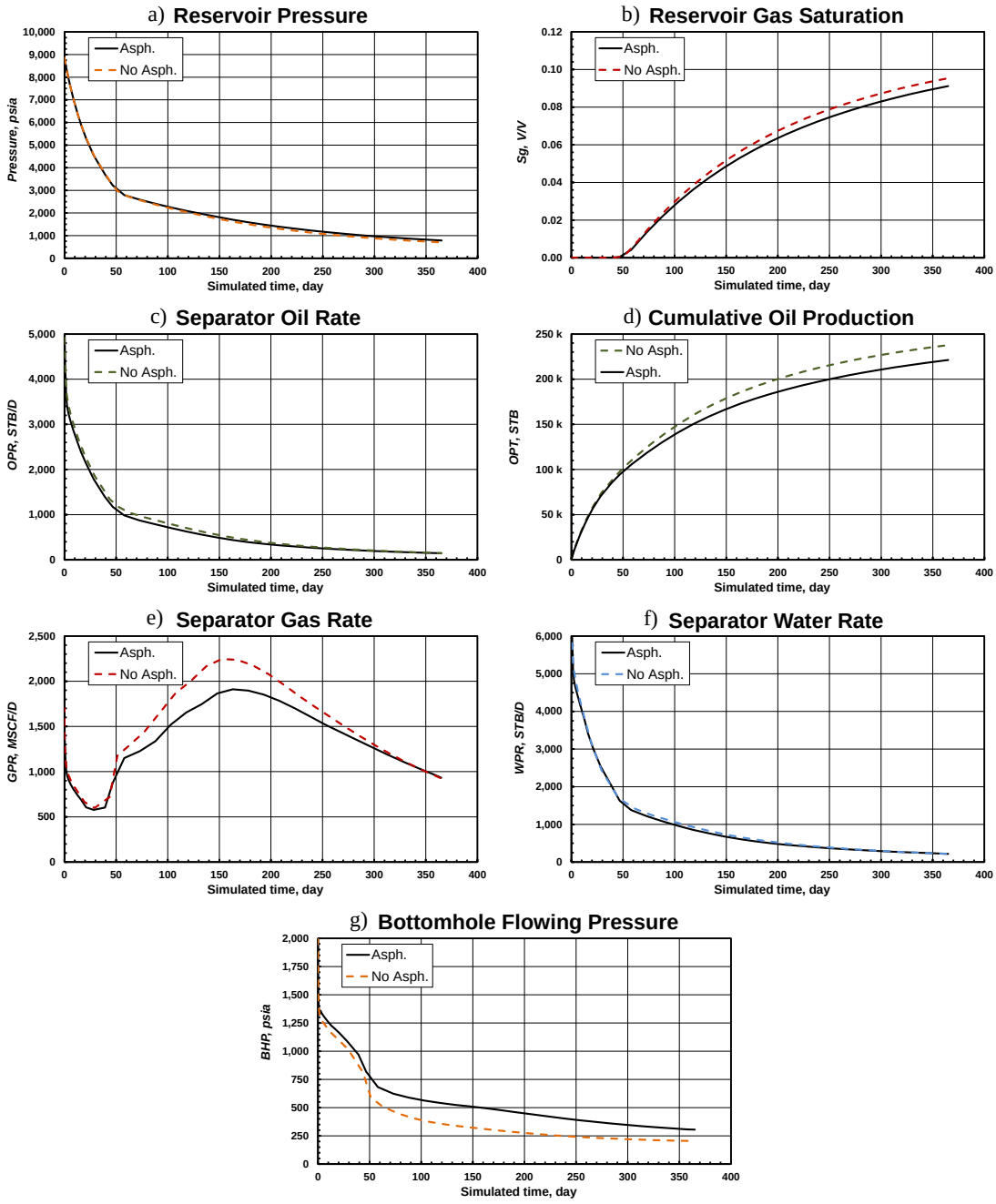

Fig. 7.6—Case 3 production performance forecast with and without asphaltene modeling. Neglecting asphaltene modeling underestimates required BHP by 160 psi in average (g), tubing and surface pipe diameter reduction due to asphaltene accretion increases pressure losses, resulting in higher BHP requirement. Cumulative oil production (d) is overestimated by 7% when neglecting solid deposition.

7.2.3 Case 4—Frequency Factor Sensitivity Impact on Asphaltene Deposition

The transport equation describing asphaltene particle movement from bulk fluid to pipeline wall contains two tunable parameters in the sticking parameter calculation, i.e. activation energy and frequency factor in Eqs. (4.37) and (4.38). Four sensitivities of frequency factor (K_d), as seen on **Table 7.4**, were performed to investigate potential scenarios for asphaltene deposition rate in the field. Actual values for tunable parameters can be obtained from laboratory or empirical field data if available.

Table 7.4—CASE 4 FREQUENCY FACTOR SENSITIVITY VALUES

Case	Frequency Factor (K_d), ft^2/s^2
Case 4a	3.23x10^1
Case 4b	1.02x10^2
Case 4c	3.23x10^2
Case 4d	1.02x10^3

Higher values of K_d increase deposition rate of asphaltene to the pipe line wall. **Fig. 7.7** illustrates the effect of this parameter on material accretion after 365 days of production. Note that Case 4d ($K_d = 1.02x10^3$ ft^2/s^2) is shown at 61 days of production, since the pipeline is entirely blocked at this time due to fast asphaltene accumulation. Under this scenario, the well requires very frequent cleanup operations or inhibitor injection, later studies in this section.

Diameter reduction in network pipelines ranged between 5% and 98% (Fig. 7.7 a) in the lower and higher sensitivities. Material deposits along the pipe varied from 1,754 lb (26 ft^3) to 25,909 lb (389 ft^3), as seen in Fig. 7.7 c and d. This demonstrates flexibility in application of the asphaltene transport method for multiple scenarios based on laboratory or field data analog wells, from slow to fast deposition rates. Forecasts can then be used to design cleaning operations and inhibitor injection programs.

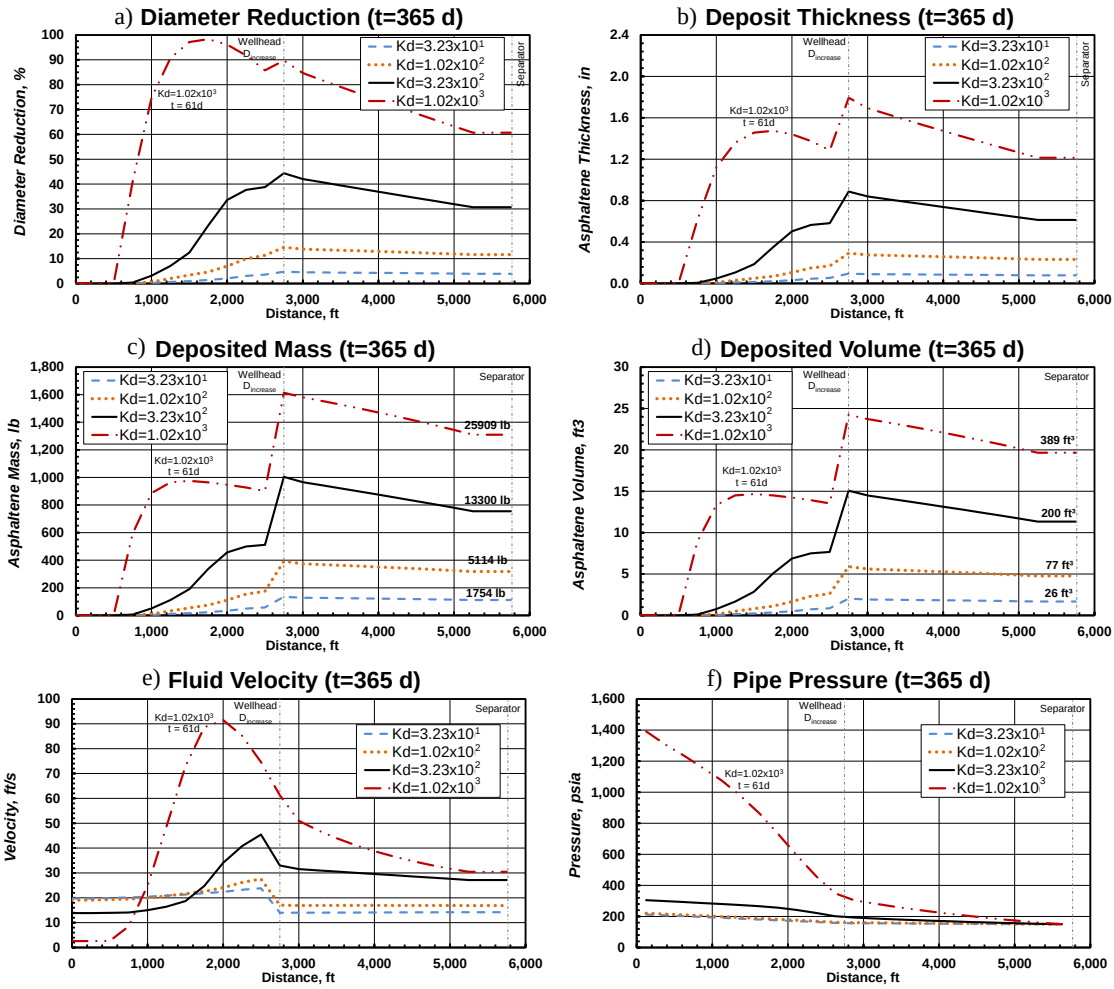

Fig. 7.7—Case 4 network asphaltene accretion and velocity profiles vs. distance for frequency factor sensitivity at the end of production. Higher values of frequency factor accelerate asphaltene deposition rates. Note that Cases 4.4 is shown at 61 days of production, asphaltene deposition with $K_d = 1.02x10^3$ is fast, pipeline flow area is blocked after 61 days, restricting production entirely (a). Observed minimum and maximum pipeline diameter reduction (a) were 5% and 98%. The velocity reduction at the wellhead (e) increases deposition, except for Case 4d where maximum velocity is observed at the maximum restriction point (1,800 ft distance). Profiles of deposited asphaltene mass (c) and volume (d) range from 1,754 lb / 26 ft^3 to 25,909 lb / 389 ft^3.

Production performance parameters for the four sensitivities are shown in **Fig. 7.8**. Increasing K_d accelerates asphaltene deposition in network pipes. Frequency factor has a negligible impact on reservoir pressure depletion (Fig. 7.8 a). Gas saturation and production rates (Fig. 7.8 b, c, e, and f) are slightly impacted, while cumulative oil production (Fig. 7.8 d) is reduced by 4.75% between Case 4a and 4c due to additional pressure losses in the system.

The greatest impact is observed for Case 4d ($K_d = 1.02x10^3$), where asphaltene deposition is accelerated and pipeline flow area is entirely blocked after 61 days of production. Production rates drop to zero and bottomhole pressure (Fig. 7.8 g) starts increasing until matching average reservoir pressure, mirroring wellbore storage effects in a build-up test.

Case 4d represents an interesting scenario since fast asphaltene deposition rates entirely block the pipeline after 61 days of production. When this condition is observed in the field, it can lead to production loss and high operational costs in cleaning up operations and chemical treatments (Ali et al. 1999).

Fig. 7.9 details pipeline asphaltene deposition results. As mentioned before, at 61 days of production, 98% of pipe diameter at 1,800 ft location is blocked with asphaltenes (Fig. 7.9 a), restricting flow rates to zero. Asphaltene layer almost covers the entire pipe area (Fig. 7.9 b), causing high deposit mass and volume. This combination of factors make cleanup operations very difficult and expensive, which highlights the importance of proper prevention plans to mitigate asphaltene deposition. A case of chemical injection in presented following, to demonstrate applications of downhole inhibitor injection.

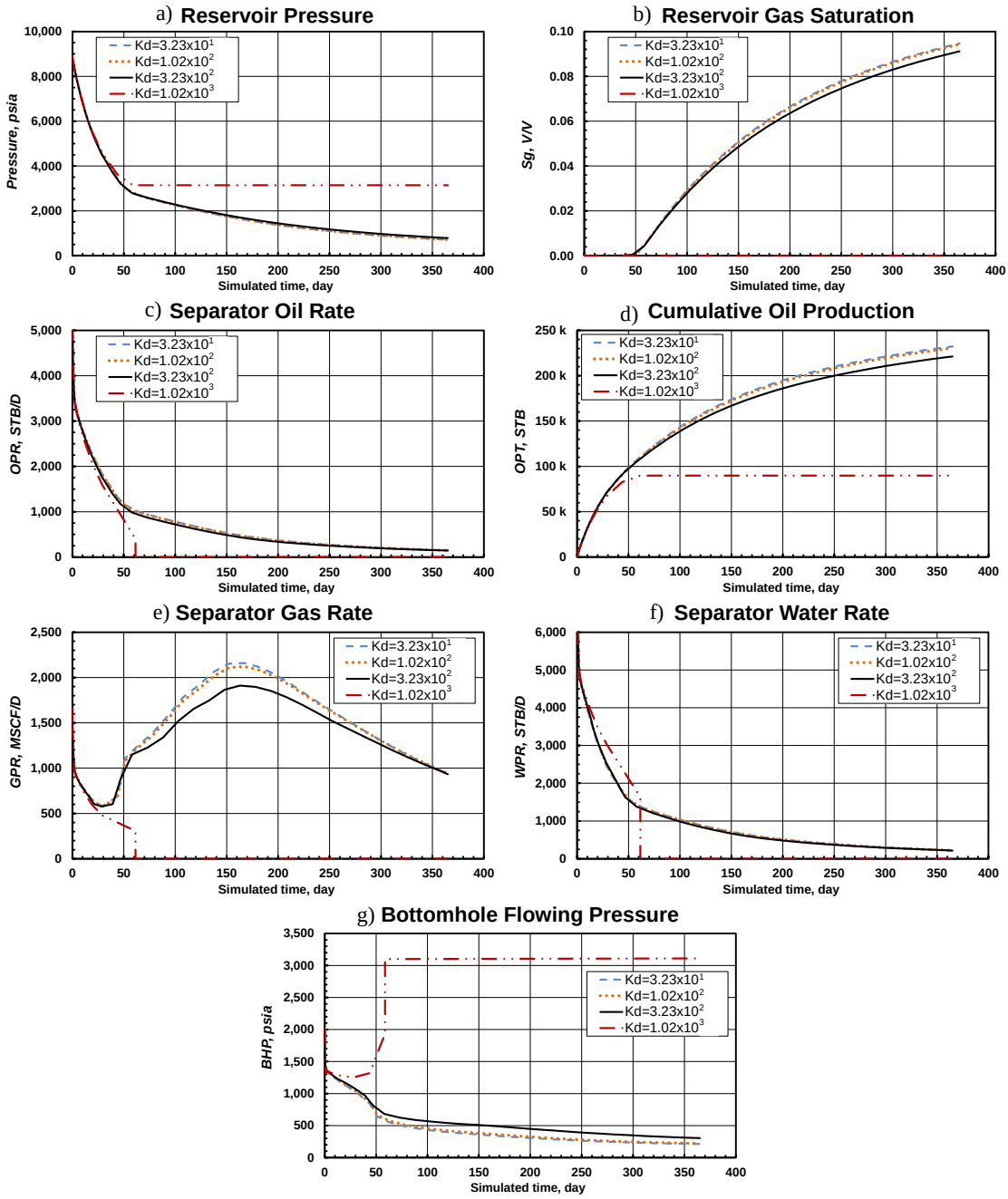

Fig. 7.8—Case 4 production performance forecast with frequency factor sensitivity. K_d sensitivity has largest impact on cumulative oil production, a 4.75% difference between Case 4a and 4c. Production is interrupted in Case 4d (dash-dotted red line). Asphaltene deposition with $K_d = 1.02x10^3$ is accelerated, pipeline flow area is blocked after 61 days, restricting production entirely (c-f). Bottomhole pressure (g) drastically increases to average reservoir pressure, mirroring a wellbore storage effect.

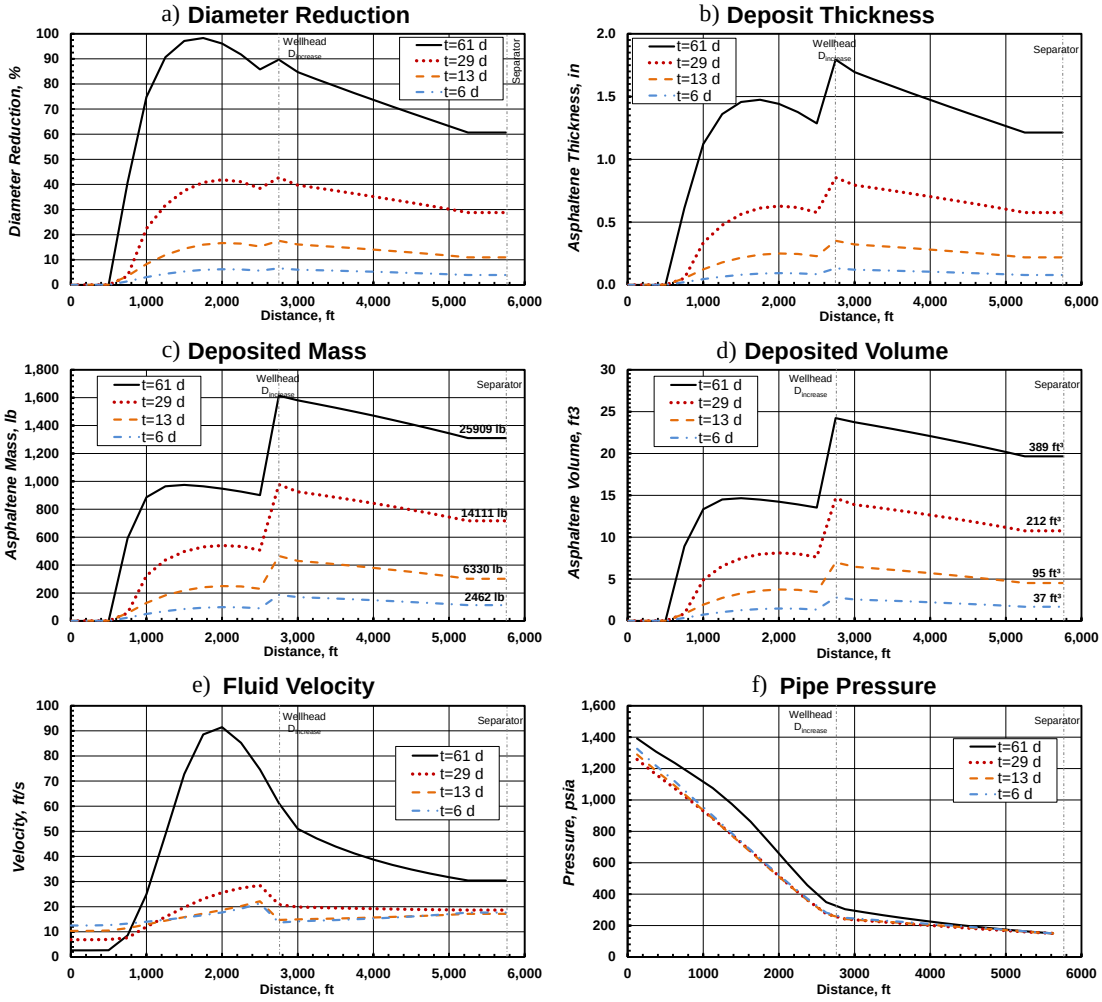

Fig. 7.9—Case 4d ($K_d = 1.02x10^3$) network asphaltene accretion and velocity profiles vs. distance for frequency factor sensitivity at the end of production (61 days). Flow is entirely restricted, reaching a 98% diameter reduction, after 61 days of production (a). Asphaltene layer almost covers the entire pipe area (b), causing high deposit mass and volume (c and d). Fluid velocity reaches high values at locations with largest diameter reduction (e).

7.2.4 Case 5—Impact of Downhole Chemical Injection on Asphaltene Deposition

Prevention of precipitation and deposition is recognized as the best technique to manage assets with high asphaltene content. The variables controlling asphaltene precipitation are pressure, temperature, and fluid composition. In Case 5, bottomhole chemical injection is performed to mitigate asphaltene accretion, introducing a thermodynamic inhibitor to mix with produced fluids. Injected inhibitor is usually recycled at surface, a separation process allows extracting a large portion of the inhibitor to be reinjected.

Toluene (Pan and Firoozabadi 2000b) is injected at bottomhole reference depth using the source term in Eq. (4.2) for network segment #1. By introducing toluene, fluid composition is modified and interaction between components reduce amount of asphaltene precipitate. Toluene component critical properties are presented in **Table 7.5** (Goodwin 1989), binary interaction coefficients (BIC) between toluene and all other components are set to zero.

Table 7.5—CASE 5 TOLUENE COMPONENT EOS PROPERTIES

Toluene Property	Value
M_w, lb/lbmol	92.1
p_c, psia	614.45
T_c,°F	609.44
ω, dimensionless	0.257
Z_{crit}, dimensionless	0.27234
$\mathcal{S}_{shift}$, dimensionless	-0.0001
BIC, dimensionless	0

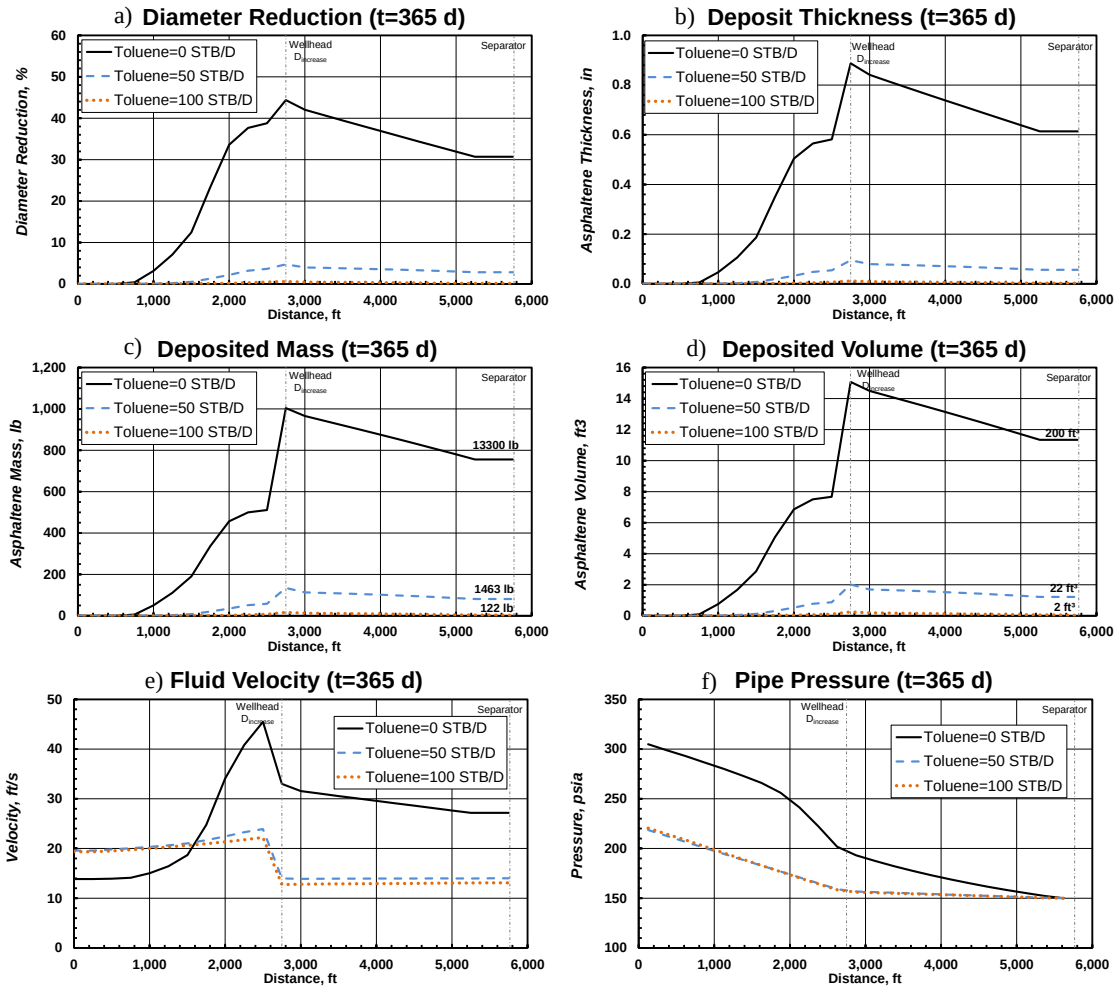

Fig. 7.10—Case 5 network asphaltene accretion and velocity profiles vs. distance for inhibitor injection sensitivity at 365 days of production. Bottomhole toluene injection effectively reduce asphaltene precipitation and deposition. Maximum diameter reduction is lowered from 44% to 5% with 50 STB/D and less the 1% with 100 STB/D injection (a). Asphaltene layer thickness (b), deposited mass (c) and volume (d) are also greatly reduced, yielding more favorable fluid velocity and pressure gradient profiles (e and f) due to decreased frictional pressure losses.

Two scenarios with toluene injection rates of 50 and 100 STB/D are compared against Case 4c ($K_d = 3.23x10^2$, in Table 7.4) as base scenario without inhibitor injection. **Fig. 7.10** shows the effectiveness of toluene as asphaltene inhibitor, maximum pipeline diameter reduction of 44% (without inhibitor injection) is reduced to 5% when injecting 50 STB/D of toluene and to less than 1% when injecting 100 STB/D (Fig. 7.10 a). Deposit layer thickness, mass, and volume (Fig. 7.10 b, c, and d) are dramatically reduced, yielding more favorable fluid velocity and pressure profiles (Fig. 7.10 e and f) due to reduced friction losses in the system.

Fig. 7.11 demonstrates the effectiveness of toluene to improve production performance. Separator oil rate, discounting the injected toluene volume (Fig. 7.11 c), is higher when inhibitor injection is applied, yielding nearly 5% (approximately 10,000 STB) increase in cumulative oil produced, as shown on Fig. 7.11 d.

Production increment is achieved through the reduction of BHP, an average of 130 psi difference, when inhibitor is injected (Fig. 7.11 g). Asphaltene accumulations require higher BHP to meet separator pressure boundary condition. Incremental gas production is observed when inhibitor is used due to a combined effect, improved oil rates increase associated gas production and also free gas production at bottomhole increases due to faster reservoir pressure depletion (reservoir gas saturation faster increment).

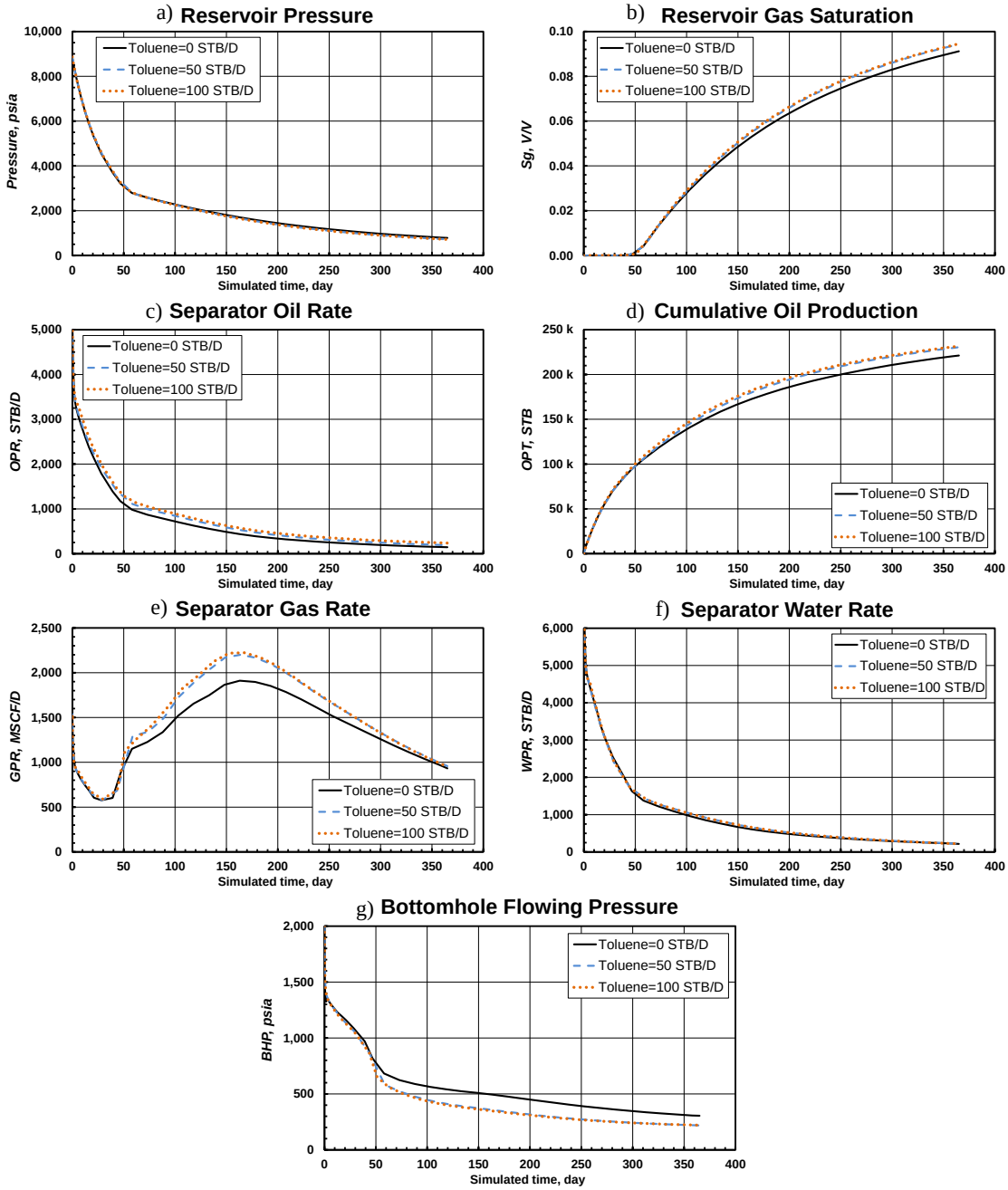

Fig. 7.11—Case 5 production performance forecast with bottomhole inhibitor injection. Bottomhole toluene injection improves production performance by reducing frictional pressure losses in the system. Nearly 5% (10,000 STB) increase in cumulative oil production (d) is achieved by reducing required BHP 130 psi in average when injecting inhibitor (g). Presented oil production rates and cumulative production already discount injected toluene volumes.

7.2.5 Case 6—Impact of Artificial Gas-Lift on Asphaltene Deposition

Artificial gas-lift is a commonly applied method to increase well productivity by injecting dry gas, usually methane, from casing's annular space into the tubing at a desired depth. Injected gas reduces overall wellbore fluid density reducing bottomhole flowing pressure, hence increasing well productivity. Mixing between produced reservoir fluid and injected gas at bottomhole modify hydrocarbon composition, altering onset asphaltene precipitation conditions. Furthermore, gas injection increases fluid velocity in wellbore and surface pipelines due to its high compressibility.

Case 6 presents a gas-lift scenario with 500 MSCF/D of methane injected at bottomhole reference depth (using the source term in Eq. (4.2) for network segment #1) to increase productivity. The objective is to evaluate gas-lift impact on asphaltene deposition in the coupled system under primary depletion conditions and compare results with Case 4c (Table 7.4) as base.

Network asphaltene accretion, velocity, and pressure profiles comparison between gas-lift and base case are presented in **Fig. 7.12**. Material deposits are reduced by nearly half when artificial gas-lift in applied in this scenario, evidenced by reduced asphaltene layer thickness, mass, and volume deposited in the pipeline (Fig. 7.12 a through d). Asphaltene deposition is greatly reduced in the vertical wellbore section from 0 to 2,000 ft distance due to high fluid velocity as gas expands. Under these conditions, high fluid velocity reduces the probability of asphaltene particles sticking to the pipe wall. Nonetheless, this behavior is not universal, some gas-lift scenarios can lead to acceleration in deposition rates, as will be shown in the stand-alone network sensitivities.

Production performance comparison for cases with and without gas-lift can be observed in **Fig. 7.13**. Only a marginal cumulative oil production of about 1% (approximately 2,500 STB) is achieved by implementing gas-lift in the system; major contribution of gas-lift in this case is reduction of asphaltene deposits due to fluid velocity increase. Presented gas

production rate in Fig. 7.13 e includes injected gas volume at bottomhole that returns to the separator, which combined with the marginal oil production rate increase amounts to a gas rate slightly greater than 500 SCF/D more than the scenario without gas-lift. BHP reduction with gas-lift is in average 70 psi (Fig. 7.13 g), a small value to significantly increase production.

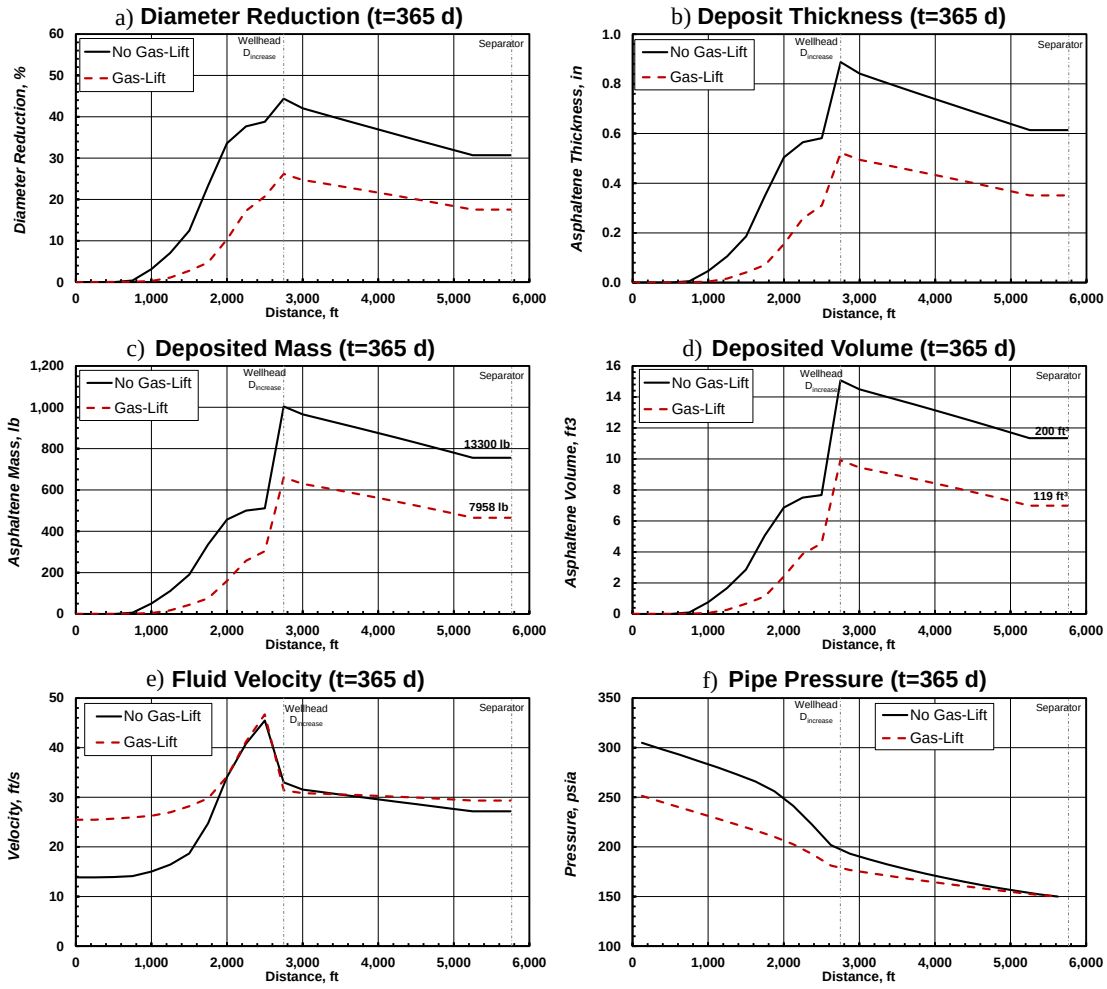

Fig. 7.12—Case 6 network asphaltene accretion and velocity profiles vs. distance for artificial gas-lift scenario at 365 days of production. Asphaltene deposition is reduced nearly by half in this case when gas-lift is applied (a through d). High fluid velocity caused by expanding gas reduce material accretion in the vertical wellbore section creating a more favorable pressure gradient profile (e, a, and d).

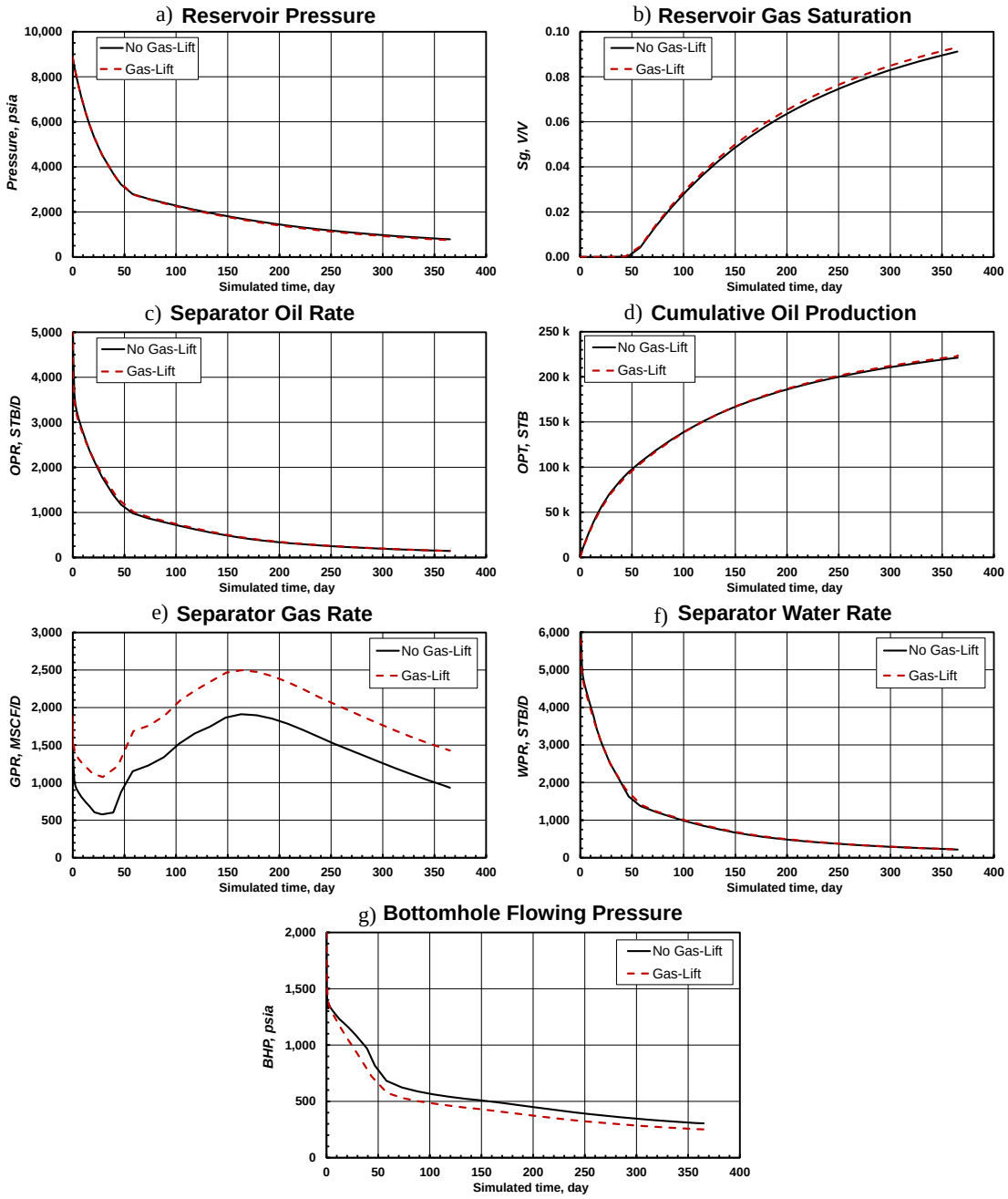

Fig. 7.13—Case 6 production performance forecast with artificial gas-lift. Application of gas-lift marginally increased cumulative oil production by 1% (approximately 2,500 STB) during one year of reservoir depletion (a and d). Gas production rate with gas-lift is presented including injected gas volume, which combined with the small oil production incremental, yield a gas rate slightly greater than 500 SCF/D more than the no gas-lift scenario (e). Average BHP reduction is only 70 psi (g).

7.3 Network Stand-Alone

Reservoir-network coupled runs allowed forecasting production performance for multiple scenarios including asphaltene deposition with sensitivities on particle transport, inhibitor injection, artificial gas-lift, and the potentially inaccurate forecasts if asphaltene deposition is neglected. In this section, additional sensitivities are performed on the stand-alone network model to develop more rigorous analysis of asphaltene deposition mechanisms and demonstrate the ability to model decoupled network cases.

Modeling the network as a stand-alone system allows controlling more variables by taking advantage of fixing bottomhole and separator boundary conditions, whereas in the coupled system only separator state can be specified and bottomhole conditions are calculated to meet surface requirements as a function of reservoir productivity. This approach enables to improve the understanding of fluid composition, pressure, and temperature impact on asphaltene precipitation and deposition in the network system.

The following scenarios use the network description shown in Section 6.2, the 8-component fluid characterization presented in Section 6.3.1, and asphaltene transport frequency factor $K_d = 3.23x10^1$ ft^2/s^2. Cases are set with a constant downhole inlet fluid composition, water cut, and pressure. Constant separator oil production rate is set as surface boundary condition (refer to Fig. 6.6 for node segment and connection indices). Models are run for 180 simulation days of production. Sensitivities are performed on bottomhole flowing pressure, artificial gas-lift injection rate, asphaltene molar composition in produced fluid, and temperature profile in the pipeline system.

7.3.1 Case 7—Bottomhole Flowing Pressure Sensitivity

Pressure profiles in wellbore and surface pipeline dictate preferential asphaltene precipitation and deposition locations in the system. On Case 7, a constant oil production rate at separator and bottomhole inlet fluid composition, water cut, and pressure are set as boundary conditions, see **Table 7.6**. Four sensitivities on BHP ranging from 1,000 to 7,000

psia (**Table 7.7**) are run to characterize impact of pressure on asphaltene deposition profiles during 180 days of production.

Table 7.6—CASE 7 BOUNDARY CONDITIONS

Location	Boundary Condition	Value
Bottomhole (Node #1)	Pressure, psia	Table 7.7
Bottomhole (Node #1)	Fluid composition	Table 6.5
Bottomhole (Node #1)	Water Cut, V/V	0.1
Separator (Connect. #24[c])	Oil Rate, STB/D	5,000
Network	Simulation time, day	180

Table 7.7—CASE 7 BOTTOMHOLE FLOWING PRESSURE SENSITIVITY VALUES

Case	BHP, psia
Case 7a	1,000
Case 7b	2,500
Case 7c	4,000
Case 7d	7,000

Fig. 7.14 displays the results for Case 7 sensitivities. Very complex relationships between fluid composition, pressure, and temperature lead to non-monotonic asphaltene deposition profiles as a function of BHP. Largest asphaltene accretion are observed for Cases 7b and 7c (BHP = 4,000 and 2,500 psia), from Fig. 7.14 a through d, which generate pressure-temperature combinations along the pipeline that are closer to the saturation point of the fluid (Fig. 6.8). Case 7a displayed the lowest deposition and greatest fluid velocities (Fig. 7.14 e) due to the elevated gas hold-up at low pressures (Fig. 7.14 f and g).

From Fig. 7.14 c, it is also noticeable that the depth at which asphaltene stars precipitating and depositing in the tubing varies depending on BHP. For BHP=1,000 psia, the onset asphaltene conditions are reached at a distance of 1,000 ft from bottomhole, a depth of 1,750 ft. For BHP=7,000 psia deposition starts at 250 ft from bottomhole, while for BHP of 4,000 and 2,500 psia deposition begins at bottomhole reference depth.

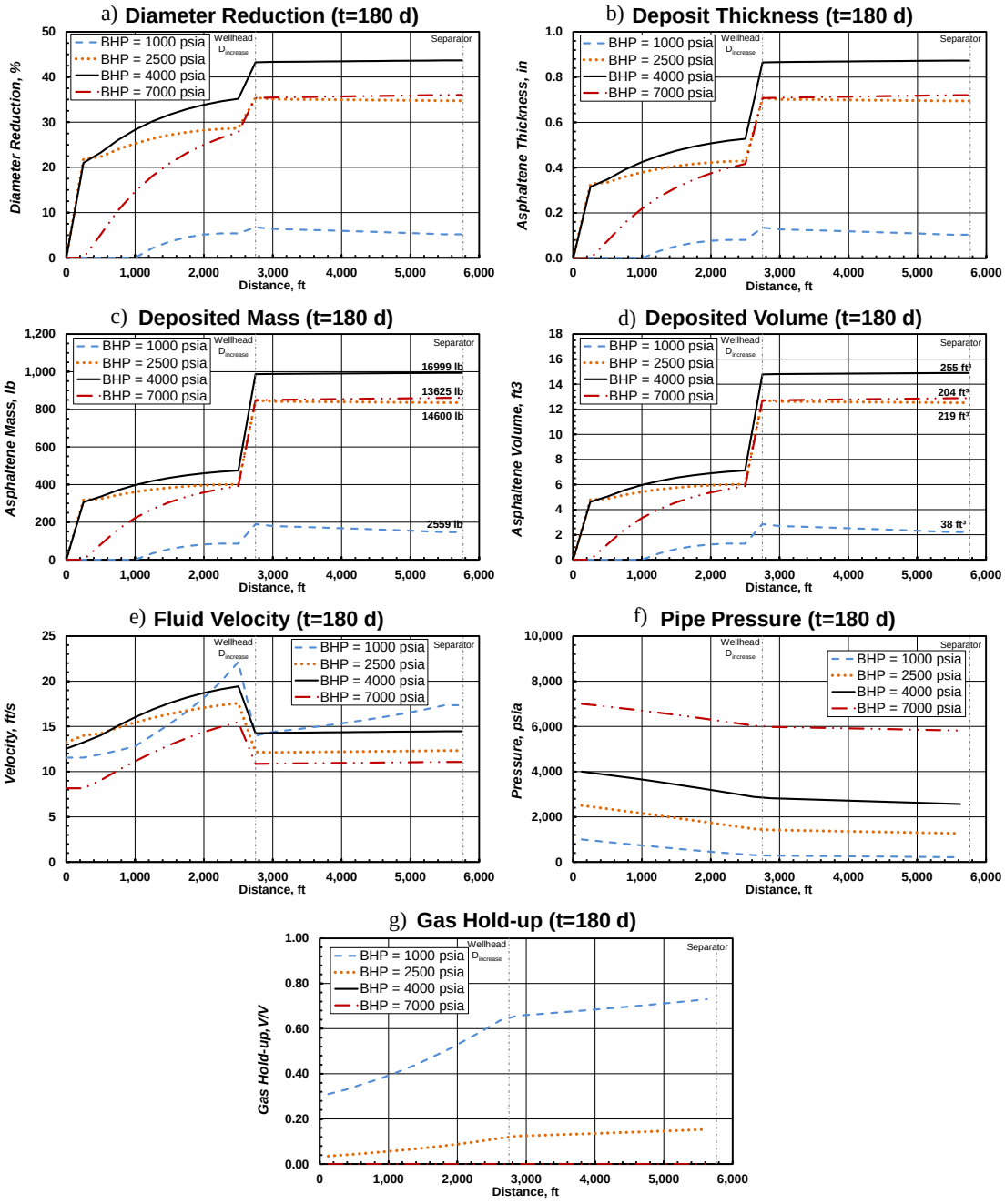

Fig. 7.14—Case 7 network properties vs. distance profiles for BHP sensitivities at 180 days of production. Highest asphaltene deposition are observed for BHP 4,000 and 2,500 psia, and lowest was found at BHP=1,000 psia (a through d). Pressure and temperature combinations closer to fluid saturation points display increased deposition e.g. BHP 4,000 and 2,500 psia.

Practical implications of asphaltene accumulation can be observed in pressure management strategies. **Fig. 7.15** displays the pressure drawdown, i.e. the difference between BHP and separator pressure, for the network system during the 180 days of production. As pipe flow area is reduced by asphaltene deposition, frictional pressure losses increase in the system, forcing to reduce separator pressure to maintain the target oil production rate constant. Case 7c (BHP=4,000 psia) displays a fast increase in pressure drawdown, from 700 to 1,430 psi after 180 days of production. If this trend continues, the well would need to be shut-in after less than a year of production, since the separator pressure has a minimum physical constraint of 14.7 psia at which the target cannot be met.

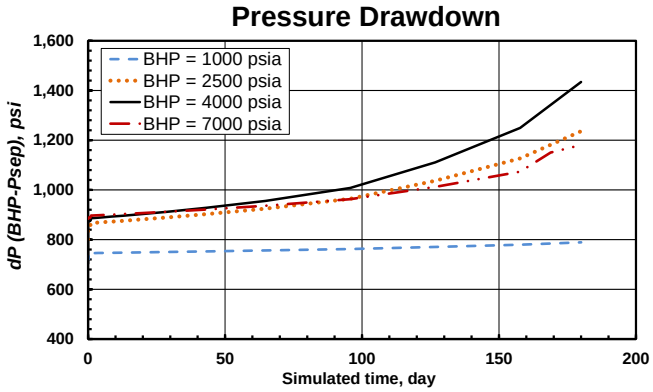

Fig. 7.15—Case 7 network pressure drawdown for BHP sensitivities. Asphaltene accumulations increase frictional pressure losses in the system as pipe flow area reduces. Larger pressure drawdown (difference between BHP and separator pressure) has to be applied for scenarios with high asphaltene deposition. BHP sensitivities of 4,000, 2,500, and 7,000 psia display largest drawdown increase in time. Maximum difference between start and end of production period is for BHP=4,000 psia, displaying a 730 psi increase in drawdown.

From this sensitivity it can be highlighted that for a constant bottomhole production composition the relationship between pipeline pressure-temperature profile and fluid saturation point dominates the asphaltene precipitation and deposition process. Asphaltene accretion was higher and faster in locations where pipeline conditions are close to the fluid saturation pressure and temperature. The accelerated deposition causes flow area reduction in pipes, increasing pressure losses in the system. Pressure drawdown must then

be increased to maintain the target rate, adding operational complexity to the field and reducing pressure management ability in the asset development plan.

7.3.2 Case 8—Artificial Gas-Lift Rate Sensitivity

The impact of artificial gas-lift on asphaltene deposition and production performance was introduced for the reservoir-network coupled Case 6 (Section 7.2.5). Case 6 operating conditions displayed low tubing pressure values, with an average BHP close to 500 psia, and asphaltene deposition was reduced due to higher fluid velocities achieved with gas-lift injection.

Case 8 intends to improve the understanding of thermodynamic and transport mechanisms of artificial gas-lift method in asphaltene deposition-prone network pipelines at high tubing pressures. BHP boundary condition is set at 7,000 psia, bottomhole produced fluid composition and water cut are also held constant, while target oil production rate at the separator is fixed at 5,000 STB/D. **Table 7.8** summarizes Case 8 boundary conditions for the simulations of 180 days of production. Four sensitivity scenarios ranging gas-lift injection rates from 0 (no gas-lift) to 1,000 SCF/D are displayed on **Table 7.9**.

Table 7.8—CASE 8 BOUNDARY CONDITIONS

Location	Boundary Condition	Value
Bottomhole (Node #1)	Pressure, psia	7,000
Bottomhole (Node #1)	Fluid composition	Table 6.5
Bottomhole (Node #1)	Water Cut, V/V	0.1
Separator (Connect. #24[c])	Oil Rate, STB/D	5,000
Network	Simulation time, day	180

Table 7.9—CASE 8 GAS-LIFT INJECTION RATE SENSITIVITY VALUES

Case	Gas-Lift Rate, MSCF/D
Case 8a	1,000
Case 8b	500
Case 8c	250
Case 8d	No Gas-Lift

Gas-lift injection rate sensitivity results are displayed in **Fig. 7.16**. Greater gas-lift rates induce larger asphaltene deposits after 180 days of production, exhibiting a monotonic relationship between injection rate and asphaltene deposition for the conditions in study. Asphaltene accretion in wellbore and surface pipeline sections is noticeably larger as gas-lift rates increase (Fig. 7.16 a through d), reaching a maximum of 302 ft^3 (75% of pipeline volume) of deposited material with 1,000 MSCF/D injection rate.

Fluid remains in single liquid phase along the pipeline system, indicating that fluid velocity increase as a function of gas injection rate is caused mainly by pipe diameter reduction, leading to unfavorable pressure profiles when gas-lift rate is increased (Fig. 7.16 e).

The overall effect of applying artificial gas-lift method under these production conditions is negative. Gas-lift injection at bottomhole increases methane content in the produced fluid mixture, reducing oil's capacity to maintain asphaltene in solution. **Table 7.10** shows bottomhole fluid compositions for the original base case and the gas-lift injection rate of 1,000 MSCF/D after both fluid mix.

The compositional change to a lighter fluid induces asphaltene precipitation at higher pressures and temperature than the original fluid composition. **Fig. 7.17** illustrates the drastic increase in asphaltene precipitation pressures and weight percent at 150 and 200 °F when the original fluid composition is mixed with the 1,000 MSCF/D gas-lift fluid.

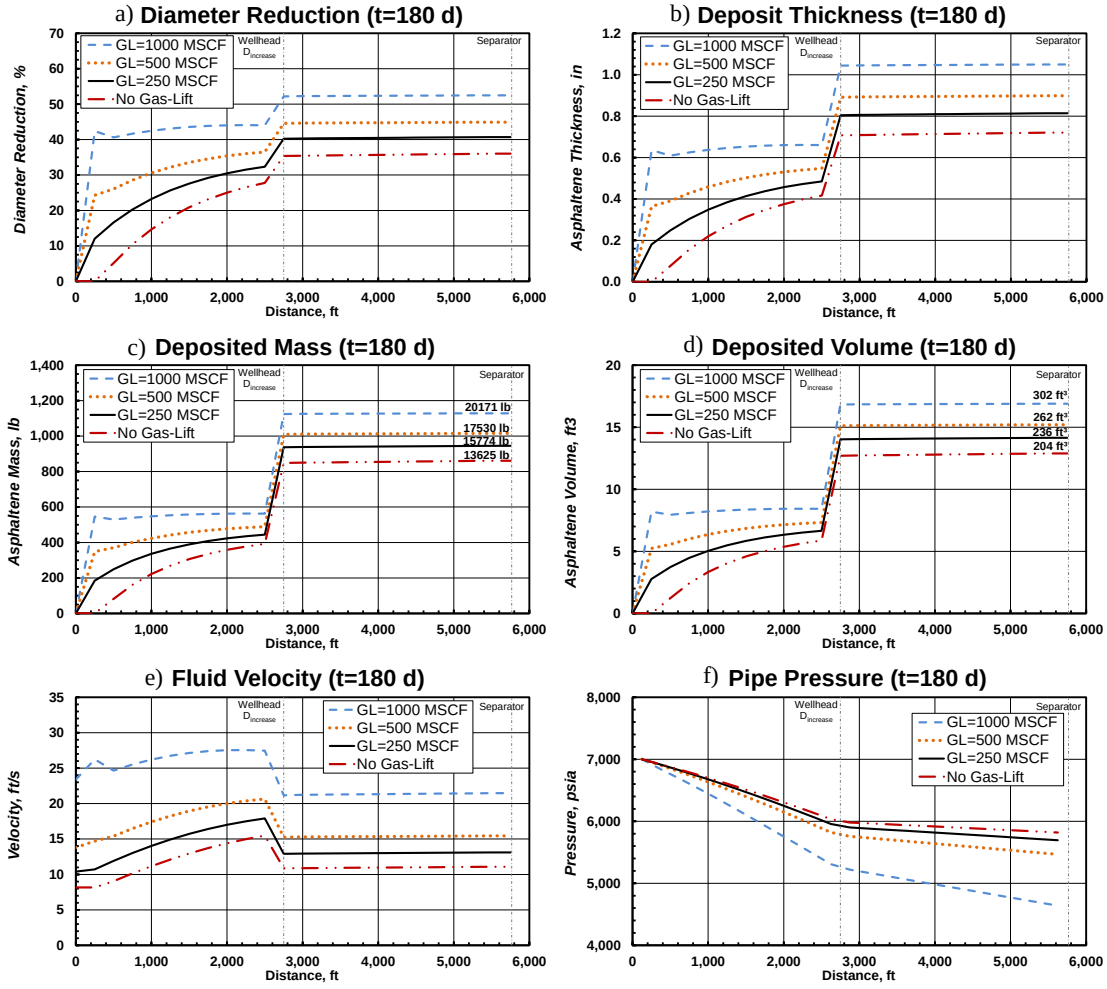

Fig. 7.16—Case 8 network properties vs. distance profiles for gas-lift injection rate sensitivities at 180 days of production. Monotonic relationship between gas-lift rate and deposited asphaltene is observed, greater injection rates cause larger material deposition (a through d). Fluid velocity increments with gas-lift rate due to faster pipe diameter reduction creating unfavorable pressure profiles at high injection rates (e and f). Fluid remains single phase liquid in all cases.

Table 7.10—CASE 8 BOTTOMHOLE FLUID COMPOSITIONS FOR ORIGINAL BASE SCENARIO AND GAS-LIFT RATE OF 1,000 MSCF/D

Component	z_i (Original)	z_i (GL=1,000 MSCF/D)
CO_2	0.02460	0.01204
C_1-N_2	0.36940	0.01829
C_2-C_3	0.07520	0.53124
C_4	0.01930	0.05590
C_5	0.01570	0.01435
C_6	0.01620	0.01167
C_{7+}	0.47145	0.35046
Asphaltene	0.00815	0.00606

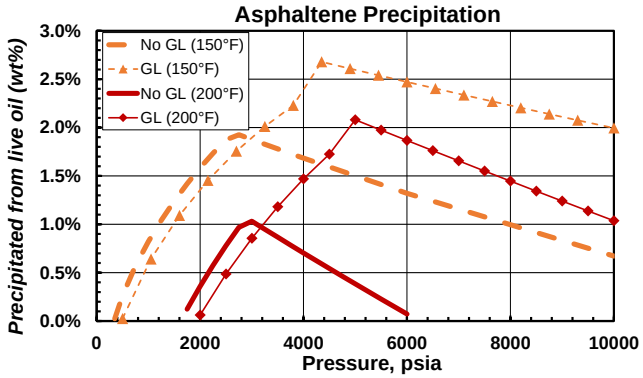

Fig. 7.17—Case 8 asphaltene precipitation envelopes for original bottomhole fluid composition and gas-lift injection rate of 1,000 MSCF/D fluid mixture at 150 and 200 °F.

Greater gas-lift injection rates led to higher volumes of asphaltene deposition in the network for Case 8. **Fig. 7.18** shows the pressure drawdown, i.e. the difference between BHP and separator pressure, for the network system during the 180 days of production for the gas-lift rate sensitivity. Pressure drawdown increases faster proportionally to gas-lift rates as a consequence of greater pipe diameter reduction and frictional pressure losses. Case 8a (GL=1,000 MSCF/D) displayed the maximum drawdown increase with 1,181 psi higher value than the base case without gas-lift.

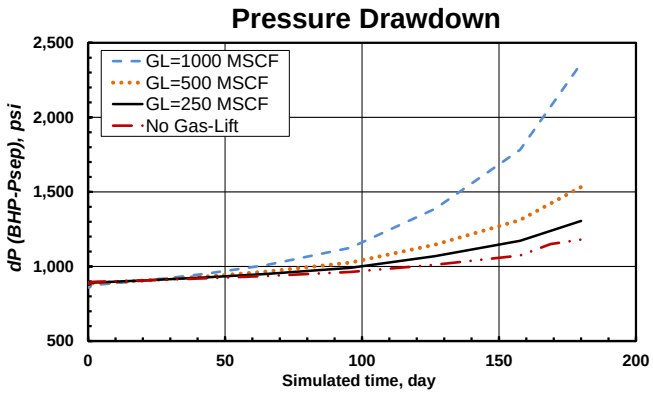

Fig. 7.18—Case 8 network pressure drawdown for gas-lift injection rate sensitivities. Asphaltene accumulations increase frictional pressure losses in the system as pipe flow area reduces due to gas-lift rate increments. Larger pressure drawdown (difference between BHP and separator pressure) difference in comparison with no gas-lift base case was found for a rate of 1,000 MSCF/D, presenting an increase of 1,181 psi after 180 days of production.

7.3.3 Case 9—Asphaltene Molar Composition Sensitivity

Asphaltene molar composition in produced fluids dictates, along with pressure and temperature, onset asphaltene conditions for precipitation and deposition. Case 9 investigates asphaltene accretion for multiple fluids with increasing asphaltene molar composition. Constant bottomhole pressure, produced water cut, fluid composition, and oil rate are fixed during the 180 days of production (**Table 7.11**).

Molar fraction of all components except C_{7+} and Asphaltene are held constant for the multiple sensitivities in fluid composition. The ratio between C_{7+} and Asphaltene was altered to generate fluids with higher Asphaltene content. **Table 7.12** presents fluid compositions for Case 9 sensitivities.

Table 7.11—CASE 9 BOUNDARY CONDITIONS

Location	Boundary Condition	Value
Bottomhole (Node #1)	Pressure, psia	1,000
Bottomhole (Node #1)	Fluid composition	Table 7.12
Bottomhole (Node #1)	Water Cut, V/V	0.1
Separator (Connect. #24[c])	Oil Rate, STB/D	5,000
Network	Simulation time, day	180

Table 7.12—CASE 9 FLUIDS FOR ASPHALTENE MOLAR COMPOSITION SENSITIVITY

Component	Case 9a z_i (Original)	Case 9b z_i	Case 9c z_i	Case 9d z_i
CO_2	0.02460	0.02460	0.02460	0.02460
C_1-N_2	0.36940	0.36940	0.36940	0.36940
C_2-C_3	0.07520	0.07520	0.07520	0.07520
C_4	0.01930	0.01930	0.01930	0.01930
C_5	0.01570	0.01570	0.01570	0.01570
C_6	0.01620	0.01620	0.01620	0.01620
C_{7+}	0.47145	0.47060	0.46960	0.46860
Asphaltene	**0.00815**	**0.00900**	**0.01000**	**0.01050**

Fig. 7.19 illustrates the asphaltene precipitation envelopes at 200 °F for fluid composition in Table 7.12. Increasing asphaltene molar fraction extends the precipitation envelope, promoting precipitation in a wider range of pressures and increasing amount of asphaltene precipitate.

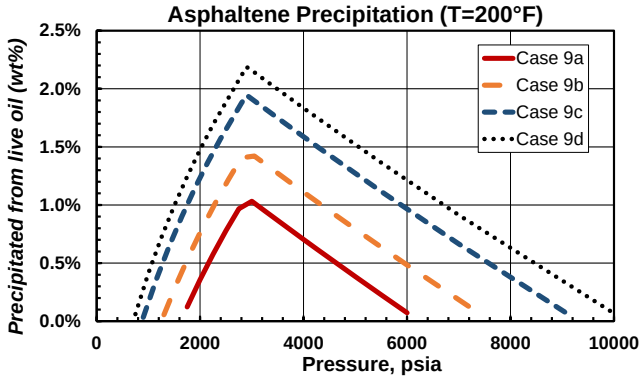

Fig. 7.19—Case 9 asphaltene precipitation envelopes for asphaltene molar composition sensitivity at 200 °F. Increased molar fraction of asphaltene component extends precipitation envelope, promoting precipitation at a wider range of pressures and with higher weight percent of solids.

Results for Case 9 sensitivities are displayed in **Fig. 7.20**. As expected from the fluid analysis and deposition envelopes presented previously, asphaltene accretion in network pipelines increases monotonically as a function asphaltene molar composition in produced fluid. The vertical wellbore section, from bottomhole to wellhead, is particularly affected

by increased solid deposition in scenarios with higher asphaltene composition (Fig. 7.20 a through d). Accentuated diameter reduction causes high frictional pressure losses in the system and high fluid velocities due to reduced pipeline flow area and greater gas hold-up (Fig. 7.20 e through f).

Scenarios with asphaltene molar compositions greater than 0.0105 (Case 9d) were unable to complete the production period of 180 days maintaining the specified oil target rate. Elevated pressure drops in the system due to fast asphaltene deposition required unphysical separator pressure values to produce 5,000 STB/D.

Increased asphaltene deposition as a function of asphaltene molar fraction intensifies the pressure drawdown required to maintain oil production target, as seen on **Fig. 7.21**. After 180 days of production, Case 9d requires 157 psi additional pressure drawdown, with respect to Case 9a, to honor boundary conditions.

Pressure drawdown in these sensitivities is controlled by separator pressure, since BHP is held constant at 1,000 psia. In field operations, separator pressure is maintain constant, hence oil rate would be severely reduced if no mitigation techniques for asphaltene deposition are implemented in fluids with high asphaltene content.

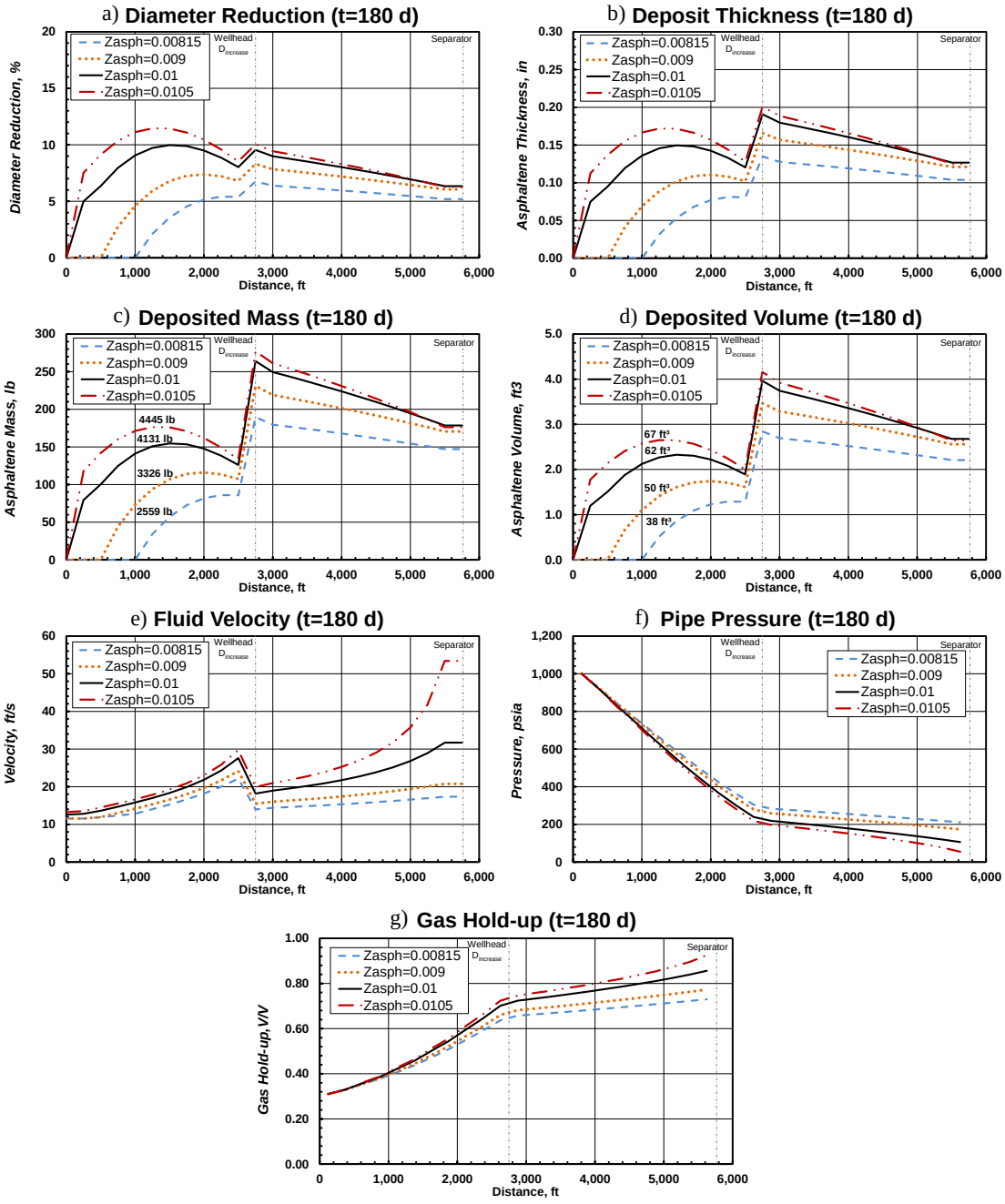

Fig. 7.20—Case 9 network properties vs. distance profiles for asphaltene molar composition sensitivities at 180 days of production. Monotonic relationship between asphaltene molar composition and deposited asphaltene is observed, greater asphaltene molar fraction cause larger material and closer to bottomhole deposition (a through d). Large pressure drops with z_{asph}=0.0105 yield high gas hold-up at separator segment and elevated fluid velocity (e through g).

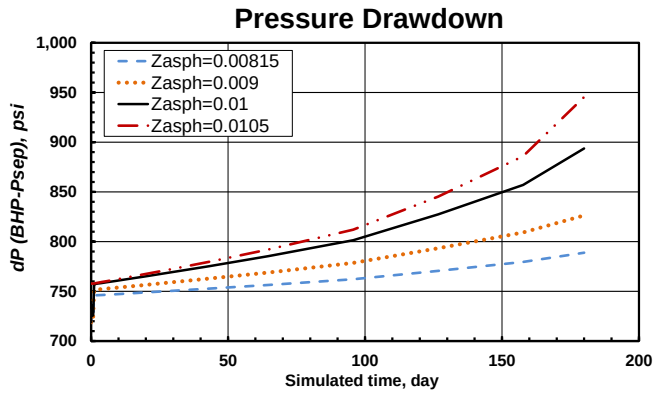

Fig. 7.21—Case 9 network pressure drawdown for asphaltene molar composition sensitivities. Asphaltene accumulations increase frictional pressure losses in the system in scenarios with high asphaltene molar composition. Larger pressure drawdown (difference between BHP and separator pressure) difference in comparison with base case of z_{asph}=0.00815 was found for z_{asph}=0.0105, presenting an increase of 157 psi after 180 days of production.

7.3.4 Case 10—Temperature Profile Sensitivity

Previous sensitivity analysis performed in BHP and fluid composition allowed to demonstrate the impact of changing conditions in the network system. The final scenarios analyzed in this study correspond to temperature profiles in the network pipelines. Case 10 presents four sensitivities varying bottomhole temperature (BHT) at well reference depth and temperature gradients in wellbore and surface pipeline.

Fig. 7.22 illustrates the temperature profiles used in Case 10. Profile 1 corresponds to the base case scenario, presented previously in Section 6.2.2, with linear temperature distributions starting with a BHT of 200 °F, a wellhead temperature (WHT) of 110 °F, and a separator temperature of 105 °F. Profile 2 has BHT, WHT, and separator temperature of 250, 160, and 140 °F respectively. Profile 3 has BHT, WHT, and separator temperature of 150, 60, and 55 °F respectively. Profile 4 is not linear, it starts at BHT of 200 °F and maintains that temperature until a depth of 2,125 ft (a 500 ft distance), gradually decreasing until stabilizing with a vertical temperature gradient of 0.036 °F/ft until reaching a WHT of 133 °F and a separator temperature of 105 °F.

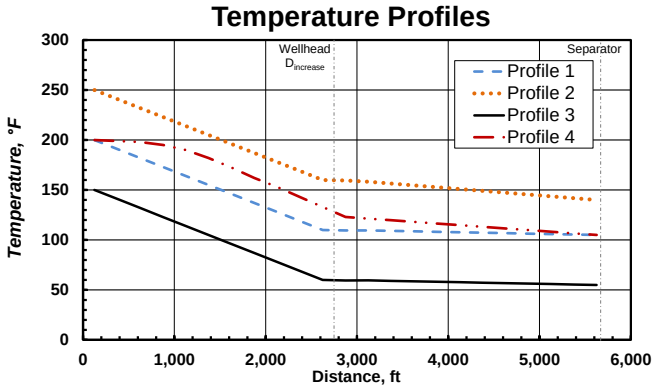

Fig. 7.22—Case 10 network temperature profile sensitivity. Four temperature profiles created with different temperature gradients in wellbore and surface pipeline.

Case 10 sensitivities are modeled with constant boundary conditions (pressure, fluid composition, water cut, and oil production rate) for 180 days of simulation, as shown on **Table 7.13**.

Table 7.13—CASE 10 BOUNDARY CONDITIONS

Location	Boundary Condition	Value
Bottomhole (Node #1)	Pressure, psia	4,000
Bottomhole (Node #1)	Fluid composition	Table 6.5
Bottomhole (Node #1)	Water Cut, V/V	0.1
Separator (Connect. #24[c])	Oil Rate, STB/D	5,000
Network	Simulation time, day	180

Scenarios with higher temperature along the network pipeline system result in reduced asphaltene accumulations (**Fig. 7.23**), especially in the vertical wellbore section where temperature drop from bottomhole to wellhead is drastic. Temperature profiles 1 through 3 display a similar asphaltene deposition pattern, solids accumulation increases with decreasing BHT. Temperature profile 4 starts at the same BHT of Profile 1, however, temperature drop in the former is less pronounced, leading to smaller asphaltene deposits in the wellbore tubing. Surface pipeline accumulations appear similar in all modeled cases.

Fluid velocity in the wellbore is elevated in cases with low temperatures due to pipe diameter reductions (Fig. 7.23 e). Surface pipeline velocity profile is comparable among

all cases. Pressure drop in the vertical wellbore section is increased in low temperature models (Fig. 7.23 f). In all the modeled scenarios in Case 10, fluid remains in single phase liquid across the network.

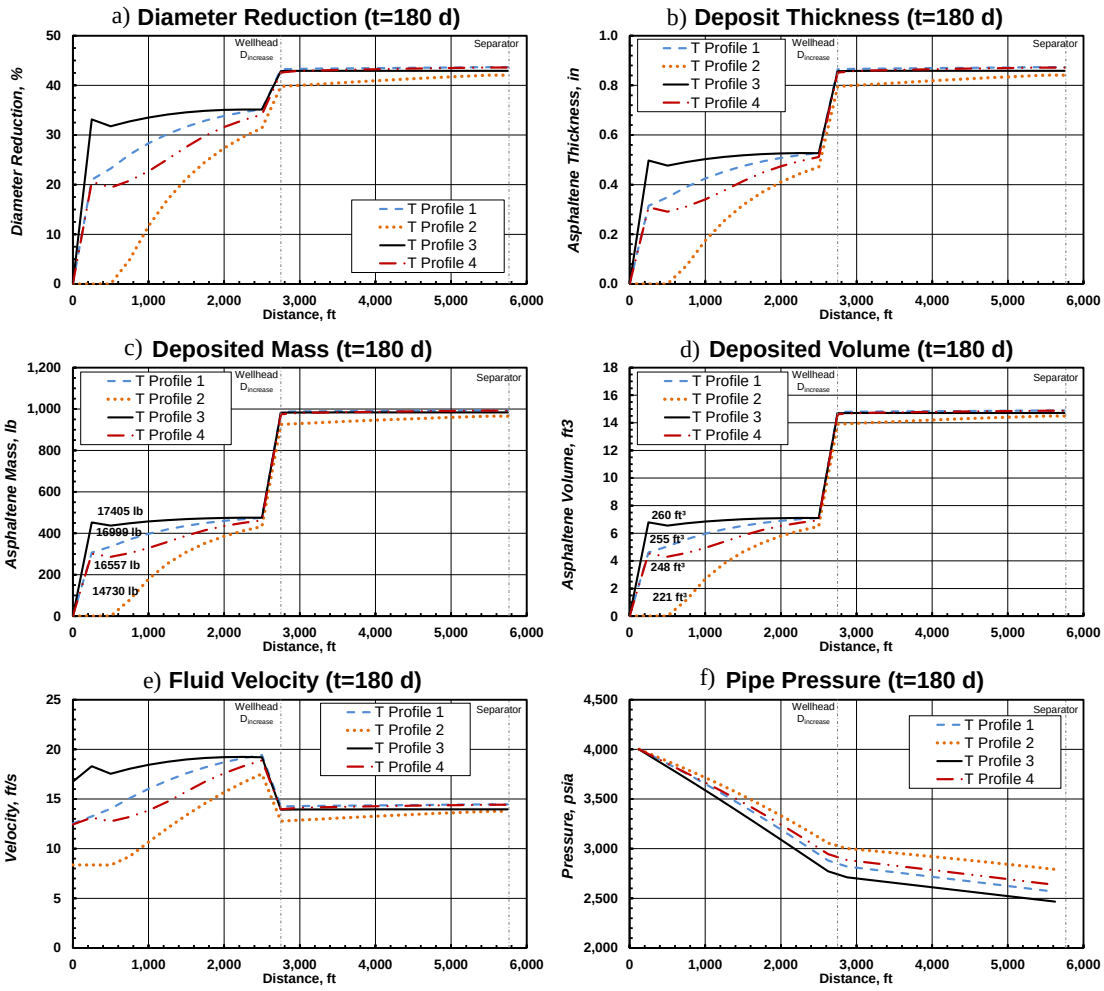

Fig. 7.23—Case 10 network properties vs. distance profiles for temperature profile sensitivities at 180 days of production. Scenarios with higher temperatures along network pipelines present less asphaltene deposition, particularly in the wellbore region, surface pipeline shows similar deposition for all cases (a through d). Fluid velocity is impacted mainly in the wellbore tubing displaying higher values in cases with lower temperatures due to formation of larger deposits, leading to higher pressure drops (e and f). Fluid remains single phase liquid in all cases.

Larger pressure drops in cases with lower temperature profiles result in larger pressure drawdowns, as seen in **Fig. 7.24**. Temperature Profile 2 displayed the smallest drawdown increase with a 344 psi increment during the 180 days of production. Profile 3 on the other hand, presented the highest with 648 psi increment from beginning to end. The difference between Profile 2 and 3 at the end of the production period is 304 psi, negatively impacting production conditions on the latter.

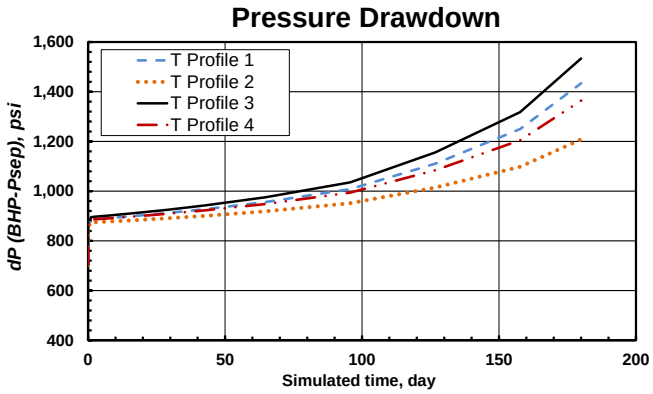

Fig. 7.24—Case 10 network pressure drawdown for temperature profile sensitivities. Profiles with lower temperatures along the network system results in larger pressure drawdown requirements to maintain production rate target.

7.4 Final Remarks on Observed Results

Pressure, temperature, and fluid composition control asphaltene deposition profiles in the production system. Performing stand-alone and integrated asset modeling enable a better understanding of reservoir and network operating conditions under a wide variety of scenarios, supporting the design of appropriate field development strategies.

Pressure management in fields with high asphaltene content is vital. The best strategy for asphaltene control is mitigation of precipitation. Often, asphaltene deposition can be prevented, or reduced, by regulating pressures in reservoir and network system. Reservoir pressure can be maintained by injecting water or gas, while network system pressure can be regulated with artificial lift methods. Proper fluid analysis is recommended before

applying these techniques to ensure compatibility and avoid undesired reactions between original and injected fluids.

Temperature, unfortunately, is not a variable easily controlled during operations. Shortly after starting a well, temperatures along the network increase providing better conditions to reduce asphaltene precipitation. Nonetheless, temperature values rapidly drop during well shut-ins, increasing precipitation potential. Artificial increase in pipe temperatures can be performed with heaters, however, this technique is very expensive to maintain for extended time periods. This leaves understanding temperature profiles as a function of rate the best approach to predict and mitigate asphaltene deposition based solely on this variable.

Produced fluid composition continuously changes as pressure falls below saturation conditions in reservoir or network system due to mobility difference in oil and gas phases. Compositional variations must be forecasted to design surface facilities, cleaning operations, and chemical injection campaigns. Fluid composition can be manipulated in the reservoir by gas or solvent injection, altering fluid behavior. Network fluid can also be modified by chemical inhibitor injection or artificial gas-lift methods. Any alterations in fluid composition may lead to positive, or negative, impact on asphaltene deposition, as demonstrated by multiple scenarios developed in this study.

CHAPTER VIII
CONCLUSIONS AND RECOMMENDATIONS

Production performance forecasts with stand-alone and integrated reservoir-network systems provide essential understanding of fluid transport mechanisms and asphaltene deposition profiles along production pipelines. This platform enables improved design of surface facilities, inhibitor injection campaigns, artificial lifting methods, and cleaning operations. This chapter summarizes main conclusions and observations in the development of this study. Recommendations for future improvements to be implemented in the presented approach are also discussed.

8.1 Conclusions

- The fully-implicit solution approach for the compositional reservoir simulator developed in this study proved robust and consistent. A complex waterflooding case with multi-segment wells, three-phase flow, and large gravity segregation effects, displayed excellent agreement with a well-established commercial simulator.

- Consistent fluid characterization with 6 and 8 components for the reservoir model was validated in Case 1, presenting a good match in reservoir performance indicators and production properties between the two fluid descriptions. In addition, a reduction of 28.6% in computational time was attained using the 6-component fluid characterization.

- The compositional delumping method for coupled reservoir-network simulations presented in Case 2 to model fluids in reservoir with 6-component and network with 8-component is robust. A strong match in results was found when comparing the delumping technique and modeling both reservoir and network with 8-

components. Computational time was reduced by 24.2% when using the delumping approach.

- Neglecting to model asphaltene deposition in network pipelines can lead to optimistic forecasts. The scenario presented in Case 3 led to a 7% (16,500 STB) overestimation in cumulative oil production after one year of production from the 40-acre synthetic model if asphaltene accretion is ignored.

- Diameter reduction due to asphaltene accretion cause additional pressure losses in the network system. Elevated frictional pressure drop limit the ability to implement pressure management techniques to control production from bottomhole to separator, ultimately leading to reduced production rates.

- Asphaltene deposition profiles along pipelines allow determining location and amount of material deposited in the system. Case 3 sample resulted in half of the network pipe volume blocked with asphaltene after a year of production. Deposition profiles can be used to design logistics for cleaning operations, a critical requirement in offshore deepwater fields due to equipment accessibility and location space constraints.

- Case 3 illustrated the effect of pipe diameter variations in the network topology on asphaltene deposition. The diameter increase from 3-in to 4-in at wellhead causes a fluid velocity reduction that triggers additional asphaltene deposition in that location.

- The asphaltene transport model describing solid particle travel from bulk fluid to pipe wall can be easily calibrated using the frequency factor constant. Models described in Case 4 represent a wide variety of scenarios from slow to fast deposition rates. Frequency factor can be obtained from laboratory or empirical

field data (analog neighbor wells) to forecast asphaltene deposition in tubing and surface pipes. Availability of these data enables the design cleanup campaigns and inhibitor injection programs.

- Scenarios with accelerated asphaltene deposition rates, represented by high frequency factor values such as Case 4d, led to great production losses after the pipeline flow is blocked by asphaltene accumulations. Cleanup operations after pipeline is obstructed are expensive and in extreme cases restoring production may not be possible. This highlights the importance of prevention and mitigation methods, e.g. pressure management and inhibitor injection.

- Bottomhole chemical injection using toluene as asphaltene inhibitor proved effective to reduce solid deposition in production network. Case 5 demonstrated that reduction in asphaltene deposited material also reduced frictional pressure losses and improved production performance.

- Design and optimization of chemical injection to mitigate asphaltene deposition in pipelines is essential to maintain normal operating conditions and improve production performance. Case 5 presented sensitivities on inhibitor injection rates for integrated reservoir-network systems, which can be used to determine optimal amounts of chemical injection under a wide variety of scenarios, reducing operating costs for the field.

- Artificial gas-lift implementation in Case 6 coupled model for natural depletion resulted in reduced asphaltene accretion. High fluid velocity in the vertical wellbore section, caused by gas expansion, decreased solids deposition rate. However, this behavior is not universal, as proven by network stand-alone sensitivities gas-lift can also severely increase asphaltene deposition at high production pressures.

- Evaluated coupled case with gas-lift did not exhibit a significant increase in cumulative oil production after one year of depletion process. Bottomhole flowing pressure reduction, of 70 psi in average with respect to no gas-lift usage, was small to substantially increase produced rates. Major benefit observed in this scenario is reduction of material deposited in the pipeline wall when using gas-lift at low bottomhole flowing pressures.

- Stand-alone network sensitivities on bottomhole flowing pressure emphasized the importance of proper reservoir and network pressure management. Asphaltene accretion increased in Case 7 scenarios where pressure-temperature conditions along wellbore and surface pipeline were close to the fluid saturation point. Pressure maintenance in both reservoir and network are key to minimize potential for asphaltene deposition.

- Scenarios with greater asphaltene deposition as a function bottomhole pressure resulted in high pressure losses due to increased friction in the system. Pressure drawdown, difference between bottomhole and separator pressures, had to be continuously increased to maintain target oil production rate.

- Case 8 revealed that gas-lift at high pressures may have an overall negative impact in production performance. Fluid resulting from mixture of original composition and injected gas-lift has lower asphaltene solubility capacity, leading to larger amounts of deposited material in pipeline and increased drawdown requirements to maintain target oil production rate.

- Asphaltene deposition envelope of lighter fluids resulting from mixture of original composition and gas-lift exhibit higher values of asphaltene onset pressure and temperature, as well as greater asphaltene precipitate weight percent, leading to increased solids deposition in the production system at high pressures.

- Produced fluids with higher asphaltene content increase solids accretion in network pipelines. Case 9 illustrated that accelerated deposition causes multiple negative effects such as high frictional pressure losses, high fluid velocities, and greater gas hold-ups in pipes.

- Fluids with high asphaltene molar composition must be analyzed and solid deposition inhibitor techniques should be implemented in fields with those characteristics. Neglecting such critical planning and development steps severely impacts operating conditions and pressure management ability, reducing production rates and asset revenue.

- Higher temperature values along the network pipeline system reduce asphaltene deposition and favor operating conditions, particularly in the vertical wellbore section where temperature changes are more drastic, as observed in Case 10 sensitivities. Offshore deepwater developments often present low production temperatures at subsea gathering system, fostering conditions for asphaltene deposition, which reinforces the need for detailed reservoir-network coupled modeling to identify inhibitor injection location and rates to optimize the production system.

8.2 Recommendations

- Implement multiphase flow calculations in pipes for network and segmented wells. Common multiphase flow correlations in the industry are based on flow regime maps, which can lead to instabilities in the numerical solution approach. Drift flux models (Shi et al. 2005) represent a potentially feasible method to characterize multiphase flow in pipelines with smooth and continuous functions suitable for numerical solution methods.

- Include heat transfer in pipelines and thermal reservoir calculations to model temperature changes in time across reservoir and network systems.

- Develop hydrate and wax modeling following a similar approach to the one developed in this study for asphaltene precipitation and deposition.

- Model asphaltene particle diameter dynamically as a function of concentration and aggregation (Akbarzadeh et al. 2007; Schneider et al. 2007).

- Expand asphaltene transport model by including solid particle removal from wall due to fluid flow shear stress and deposition during well shut-in.

- Generate and run scenarios with multiple wells, and reservoirs, produced through the same network. Improve production allocation strategies via application of intelligent system controls, chokes, etc.

- Build capability of managing additional inline equipment for network, e.g. compressors, pumps, heat exchangers, complex valves, etc.

- Model reservoir-network system from actual field and production data, with special interest in deep water assets. Proper characterization from laboratory experiments on fluid samples should be performed to calibrate equation of state parameters. Asphaltene deposition laboratory studies and empirical data from field can be used to calibrate the solid transport parameters from bulk fluid to pipeline wall.

REFERENCES

Abel, W., Jackson, R.F., and Wattenbarger, R.A. 1970. Simulation of a Partial Pressure Maintenance Gas Cycling Project with a Compositional Model, Carson Creek Field, Alberta. *Journal of Petroleum Technology* (January): 38-46. SPE 2580-PA.

Acs, G., Doleschall, S., and Farkas, E. 1985. General Purpose Compositional Model. *SPE Journal* **25** (4): 543-553.

Akbarzadeh, K., Hammami, A., Kharrat, A. et al. 2007. Asphaltenes—Problematic but Rich in Potential. *Oilfield Review* (Summer): 22-43.

Al-Mutairi, S.M., Hayder, E.M., Al-Shammari, A.T. et al. 2010. A Study of Coupling Surface Network to Reservoir Simulation Model in a Large Middle East Field. SPE 127976-MS.

Ali, J., Betancourt, J., and Avila, C. 1999. A Methodology for Asphaltene Control in Production Facilities in North of Monagas, Venezuela. Paper presented at the ATCE, Houston, TX. SPE 56572-MS.

Aziz, K. and Settari, A. 1979. Petroleum Reservoir Simulation. Applied Science Publishers LTD, London, UK. First Edition. ISBN 0-85334-787-5.

Beggs, D.H. and Brill, J.P. 1973. A Study of Two-Phase Flow in Inclined Pipes. *Journal of Petroleum Technology* **25** (5): 607-617. SPE 4007-PA.

Bird, R.B., Lightfoot, E.N., and Stewart, W.E. 2002. Transport Phenomena. Wiley, New York, NY, US. Second Edition. ISBN 9780471364740.

Burke, N.E., Hobbs, R.E., and Kashou, S.F. 1990. Measurement and Modeling of Asphaltene Precipitation (Includes Associated Paper 23831). *Journal of Petroleum Technology* (November): 1440-1446. SPE 18273-PA.

Byers, T.J. 2000. Preconditioned Newton Methods for Simulation of Reservoirs with Surface Facilities. Doctor of Philosophy Dissertation, Stanford University.

Chien, M.C.H., Lee, S.T., and Chen, W.H. 1985. A New Fully Implicit Compositional Simulator. Paper presented at the Reservoir Simulation Symposium, Dallas, TX. SPE 13385-MS.

Civan, F., 2000. Reservoir Formation Damage: Fundamentals, Modeling, Assessment, and Mitigation. Gulf Publishing Company, Houston, TX, US. First Edition. ISBN 0-88415-301-0

Coats, B.K., Fleming, G.C., Watts, J.W. et al. 2003. A Generalized Wellbore and Surface Facility Model, Fully Coupled to a Reservoir Simulator. Paper presented at the Reservoir Simulation Symposium, Houston, TX. SPE 79704-MS.

Coats, K. 1982. Reservoir Simulation: State of the Art (Includes Associated Papers 11927 and 12290). *Journal of Petroleum Technology* **34** (8): 1633-1642. SPE 10020-PA.

Coats, K.H. 1980. An Equation of State Compositional Model. *SPE Journal* (October): 363-376. SPE 8284-PA.

Dake, L.P. 1978. Fundamentals of Reservoir Engineering. Elsevier, Amsterdam, The Netherlands. First Edition. ISBN 978-0-444-41830-2.

Darcy, H. 1856. Les Fontaines Publiques De La Ville De Dijon. Trans Bobeck. Bibliothèque Nationale de France, Paris, France. First Edition. ISBN 0-7575-0540-6.

Dempsey, J.R., Patterson, J.K., Coats, K.H. et al. 1971. An Efficient Model for Evaluating Gas Field Gathering System Design. *Journal of Petroleum Technology* (September): 1067-1073. SPE 3161-PA.

Dukler, A.E., Wicks, M., and Cleveland, R.G. 1964. Frictional Pressure Drop in Two-Phase Flow: B. An Approach through Similarity Analysis. *AIChE Journal* **10** (1): 44-51.

Duns, H., Jr. and Ros, N.C.J. 1963. Vertical Flow of Gas and Liquid Mixtures in Wells. WPC.

Eaton, B.A., Knowles, C.R., and Silberbrg, I.H. 1967. The Prediction of Flow Patterns, Liquid Holdup and Pressure Losses Occurring During Continuous Two-Phase Flow in Horizontal Pipelines. *Journal of Petroleum Technology* (June): 815-828. SPE 1525-PA.

Economides, M., Hill, D., and Ehlig-Economides, C. 1993. Petroleum Production Systems. Prentice Hall, PTR, Westford, MA, US. First Edition. ISBN 0-13-658683-X.

Ellul, I.R., Saether, G., and Shippen, M.E. 2004. The Modeling of Multiphase Systems under Steady-State and Transient Conditions - a Tutorial. Paper presented at the PSIG Annual Meeting, Palm Springs, CA. PSIG.

Fleming, G. and Wong, T. 2013. Fully Coupled Simulation of Multiple Compositional Reservoirs with a Shared Facility Network. Paper presented at the Reservoir Simulation Symposium, The Woodlands, TX. SPE 163632-MS.

Fussell, L.T. and Fussell, D.D. 1979. An Iterative Technique for Compositional Reservoir Models. *SPE Journal* (August): 211-220. SPE 6891-PA.

Geng, A. and Liao, Z. 2002. Kinetic Studies of Asphaltene Pyrolyses and Their Geochemical Applications. *Applied Geochemistry* **17** (12): 1529-1541.

Ghorayeb, K., Holmes, J., Torrens, R. et al. 2003. A General Purpose Controller for Coupling Multiple Reservoir Simulations and Surface Facility Networks. Paper presented at the Reservoir Simulation Symposium, Houston, TX. SPE 79702-MS.

Ghorayeb, K., Limsukhon, M., Dashti, Q.M. et al. 2008. Multiple Reservoir Simulations Integration: An Alternative to Full Field Simulation in the North Kuwait Jurassic Complex. Paper presented at the ATCE, Denver, CO. SPE 115881-MS.

Gonzalez, D.L., Hirasaki, G.J., Creek, J. et al. 2007. Modeling of Asphaltene Precipitation Due to Changes in Composition Using the Perturbed Chain Statistical Associating Fluid Theory Equation of State. *Energy & Fuels* **21** (3): 1231-1242.

Gonzalez, K.G. 2013. Development of a Compositional Reservoir Simulator for Asphaltene Precipitation Based on a Thermodynamically Consistent Model. Master of Science Thesis, Texas A&M University.

Goodwin, R.D. 1989. Toluene Thermophysical Properties from 178 to 800 K at Pressures to 1000 Bar. *Journal of Physical and Chemical Reference Data* **18** (4): 1565-1636.

Gupta, A.K. 1986. A Model for Asphaltene Flocculation Using an Equation of State. Master of Science Thesis, Department of Chemical and Petroleum Engineering, University of Calgary.

Guyaguler, B., Zapata, V.J., Cao, H. et al. 2011. Near-Well-Subdomain Simulations for Accurate Inflow-Performance-Relationship Calculation to Improve Stability of Reservoir/Network Coupling. *SPE Reservoir Evaluation & Engineering* (October): 634-643. SPE 141207-PA.

Hagedorn, A.R. and Brown, K.E. 1965. Experimental Study of Pressure Gradients Occurring During Continuous Two-Phase Flow in Small-Diameter Vertical Conduits. *Journal of Petroleum Technology* **17** (4): 475-484. SPE 940-PA.

Holmes, J.A., Barkve, T., and Lund, O. 1998. Application of a Multisegment Well Model to Simulate Flow in Advanced Wells. Paper presented at the European Petroleum Conference, The Hague, The Netherlands. SPE 50646-MS.

Iranshahr, A., Voskov, D.V., and Tchelepi, H.A. 2009. Phase Equilibrium Computations are no Longer the Bottleneck in Thermal Compositional EOS Based Simulation. Paper presented at the Reservoir Simulation Symposium, The Woodlands, TX. SPE 119166-MS.

Jiang, Y. 2007. Techniques for Modeling Complex Reservoirs and Advanced Wells. Doctor of Philosophy Dissertation, Stanford University.

Kern, D.Q. and Seaton, R.A. 1959. A Theoretical Analysis of Thermal Surface Fouling. *British Chemical Engineering* **4** (5): 258-262.

Killough, J., Fleming, G., Engle, C. et al. 2013. Surface Facilities and Reservoir Modeling of a Middle Eastern Multi-Reservoir Complex. *International Journal of Engineering and Applied Sciences* **1** (4): 165-183.

Leibovici, C.F., Barker, J.W., and Wache, D. 2000. Method for Delumping the Results of Compositional Reservoir Simulation. *SPE Journal* **5** (2): 227-235. SPE 64001-PA.

Leontaritis, K.J. and Mansoori, G.A. 1987. Asphaltene Flocculation During Oil Production and Processing: A Thermodynamic Collodial Model. Paper presented at the SPE International Symposium on Oilfield Chemistry, San Antonio, Texas. SPE 16258-MS.

Li, Z. and Firoozabadi, A. 2010a. Cubic-Plus-Association Equation of State for Asphaltene Precipitation in Live Oils. *Energy & Fuels* **24** (5): 2956-2963.

Li, Z. and Firoozabadi, A. 2010b. Modeling Asphaltene Precipitation by N-Alkanes from Heavy Oils and Bitumens Using Cubic-Plus-Association Equation of State. *Energy & Fuels* **24** (2): 1106-1113.

Litvak, M.L. and Darlow, B.L. 1995. Surface Network and Well Tubinghead Pressure Constraints in Compositional Simulation. Paper presented at the 13th Symposium on Reservoir Simulation, San Antonio, TX. SPE 29125-MS.

Liu, K. 1997. New Strategies and Procedures for Efficient Compositional Reservoir Simulation. Doctor of Philosophy Dissertation, Texas A&M University.

Lohrenz, J., Bray, B.G., and Clark, C.R. 1964. Calculating Viscosities of Reservoir Fluids from Their Compositions. *SPE Journal* (October):1171-1176. SPE 915-PA.

Mathworks. Matlab R2014a. MathWorks Inc.

McCain, W.D. 1990. Properties of Petroleum Fluids. Pennwell Books, Tulsa, OK, US. Second Edition. ISBN 9780878143351.

Michelsen, M. and Mollerup, J. 2007. Thermodynamic Models: Fundamentals & Computational Aspects. Tie-Line Publications, Denmark. Second Edition. ISBN 87-989961-3-4.

Nghiem, L.X., Fong, D.K., and Aziz, K. 1981. Compositional Modeling with an Equation of State. *SPE Journal* **21** (6): 687-556. SPE 9306-PA.

Orkiszewski, J. 1967. Predicting Two-Phase Pressure Drops in Vertical Pipe. *Journal of Petroleum Technology* (June): 829-838. SPE 1546-PA.

Pan, H. and Firoozabadi, A. 2000a. Thermodynamic Micellization Model for Asphaltene Precipitation from Reservoir Crudes at High Pressures and Temperatures. *SPE Production & Operations* **15** (1): 58-65. SPE 60842-PA.

Pan, H. and Firoozabadi, A. 2000b. Thermodynamic Micellization Model for Asphaltene Precipitation Inhibition. *AIChE Journal* **46** (2): 416-426.

Papavergos, P.G. and Hedley, A.B. 1984. Particle Deposition Behaviour from Turbulent Flows. *Chemical Engineering Research and Design* **62** (5): 275-295.

Peaceman, D.W. 1978. Interpretation of Well-Block Pressures in Numerical Reservoir Simulation (Includes Associated Paper 6988). *SPE Journal* (June):183-194. SPE 6893-PA.

Peaceman, D.W. 1983. Interpretation of Well-Block Pressures in Numerical Reservoir Simulation with Nonsquare Grid Blocks and Anisotropic Permeability. *SPE Journal* (June):531-543. SPE 10528-PA.

Peaceman, D.W. 1990. Interpretation of Wellblock Pressures in Numerical Reservoir Simulation: Part 3 -- Off-Center and Multiple Wells within a Wellblock. *SPE Reservoir Engineering* (May): 227-232. SPE 16976-PA.

Pedersen, K.S. and Christensen, P.L. 2006. Phase Behavior of Petroleum Reservoir Fluids.CRC/Taylor & Francis, Boca Raton, FL, US. ISBN 0-8247-0694-3.

Péneloux, A., Rauzy, E., and Fréze, R. 1982. A Consistent Correction for Redlich-Kwong-Soave Volumes. *Fluid Phase Equilibria* **8** (1): 7-23.

Peng, D.-Y. and Robinson, D.B. 1976. A New Two-Constant Equation of State. *Industrial & Engineering Chemistry Fundamentals* **15** (1): 59-64.

Rachford, H.H., Jr. and Rice, J.D. 1952. Procedure for Use of Electronic Digital Computers in Calculating Flash Vaporization Hydrocarbon Equilibrium. *Petroleum Transactions* **195** (Techincal Note 136): 327-328. SPE 952327-G.

Rafiqul-Islam, M., Moussavizadegan, S.H., Mustafiz, S. et al. 2010. Advanced Petroleum Reservoir Simulation. Scrivener-Wiley, Hoboken, NJ, US. ISBN 978-0-470-625811.

Ramirez-Jaramillo, E., Lira-Galeana, C., and Manero, O. 2006. Modeling Asphaltene Deposition in Production Pipelines. *Energy & Fuels* **20** (3): 1184-1196.

Schlumberger. Eclipse Technical Description and Reference Manual 2014.1. Schlumberger.

Schneider, M.H., Andrews, A.B., Mitra-Kirtley, S. et al. 2007. Asphaltene Molecular Size by Fluorescence Correlation Spectroscopy. *Energy & Fuels* **21** (5): 2875-2882.

Shi, H., Holmes, J.A., Diaz, L.R. et al. 2005. Drift-Flux Parameters for Three-Phase Steady-State Flow in Wellbores. *SPE Journal* (June): 130-137. SPE 89836-PA.

Shirdel, M. 2013. Development of a Coupled Wellbore-Reservoir Compositional Simulator for Damage Prediction and Remediation. Doctor of Philosophy Dissertation, University of Texas.

Stone, H.L. 1973. Estimation of Three-Phase Relative Permeability and Residual Oil Data. *Journal of Canadian Petroleum Technology* **12** (4): 53-61.

Thomas, F.B., Bennion, D.B., Bennion, D.W. et al. 1992. Experimental and Theoretical Studies of Solid Precipitation from Reservoir Fluid. *Journal of Canadian Petroleum Technology* **31** (1): 22-31.

Vargas, F.M., Gonzalez, D.L., Hirasaki, G.J. et al. 2009. Modeling Asphaltene Phase Behavior in Crude Oil Systems Using the Perturbed Chain Form of the Statistical Associating Fluid Theory (PC-SAFT) Equation of State. *Energy & Fuels* **23** (3): 1140-1146.

Watkinson, A.P. 1968. Particulate Fouling of Sensible Heat Exchangers. Doctor of Philosophy Dissertation, The University of British Columbia.

Watts, J.W. 1986. A Compositional Formulation of the Pressure and Saturation Equations. *SPE Reservoir Engineering* (May): 243-252. SPE 12244-PA.

Watts, J.W., Fleming, G.C., and Lu, Q. 2009. Determination of Active Constraints in a Network. Paper presented at the Reservoir Simulation Symposium, The Woodlands, TX. SPE 118877-MS.

Wong, T.W., Firoozabadi, A., and Aziz, K. 1990. Relationship of the Volume-Balance Method of Compositional Simulation to the Newton-Raphson Method. *SPE Reservoir Engineering* (August): 415-422. SPE 18424-PA.

Wylie, E.B., Stoner, M.A., and Streeter, V.L. 1971. Network: System Transient Calculations by Implicit Method. *SPE Journal* (December): 356-362. SPE 2963-PA.

Yan, W., Michelsen, M.L., and Stenby, E.H. 2011. On Application of Non-Cubic EOS to Compositional Reservoir Simulation. Paper presented at the 73th EAGE Annual Conference and Exhibition incorporating SPE Europec Vienna, Austria.

Young, L.C. and Stephenson, R.E. 1983. A Generalized Compositional Approach for Reservoir Simulation. *SPE Journal* (October): 727-742. SPE 10516-PA

APPENDIX A

This appendix presents the calculation procedure for vapor/liquid equilibrium (VLE) using Peng-Robinson (PR) (Peng and Robinson 1976) cubic equation of state (EOS), shown in Eq. (A.1).

$$p = \frac{RT}{\upsilon - b} - \frac{(a\alpha)}{\upsilon^2 + 2\upsilon b - b^2} \quad \text{..... (A.1)}$$

Or in its cubic form based on the compressibility factor, $Z = \frac{pV}{nRT}$:

$$Z^3 - (1 - B)Z^2 + (A - 3B^2 - 2B)Z - (AB - B^2 - B^3) = 0 \quad \text{..... (A.2)}$$

With,

$$A = \frac{p(a\alpha)}{(RT)^2} \quad \text{..... (A.3)}$$

$$B = \frac{pb}{RT} \quad \text{..... (A.4)}$$

$$(a\alpha) = \sum_i \sum_j x_i x_j \sqrt{a_i a_j \alpha_i \alpha_j}(1 - \kappa_{ij}) \quad \text{..... (A.5)}$$

$$b = \sum_i x_i b_i \quad \text{..... (A.6)}$$

$$a_i = 0.45724 \frac{R^2 T_{ci}^2}{p_{ci}^2} \quad \text{..... (A.7)}$$

$$b_i = 0.07780 \frac{RT_{ci}}{p_{ci}} \quad \text{..... (A.8)}$$

$$\alpha_i = \left[1 + m_i \left(1 - \sqrt{\frac{T}{T_{ci}}}\right)\right]^2 \quad \text{..... (A.9)}$$

$$m_i = 0.37464 + 1.54226\,\omega_i - 0.2699\,\omega_i^2;\ \omega_i < 0.49$$
$$m_i = 0.379642 + 1.48503\,\omega_i - 0.164423\,\omega_i^2 + 0.01667\,\omega_i^3;\ \omega_i \geq 0.49 \quad \text{... (A.10)}$$

Thermodynamic equilibrium for a compositional fluid is reached when phase fugacities for each component are equal, evaluating Eq. (A.11). Related to the chemical potential concept, this implies that for all components, the molecular transfer rate from liquid to vapor phase equals the molecular transfer rate from vapor to liquid phase, reaching equilibrium.

$$\hat{f}_i^l = \hat{f}_i^v \quad ; \quad i = 1\ to\ n_c \quad \text{..... (A.11)}$$

Applying logarithm function, Eq. (A.11) can be re-written as follows:

$$ln\left(\frac{\hat{f}_i^v}{\hat{f}_i^l}\right) = 0 \quad ; \quad i = 1\ to\ n_c \quad \text{..... (A.12)}$$

Fugacity coefficients can be expressed, by definition, in terms of component phase fugacity, composition, and pressure:

$$\hat{\varphi}_i^v = \frac{\hat{f}_i^v}{y_i p} \ \ and \ \ \hat{\varphi}_i^l = \frac{\hat{f}_i^l}{x_i p} \quad \text{..... (A.13)}$$

In addition, the component equilibrium ratio (K_i) is defined as the proportion of vapor to liquid molar composition.

$$K_i = \frac{y_i}{x_i} = \frac{\hat{\varphi}_i^l}{\hat{\varphi}_i^v} \quad \text{.....(A.14)}$$

Combining Eqs. (A.12) through (A.14) yields the fugacity residual for two-phase VLE:

$$lnK_i + ln\hat{\varphi}_i^v - \hat{\varphi}_i^l = 0 \quad \text{.....(A.15)}$$

The VLE or flash calculation can be performed using Newton-Raphson or successive substitution scheme, as follows (Michelsen and Mollerup 2007):

a. A first estimate of K-values is obtained from Wilson's approximation (if no *a priori* value is known from other source). Wilson's equilibrium ratio estimate is a function of system pressure (p), temperature (T), and component critical pressure (p_{c_i}) and temperature (T_{c_i}), and acentric factor (ω_i).

$$lnK_i = ln\left(\frac{p_{c_i}}{p}\right) + 5.373(1+\omega_i)\left(1 - \frac{T_{c_i}}{T}\right) \quad \text{.....(A.16)}$$

b. Using Newton's method and the Rachford-Rice equation (Rachford and Rice 1952), calculate the vapor molar fraction f_v:

$$\sum_{i=1}^{n_c}(y_i - x_i) = \sum_{i=1}^{n_c}\frac{z_i(K_i-1)}{1+f_v(K_i-1)} = 0 \quad \text{.....(A.17)}$$

c. Calculate vapor and liquid phases molar fractions, with Eq. (A.18).

$$x_i = \frac{z_i}{1+f_v(K_i-1)} \quad and \quad y_i = \frac{z_i K_i}{1+f_v(K_i-1)} \quad \text{.....(A.18)}$$

d. Calculate fugacity coefficients for each component i and each phase α following the expression based on PR-EOS:

$$ln(\hat{\varphi}_i^{\alpha}) = \frac{B_i}{B}(Z^{\alpha} - 1) - ln(Z^{\alpha} - B^{\alpha}) + \frac{A^{\alpha}}{2\sqrt{2}B^{\alpha}}\left[\frac{B_i}{B^{\alpha}} - \frac{2\sum_{j=1}^{n_c} x_j^{\alpha}(a\alpha)_{ij}}{(a\alpha)^{\alpha}}\right] ln(\beta^{\alpha}) \quad \text{.....(A.19)}$$

Where:

$$(a\alpha)_{ij} = \sqrt{a_i a_j \alpha_i \alpha_j}(1 - \kappa_{ij}) \quad \text{.....(A.20)}$$

$$\beta^{\alpha} = \frac{Z^{\alpha} + \left(1 + \sqrt{2}\right)B^{\alpha}}{Z^{\alpha} - \left(1 - \sqrt{2}\right)B^{\alpha}} \quad \text{.....(A.21)}$$

e. Update equilibrium ratios from iteration k to $k + 1$.

$$K_i^{k+1} = K_i^k \left(\frac{\hat{\varphi}_i{}^{v}}{\hat{\varphi}_i{}^{l}}\right) \quad \text{.....(A.22)}$$

f. Evaluate convergence with Eq. (A.23) and repeat from step b until desired criteria are met (e.g. $\varepsilon = 1 \times 10^{-10}$).

$$\sum_{i=1}^{n_c} \frac{z_i(K_i - 1)}{1 + f_v(K_i - 1)} \leq \varepsilon \quad \text{.....(A.23)}$$

APPENDIX B

This appendix details the finite-difference discretization process for water and hydrocarbon components hydraulic diffusivity equations. Central difference spatial discretization and backward difference time discretization is applied to differential expressions to create the residual form for a fully-implicit system of equation.

B.1. Water Hydraulic Diffusivity

The differential form for water hydraulic diffusivity in porous media, Eq. (B.1), can be divided in three main components, from left to right: convective flow, accumulation, well source/sink.

$$\nabla \cdot \left[\beta_c \vec{\vec{k}} A \frac{k_{rw}}{\mu_w} \nabla \Phi_w\right] = V_b \frac{\partial}{\partial t}[\phi W] + \rho_w q_w \quad \text{..... (B.1)}$$

Where,

k_{rw} is water relative permeability, [dimensionless]

μ_w is water viscosity, [cP]

$\vec{\vec{k}}$ is rock permeability tensor, [mD]

Φ_w is water potential, [psia]

A is area perpendicular to flow direction, [ft^2]

V_b is gridblock rock bulk volume, [ft^3]

ϕ is rock porosity, [ft^3/ft^3]

W is mass of water per unit pore volume, [lb/ft^3]

q_w is volumetric water rate from a well, [ft^3/day]

ρ_w is water density, [lb/ft^3]

$\beta_c = 0.00633$ is the conversion constant for field units

B.1.1 Water Convective Flow Term (Spatial Discretization)

This term is represented by the gridblock flow divergence, which can be expressed as the finite-difference summation of fluxes from the central gridblock to its neighbors (East, West, North, South, Bottom, and Top). Central difference formulation yields:

$$\begin{aligned}\nabla \cdot [a_w \nabla \Phi_w] = {} & a_{wE}\Delta\Phi_{wE} + a_{wW}\Delta\Phi_{wW} \\ & + a_{wN}\Delta\Phi_{wN} + a_{wS}\Delta\Phi_{wS} \\ & + a_{wB}\Delta\Phi_{wB} + a_{wT}\Delta\Phi_{wT}\end{aligned} \quad \text{..... (B.2)}$$

Water transmissibility between the central gridblock and its neighbors $a_{w\eta}$ ($\eta = E, W, N, S, B, T$) is given by the product of the interblock geometric transmissibility T_η and water mobility $\lambda_{w\eta}$.

$$a_{w\eta} = T_\eta \lambda_{w\eta} \quad \text{..... (B.3)}$$

The interblock geometric transmissibility component is a function of gridblock size ($\Delta x, \Delta \text{y}, \text{and } \Delta \text{z}$) and permeability ($\vec{\vec{k}}$), which are considered constant during the simulation. The following equations display interblock geometric transmissibility equations between neighbor cells.

$$T_E = 2\beta_c \left[\frac{(k_x \Delta y \Delta z)_i \, (k_x \Delta y \Delta z)_{i+1}}{(k_x \Delta y \Delta z)_i \Delta x_{i+1} + (k_x \Delta y \Delta z)_{i+1} \Delta x_i} \right]$$

$$T_W = 2\beta_c \left[\frac{(k_x \Delta y \Delta z)_i \, (k_x \Delta y \Delta z)_{i-1}}{(k_x \Delta y \Delta z)_i \Delta x_{i-1} + (k_x \Delta y \Delta z)_{i-1} \Delta x_i} \right]$$

$$T_N = 2\beta_c \left[\frac{\left(k_y \Delta x \Delta z\right)_j \left(k_y \Delta x \Delta z\right)_{j+1}}{\left(k_y \Delta x \Delta z\right)_j \Delta y_{j+1} + \left(k_y \Delta x \Delta z\right)_{j+1} \Delta y_j} \right]$$

$$T_S = 2\beta_c \left[\frac{\left(k_y \Delta x \Delta z\right)_j \left(k_y \Delta x \Delta z\right)_{j-1}}{\left(k_y \Delta x \Delta z\right)_j \Delta y_{j-1} + \left(k_y \Delta x \Delta z\right)_{j-1} \Delta y_j} \right] \quad \text{..... (B.4)}$$

$$T_B = 2\beta_c \left[\frac{(k_z \Delta x \Delta y)_k \, (k_z \Delta x \Delta y)_{k+1}}{(k_z \Delta x \Delta y)_k \Delta z_{k+1} + (k_z \Delta x \Delta y)_{k+1} \Delta z_k} \right]$$

$$T_T = 2\beta_c \left[\frac{(k_z \Delta x \Delta y)_k \, (k_z \Delta x \Delta y)_{k-1}}{(k_z \Delta x \Delta y)_k \Delta z_{k-1} + (k_z \Delta x \Delta y)_{k-1} \Delta z_k} \right]$$

Water mobility is a dynamic property (potentially changes at each iteration and time-step), defined as a function of interblock water relative permeability, density, and viscosity. Interblock water viscosity and density are calculated using volume-weighted arithmetic average between neighbor cells. Relative permeability is a function of fluid saturation in the pore space; upwind (or upstream) permeability is used in this formulation to enhance solution stability.

$$\lambda_{w\eta} = \left(k_{rw} \frac{\rho_w}{\mu_w} \right)_\eta \quad \text{..... (B.5)}$$

The water potential difference between central and neighbor cells (denoted by subscript η), using capillary pressure definition, can be expressed as a function of oil pressure p_o, oil-water capillary pressure p_{cow}, and height difference Δz (Note g_c as the gravity constant).

$$\Delta\Phi_{w\eta} = \left(\Phi_{w\eta} - \Phi_{wC}\right) = \Delta p_{o\eta} - \Delta p_{cow_\eta} - \gamma_{w\eta}\Delta z_\eta$$
$$\Delta\Phi_{w\eta} = \left(p_{o\eta} - p_{oC}\right) - \left(p_{cow_\eta} - p_{cow_C}\right) - g_c\left(\frac{\rho_{w\eta} + \rho_{wC}}{2}\right)\left(z_\eta - z_C\right) \quad \text{..... (B.6)}$$

This expression requires additional manipulation, since capillary pressures are a function of fluid saturation, which is not one of the independent primary variables. Instead, capillary pressures must be expressed as a function of water mass per unit volume (W). Using chain rule and chord-slope approach, the final form for the convective flow equation can be expressed, as shown below, as a summation of fluxes from the six surfaces of the cell.

$$\nabla \cdot [a_w \nabla \Phi_w] = \sum_{\eta=1}^{6}\left[a_{w\eta}\left(\Delta p_{o\eta} - \gamma_{w\eta}\Delta z_\eta\right) - \frac{a_{w\eta}p'_{cow_\eta}}{\rho_{w\eta}}\Delta W_\eta\right] \quad \text{..... (B.7)}$$

Eq. (B.8) shows the oil-water capillary pressure spatial chord-slope between central and neighbor cells, while Eq. (B.9) presents de definition of ΔW_η.

$$p'_{cow_\eta} = \frac{p_{cow_\eta} - p_{cow_c}}{S_{w_\eta} - S_{w_C}} \quad \text{..... (B.8)}$$

$$\Delta W_\eta = W_\eta - W_C \quad \text{..... (B.9)}$$

B.1.2 Water Accumulation Term (Time Discretization)

Discretization in time is performed using backward difference formulation, implementing an implicit approach for system of equations solution. Final form must be expressed displaying primary independent variables in the new time level $n + 1$.

$$V_b \frac{\partial}{\partial t}[\phi W] = \frac{V_b}{\Delta t}[\Delta_\tau(\phi W)] = \frac{V_b}{\Delta t}[W^n \Delta_\tau(\phi) + \phi^{n+1}\Delta_\tau(W)] \quad \text{..... (B.10)}$$

The previous expression can be derived from the time chord-slope approach shown below. The example below was developed for discretization of four variables; Eq. (B.10) is a special case of this formulation where two of the variables can be set to unit and the expression is simplified.

$$\begin{aligned}\Delta_\tau(uvxy) &= (uvxy)^{n+1} - (uvxy)^n \\ &= (vxy)^n\Delta_\tau(u) + u^{n+1}(xy)^n\Delta_\tau(v) \\ &+ (uv)^{n+1}(y)^n\Delta_\tau(x) + (uvx)^{n+1}\Delta_\tau(y)\end{aligned} \quad \text{..... (B.11)}$$

Since porosity is a function of pressure, the chain rule can be applied to express its time derivative in terms of pressure, as presented in the following equation.

$$\Delta_\tau(\phi) = \frac{\partial\phi}{\partial t} = \frac{\partial\phi}{\partial p}\frac{\partial p}{\partial t} = \frac{\phi^{n+1} - \phi^n}{p^{n+1} - p^n}\Delta_\tau(p) = \phi'\Delta_\tau(p) \quad \text{..... (B.12)}$$

Finally, the water accumulation term can be expressed with primary independent variables in the new time level.

$$V_b\frac{\partial}{\partial t}[\phi W] = \frac{V_b}{\Delta t}[W^n\phi'(p^{n+1} - p^n) + \phi^{n+1}(W^{n+1} - W^n)] \quad \text{..... (B.13)}$$

B.1.3 Water Equation Residual Form

Final expression for the water equation can be written in residual form, see below. Including well source/sink term, all coefficients in the equation must be calculated in the new time level, hence the fully-implicit approach, solved through a Newton-Raphson scheme.

$$R_w = \frac{V_b}{\Delta t}[W^n \phi'(p_{oC}^{n+1} - p_{oC}^n) + \phi^{n+1}(W^{n+1} - W^n)]$$
$$- \sum_{\eta=1}^{6}\left[a_{w\eta}^{n+1}\left(\Delta p_{o\eta}^{n+1} - \gamma_{w\eta}^{n+1}\Delta z_\eta\right) - \frac{a_{w\eta}^{n+1} p_{cow_\eta}^{\prime\,(n+1)}}{\rho_{w\eta}^{n+1}}\Delta W_\eta^{n+1}\right] \quad \text{..... (B.14)}$$
$$+ WI_w^{n+1}\left(p_{oC}^{n+1} - p_{cow}^{n+1} - p_{wf}^{n+1}\right)$$

B.2. Hydrocarbon Component Hydraulic Diffusivity

Similarly to the water equation, the differential form for hydrocarbon hydraulic diffusivity in porous media, Eq. (B.15), can be divided in three main components, from left to right: convective flow, accumulation, well source/sink.

$$\nabla \cdot \left[\beta_c \vec{\vec{k}} A\left(x_i \frac{k_{ro}}{\mu_o}\nabla\Phi_o + y_i \frac{k_{rg}}{\mu_g}\nabla\Phi_g\right)\right] = V_b \frac{\partial}{\partial t}[\phi F_i] + \dot{n}_i \quad ; \quad i = 1\ to\ n_c \quad \text{..... (B.15)}$$

Where,

k_{ro} and k_{rg} are oil and gas relative permeability, [dimensionless]

μ_o and μ_g are oil and gas viscosity, [cP]

x_i and y_i are liquid and vapor molar fractions of component *i* respectively, [lbmol/lbmol]

$\vec{\vec{k}}$ is rock permeability tensor, [mD]

Φ_o and Φ_g are oil and gas potential, [psia]

A is area perpendicular to flow direction, [ft^2]

V_b is gridblock rock bulk volume, [ft^3]

ϕ is rock porosity, [ft^3/ft^3]

F_i is number of moles of component i per unit pore volume, [lbmol/ft^3]

$\dot{n}_i$ is molar rate of component i from a well, [lbmol/day]

n_c is the number of hydrocarbon components

$\beta_c = 0.00633$ is the conversion constant for field units

B.2.1 Hydrocarbon Component Convective Flow Term (Spatial Discretization)

This term is represented by the gridblock component flow divergence of oil and gas phases, which can be expressed as the finite-difference summation of fluxes from the central gridblock to its neighbors (East, West, North, South, Bottom, and Top). Central difference formulation yields:

$$\begin{aligned}\nabla \cdot \left[a_o x_i \nabla\Phi_o + a_g y_i \nabla\Phi_g\right] &= a_{oE} x_{iE} \Delta\Phi_{oE} + a_{oW} x_{iW} \Delta\Phi_{oW} \\ &+ a_{oN} x_{iN} \Delta\Phi_{oN} + a_{oS} x_{iS} \Delta\Phi_{oS} \\ &+ a_{oB} x_{iB} \Delta\Phi_{oB} + a_{oT} x_{iT} \Delta\Phi_{oT} \\ &+ a_{gE} y_{iE} \Delta\Phi_{gE} + a_{gW} y_{iW} \Delta\Phi_{gW} \\ &+ a_{gN} y_{iN} \Delta\Phi_{gN} + a_{gS} y_{iS} \Delta\Phi_{gS} \\ &+ a_{gB} y_{iB} \Delta\Phi_{gB} + a_{gT} y_{iT} \Delta\Phi_{gT}\end{aligned} \quad \text{..... (B.16)}$$

Oil and gas transmissibility between the central gridblock and its neighbors $a_{o\eta}$ and $a_{g\eta}$ ($\eta = E, W, N, S, B, T$) are given by the product of the interblock geometric transmissibility T_η, defined previously in Eq. (B.4), and oil and gas mobility ($\lambda_{o\eta}$ and $\lambda_{g\eta}$).

$$\begin{aligned}a_{o\eta} &= T_\eta \lambda_{o\eta} \\ a_{g\eta} &= T_\eta \lambda_{g\eta}\end{aligned} \quad \text{..... (B.17)}$$

Oil and gas mobilities are calculated as a function of phase relative permeability $k_{r\alpha}$, molar density $\tilde{\rho}_\alpha$, and viscosity μ_α. Interblock hydrocarbon phase viscosity and density are calculated using volume- and mass-weighted arithmetic average between neighbor cells. Relative permeability is a function of fluid saturation in the pore space; upwind (or upstream) permeability is used in this formulation to enhance solution stability.

$$\lambda_{o\eta} = \left(k_{ro}\frac{\tilde{\rho}_o}{\mu_o}\right)_\eta$$
$$\lambda_{g\eta} = \left(k_{rg}\frac{\tilde{\rho}_g}{\mu_g}\right)_\eta \quad \text{..... (B.18)}$$

Oil potential difference between central and neighbor cells (denoted by subscript η) can be expressed as a function of oil pressure p_o and height difference Δz (Note g_c as the gravity constant).

$$\Delta\Phi_{o\eta} = \left(\Phi_{o\eta} - \Phi_{oC}\right) = \Delta p_{o\eta} - \gamma_{o\eta}\Delta z_\eta$$
$$\Delta\Phi_{o\eta} = \left(p_{o\eta} - p_{oC}\right) - g_c\left(\frac{\rho_{o\eta} + \rho_{oC}}{2}\right)\left(z_\eta - z_C\right) \quad \text{..... (B.19)}$$

Gas-potential difference is expressed similarly, including in this instance the gas-oil capillary pressure.

$$\Delta\Phi_{g\eta} = \left(\Phi_{g\eta} - \Phi_{gC}\right) = \Delta p_{o\eta} + \Delta p_{cgo_\eta} - \gamma_{g\eta}\Delta z_\eta$$
$$\Delta\Phi_{g\eta} = \left(p_{o\eta} - p_{oC}\right) + \left(p_{cgo_\eta} - p_{cgo_C}\right) - g_c\left(\frac{\rho_{g\eta} + \rho_{gC}}{2}\right)\left(z_\eta - z_C\right) \quad \text{..... (B.20)}$$

Using chain rule and spatial chord-slope approach to account for capillary pressure dependence on phase saturation, the final form of the hydrocarbon convective flow equation is shown below, as a summation of fluxes from the six surfaces of the cell. Note that spatial chord-slopes of capillary pressure and gas saturation are defined similarly as presented in Eq. (B.8), accounting the variables as function of gas saturation and F_i respectively.

$$\nabla \cdot \left[a_o x_i \nabla \Phi_o + a_g y_i \nabla \Phi_g\right]$$
$$= \sum_{\eta=1}^{6} \left[a_{o\eta} x_i \left(\Delta p_{o\eta} - \gamma_{o\eta} \Delta z_\eta\right)\right]$$
$$+ \sum_{\eta=1}^{6} \left[a_{g\eta} y_i \left(\Delta p_{o\eta} - \gamma_{g\eta} \Delta z_\eta\right)\right] + \sum_{\eta=1}^{6} \left[a_{g\eta} y_i p'_{cgo_\eta} S'_{g_\eta} \Delta F_i\right] \quad \text{..... (B.21)}$$

B.2.2 Hydrocarbon Component Accumulation Term (Time Discretization)

Discretization in time is performed using backward difference formulation, aiming an implicit system of equations solution.

$$V_b \frac{\partial}{\partial t}[\phi F_i] = \frac{V_b}{\Delta t}[\Delta_\tau(\phi F_i)] = \frac{V_b}{\Delta t}[F_i^n \Delta_\tau(\phi) + \phi^{n+1} \Delta_\tau(F_i)] \quad \text{..... (B.22)}$$

Applying time chord-slope, from Eq. (B.11), and chain rule on the porosity derivative, the final form of the hydrocarbon component accumulation term yields:

$$V_b \frac{\partial}{\partial t}[\phi F_i] = \frac{V_b}{\Delta t}[F_i^n \phi'(p^{n+1} - p^n) + \phi^{n+1}(F_i^{n+1} - F_i^n)] \quad \text{..... (B.23)}$$

B.2.3 Hydrocarbon Component Equation Residual Form

Finally, the residual form of the hydrocarbon component i hydraulic diffusivity equation is obtained by combining Eqs. (B.15), (B.21), (B.23), and well source/sink term.

$$
\begin{aligned}
R_i = \frac{V_b}{\Delta t}\left[F_i^n \phi'(p_{oC}^{n+1} - p_{oC}^n) + \phi^{n+1}(F_i^{n+1} - F_i^n)\right] \\
- \sum_{\eta=1}^{6}\left[a_{o\eta}^{n+1} x_i^{n+1}\left(\Delta p_{o\eta} - \gamma_{o\eta}^{n+1}\Delta z_\eta\right)\right] \\
- \sum_{\eta=1}^{6}\left[a_{g\eta}^{n+1} y_i^{n+1}\left(\Delta p_{o\eta} - \gamma_{g\eta}^{n+1}\Delta z_\eta\right)\right] \\
- \sum_{\eta=1}^{6}\left[\left(a_{g\eta} y_i p'_{cgo_\eta} S'_{g_\eta}\right)^{n+1} \Delta F_i\right] \\
+ WI_o^{n+1} x_i^{n+1}\left(p_{oC}^{n+1} - p_{wf}^{n+1}\right) \\
+ WI_g^{n+1} y_i^{n+1}\left(p_{oC}^{n+1} + p_{cgo}^{n+1} - p_{wf}^{n+1}\right)
\end{aligned}
\qquad \text{..... (B.24)}
$$

APPENDIX C

Appendix C details reservoir model properties including horizontal permeability distribution (**Fig. C.1**), relative permeability and capillary pressure tables (**Table C.1**), and water properties (**Table C.2**). Relative permeability curves are processed using the Stone II (Stone 1973) model.

	1	2	3	4	5	6	7	8	9	10	11	12	13	14	15
1	1707.5	2159.2	2386.2	2474.9	2341.2	2096.3	1891.8	1743.2	1586.4	1456.3	1353.3	1277.3	1198.6	1129.6	1075.4
2	1591.8	2604.5	1889.8	2690.2	1795.5	1038.6	868.8	710.6	372.2	305.7	452.4	685.7	473.1	346.6	373.1
3	1843.0	2744.4	3246.0	2487.7	2277.7	1493.9	969.7	541.1	498.9	514.7	721.6	678.4	458.1	312.7	217.9
4	1818.4	2079.9	1783.4	1848.6	1573.9	1764.2	1227.7	509.1	431.5	530.0	587.1	437.9	485.9	372.2	213.8
5	1649.0	1295.3	1320.2	1165.1	1287.7	1685.7	1356.0	722.6	455.7	430.3	361.8	249.3	295.0	342.7	229.8
6	1549.9	721.3	817.5	1001.5	1023.9	1211.0	890.1	700.1	521.0	377.8	318.0	187.8	171.6	225.8	258.2
7	1480.4	678.6	681.9	761.1	850.0	992.6	1021.3	991.3	795.7	355.1	243.2	226.0	174.9	219.0	260.9
8	1404.8	585.5	349.3	519.6	650.7	647.2	804.5	1028.9	738.7	297.4	271.9	212.8	127.9	136.5	174.4
9	1294.8	552.5	475.1	486.1	474.1	421.2	550.6	598.5	528.9	300.2	184.0	168.1	109.3	74.2	70.7
10	1190.2	351.3	359.4	502.9	481.3	405.6	504.6	289.3	213.5	146.1	99.1	125.6	115.1	78.3	72.4
11	1098.9	222.2	200.4	225.4	328.3	325.7	351.4	232.2	143.2	98.8	85.8	94.3	121.9	89.9	66.3
12	1020.6	135.6	82.6	105.6	201.2	237.2	300.2	256.3	174.2	134.5	85.0	82.6	89.4	82.2	92.9
13	955.3	152.9	135.3	164.1	230.2	229.6	322.5	272.9	211.5	129.7	77.3	72.9	69.2	111.1	106.1
14	895.1	187.2	212.1	191.5	257.4	380.4	350.3	295.3	182.0	117.3	82.0	71.4	102.9	170.0	198.6
15	845.0	158.4	191.7	239.1	269.2	325.9	235.7	233.4	195.6	131.9	80.0	59.0	151.7	203.6	156.7

Fig. C.1—Layer horizontal permeability distribution. Each reservoir model layer displays the same distribution.

Table C.1—THREE-PHASE RELATIVE PERMEABILITY AND CAPILLARY PRESSURE FOR RESERVOIR MODEL

Water			Gas			Oil		
S_w	k_{rw}	p_{cow}	S_g	k_{rg}	p_{cgo}	S_o	k_{row}	k_{rog}
0.16	0	50.0	0	0	0	0	0	0
0.18	0	41.0	0.04	0.005	0	0.04	0	0
0.20	0.002	32.0	0.08	0.013	0	0.08	0	0
0.24	0.010	21.0	0.12	0.026	0	0.12	0	0
0.28	0.020	15.5	0.16	0.040	0	0.16	0	0
0.32	0.033	12.0	0.20	0.058	0	0.20	0	0
0.36	0.049	9.2	0.24	0.078	0	0.24	0	0
0.40	0.066	7.0	0.28	0.100	0	0.28	0.005	0.005
0.44	0.090	5.3	0.32	0.126	0	0.32	0.012	0.012
0.48	0.119	4.2	0.36	0.156	0	0.36	0.024	0.024
0.52	0.150	3.4	0.40	0.187	0	0.40	0.040	0.040
0.56	0.186	2.7	0.44	0.222	0	0.44	0.060	0.060
0.60	0.227	2.1	0.48	0.260	0	0.48	0.082	0.082
0.64	0.277	1.7	0.56	0.349	0	0.52	0.112	0.112
0.68	0.330	1.3	0.60	0.400	0	0.56	0.150	0.150
0.72	0.390	1.0	0.64	0.450	0	0.60	0.196	0.196
0.76	0.462	0.7	0.68	0.505	0	0.68	0.315	0.315
0.80	0.540	0.5	0.72	0.562	0	0.72	0.400	0.400
0.84	0.620	0.4	0.76	0.620	0	0.76	0.513	0.513
0.88	0.71	0.3	0.80	0.680	0	0.80	0.650	0.650
0.92	0.8	0.2	0.84	0.740	0	0.84	0.800	0.800
0.96	0.9	0.1	--	--	--	--	--	--
1	1	0	--	--	--	--	--	--

Table C.2—WATER VOLUMETRIC FACTOR AND VISCOSITY AS A FUNCTION OF PRESSURE

Pressure, psia	B_w, bbl/STB	μ_w, cP
14.7	1.0472	0.31549
25	1.0472	0.31548
50	1.0471	0.31546
75	1.0470	0.31543
100	1.0470	0.31541
150	1.0468	0.31536
200	1.0466	0.31532
300	1.0463	0.31522
400	1.0460	0.31513
800	1.0448	0.31475
1,200	1.0435	0.31437
1,600	1.0423	0.31399
2,000	1.0410	0.31362
2,400	1.0398	0.31324
2,800	1.0385	0.31287
3,200	1.0373	0.31249
3,600	1.0360	0.31212
4,000	1.0348	0.31174
4,400	1.0335	0.31137
4,800	1.0323	0.31099
5,200	1.0311	0.31062
5,600	1.0298	0.31025
6,000	1.0286	0.30988
6,400	1.0274	0.30951
6,800	1.0261	0.30913
7,200	1.0249	0.30876
7,600	1.0237	0.30839
8,000	1.0224	0.30802
8,400	1.0212	0.30765
8,800	1.0200	0.30729
9,200	1.0188	0.30692
9,600	1.0175	0.30655
10,000	1.0163	0.30618